OCT 17 1987

1051-4-11

Y3.N83:25/4954

NUREG/CR-4954

Long-Term Performance of Spent Fuel Waste Forms

ORIGINAL

Prepared by J. L. Means, A. J. Markworth, J. K. McCoy, M. P. Failey, M. J. Stenhouse, R. Kohli, G. C. Taylor

Battelle Columbus Division

Prepared for
U.S. Nuclear Regulatory Commission

COMPLETED

NOTICE

This report was prepared as an account of work sponsored by an agency of the United States Government. Neither the United States Government nor any agency thereof, or any of their employees, makes any warranty, expressed or implied, or assumes any legal liability of responsibility for any third party's use, or the results of such use, of any information, apparatus, product or process disclosed in this report, or represents that its use by such third party would not infringe privately owned rights.

NOTICE

Availability of Reference Materials Cited in NRC Publications

Most documents cited in NRC publications will be available from one of the following sources:

1. The NRC Public Document Room, 1717 H Street, N.W.
   Washington, DC 20555
2. The Superintendent of Documents, U.S. Government Printing Office, Post Office Box 37082,
   Washington, DC 20013-7082
3. The National Technical Information Service, Springfield, VA 22161

Although the listing that follows represents the majority of documents cited in NRC publications, it is not intended to be exhaustive.

Referenced documents available for inspection and copying for a fee from the NRC Public Document Room include NRC correspondence and internal NRC memoranda; NRC Office of Inspection and Enforcement bulletins, circulars, information notices, inspection and investigation notices; Licensee Event Reports; vendor reports and correspondence; Commission papers; and applicant and licensee documents and correspondence.

The following documents in the NUREG series are available for purchase from the GPO Sales Program: formal NRC staff and contractor reports, NRC-sponsored conference proceedings, and NRC booklets and brochures. Also available are Regulatory Guides, NRC regulations in the *Code of Federal Regulations*, and *Nuclear Regulatory Commission Issuances*.

Documents available from the National Technical Information Service include NUREG-series reports and technical reports prepared by other federal agencies and reports prepared by the Atomic Energy Commission, forerunner agency to the Nuclear Regulatory Commission.

Documents available from public and special technical libraries include all open literature items, such as books, journal and periodical articles, and transactions. *Federal Register* notices, federal and state legislation, and congressional reports can usually be obtained from these libraries.

Documents such as theses, dissertations, foreign reports and translations, and non-NRC conference proceedings are available for purchase from the organization sponsoring the publication cited.

Single copies of NRC draft reports are available free, to the extent of supply, upon written request to the Division of Information Support Services, Distribution Section, U.S. Nuclear Regulatory Commission, Washington, DC 20555.

Copies of industry codes and standards used in a substantive manner in the NRC regulatory process are maintained at the NRC Library, 7920 Norfolk Avenue, Bethesda, Maryland, and are available there for reference use by the public. Codes and standards are usually copyrighted and may be purchased from the originating organization or, if they are American National Standards, from the American National Standards Institute, 1430 Broadway, New York, NY 10018.

NUREG/CR-4954
RW

Long-Term Performance of Spent Fuel Waste Forms

Manuscript Completed: June 1987
Date Published: September 1987

Prepared by
J. L. Means, A. J. Markworth, J. K. McCoy, M. P. Failey
M. J. Stenhouse, R. Kohli, G. C. Taylor

Battelle Columbus Division
505 King Avenue
Columbus, Ohio 43201-2693

Prepared for
Division of Engineering
Office of Nuclear Regulatory Research
U.S. Nuclear Regulatory Commission
Washington, DC 20555
NRC FIN B6764

PREVIOUS REPORTS IN SERIES

NUREG/CR-3405, Volume 1: "Long-Term Performance of Materials Used for High-Level Waste Packaging: Annual Report, March 1982-April 1983."

NUREG/CR-3427, Volume 1: "Long-Term Performance of Materials Used for High-Level Waste Packaging: Quarterly Report, April-June 1983."

NUREG/CR-3427, Volume 2: "Long-Term Performance of Materials Used for High-Level Waste Packaging: Quarterly Report, July-September 1983."

NUREG/CR-3427, Volume 3: "Long-Term Performance of Materials Used for High-Level Waste Packaging: Quarterly Report, October-December 1983."

NUREG/CR-3427, Volume 4: "Long-Term Performance of Materials Used for High-Level Waste Packaging: Annual Report, April 1983-April 1984."

NUREG/CR-3900, Volume 1: "Long-Term Performance of Materials Used for High-Level Waste Packaging: Quarterly Report, April-June 1984."

NUREG/CR-3900, Volume 2: "Long-Term Performance of Materials Used for High-Level Waste Packaging: Quarterly Report, July-September 1984."

NUREG/CR-3900, Volume 3: "Long-Term Performance of Materials Used for High-Level Waste Packaging: Quarterly Report, October-December 1984."

NUREG/CR-3900, Volume 4: "Long-Term Performance of Materials Used for High-Level Waste Packaging: Annual Report, April 1984-April 1985."

NUREG/CR-4379, Volume 1: "Long-Term Performance of Materials Used for High-Level Waste Packaging: Quarterly Report, April-June 1985."

NUREG/CR-4379, Volume 2: "Long-Term Performance of Materials Used for High-Level Waste Packaging: Quarterly Report, July-September 1985."

NUREG/CR-4379, Volume 3: "Long-Term Performance of Materials Used for High-Level Waste Packaging: Quarterly Report, October-December 1985."

NUREG/CR-4379, Volume 4: "Long-Term Performance of Materials Used for High-Level Waste Packaging: Annual Report, April 1985-March 1986."

NUREG/CR-4795: "Long-Term Performance of High-Level Glass Waste Forms: Topical Report, September 1987."

NUREG/CR-4956: "System Performance of High-Level Waste Package Components: Topical Report, September 1987."

NUREG/CR-4955: "Long-Term Performance of Container Materials for High-Level Waste: Topical Report, September 1987."

ABSTRACT

This report describes the results of a 2-year experimental program to investigate the leaching/dissolution characteristics of spent fuel in simulated groundwaters. Experiments were conducted to evaluate the leaching of unirradiated UO_2 in simulated groundwaters both in the presence and absence of an external radiation field. Other experiments characterized the dissolution behavior of spent fuel under the same conditions as for UO_2. Leach data were interpreted in terms of rates and mechanisms of radionuclide release, thus providing insight on leach behavior under realistic repository conditions. Uranium release from both unirradiated and irradiated UO_2 appeared to be solubility controlled, with only minor leachate compositional effects on the uranium concentrations. When leached in the presence of a radiation field, unirradiated UO_2 produced elevated uranium concentrations only in the brine leachates. The leaching of both cesium and iodine from spent fuel was rapid and linear with the surface-area-to-volume (S/V) ratio. Similar to cesium and iodine, strontium release was nearly proportional to S/V. However, unlike cesium and iodine, strontium release was strongly affected by leachate composition, with greater release associated with lower pH.

A model describing the kinetics of spent fuel/UO_2 dissolution was developed, complementing the experimental studies. For fixed values of the time constant and kinetic exponent, the model predicts that the effect of water chemistry on spent fuel dissolution is largely limited to affecting the saturation concentration of uranium in the aqueous solution. This result contrasts sharply with results obtained previously for glass dissolution.

TABLE OF CONTENTS

		Page	
EXECUTIVE SUMMARY		1	
1. INTRODUCTION		1-1	3
1.1 Objectives and Approach		1-1	3
1.2 Report Organization		1-3	5
2. LEACH TESTING AND ANALYTICAL PROCEDURES		2-1	6
2.1 Experimental Methods		2-1	6
2.1.1 Leachate Composition		2-1	6
2.1.2 Apparatus Design		2-1	6
2.1.3 Test Procedures		2-5	10
2.2 Analytical Methods		2-6	11
2.2.1 Radionuclide Analyses		2-6	11
	2.2.1.1 Uranium	2-6	11
	2.2.1.2 Cesium-134 and Cesium-137	2-6	11
	2.2.1.3 Iodine-129	2-6	11
	2.2.1.4 Strontium-90	2-7	12
	2.2.1.5 Actinides	2-7	12
2.2.2 Eh and pH Measurements		2-8	13
2.2.3 UO_2 Surface Analysis		2-8	13
2.3 References for Chapter 2		2-10	14
3. ANALYTICAL RESULTS		3-1	16
3.1 Eh/pH Trends		3-1	16
3.1.1 Eh		3-1	16
3.1.2 pH		3-2	17
3.2 Leach Data		3-3	18
3.2.1 Uranium		3-4	19
	3.2.1.1 Unirradiated UO_2, No External Radiation Field	3-4	19
	3.2.1.2 Unirradiated UO_2, External Radiation Field	3-4	19
	3.2.1.3 Spent Fuel Uranium	3-4	19

TABLE OF CONTENTS
(CONTINUED)

		Page	
3.2.2	Cesium	3-4	19
3.2.3	Iodine	3-10	25
3.2.4	Strontium	3-10	25
3.2.5	Americium	3-23	38
3.2.6	Curium	3-23	38
3.2.7	Plutonium	3-30	45
3.3	Leached UO_2 Surface Characteristics	3-40	55
3.4	References for Chapter 3	3-43	58
4.	LEACHING MECHANISMS	4-1	59
4.1	Uranium	4-1	59
4.2	Cesium and Iodine	4-6	64
4.3	Strontium	4-8	66
4.4	Other Actinides	4-8	66
4.5	References for Chapter 4	4-14	72
5.	UO_2/SPENT-FUEL DISSOLUTION MODELING	5-1	73
5.1	Previous Studies in Mineral-Dissolution Modeling	5-1	73
5.1.1	General Concepts	5-1	73
5.1.2	Rate-Controlling Processes in Mineral Dissolution	5-1	73
5.1.3	Analyses of Mineral-Dissolution Kinetics	5-4	76
5.1.4	Application of Dissolution-Rate Equation	5-5	77
5.2	UO_2-Dissolution Model Development	5-6	78
5.2.1	Review of Existing UO_2-Dissolution Models	5-6	78
5.2.2	Battelle UO_2-Dissolution Model	5-7	79
5.3	Application of UO_2 Dissolution Model	5-8	80
5.4	References for Chapter 5	5-11	83
6.	CONCLUSIONS	6-1	86
APPENDIX A.	SPENT FUEL CHARACTERISTICS	A-1	89
APPENDIX B.	DISTRIBUTION OF RADIONUCLIDES IN SPENT FUEL	B-1	112
APPENDIX C.	TABULATED LEACHATE DATA	C-1	121
APPENDIX D.	WATER CHEMISTRY	D-1	134
APPENDIX E.	QUALITY ASSURANCE PROCEDURES	E-1	141

LIST OF FIGURES

		Page	
Figure 2.1.	Schematic of reaction vessel used for UO_2 and spent fuel pulsed-flow leach tests	2-4	9
Figure 2.2.	Schematic of cell designed for in-line Eh (platinum electrode) measurement in leachates	2-9	14
Figure 3.1.	Average uranium concentrations vs. time for all leachates, unirradiated UO_2, no external radiation field, with (a) S/V = 50 m^{-1} and (b) S/V = 5 m^{-1}	3-5	20
Figure 3.2.	Average uranium concentrations vs. time, all leachates, unirradiated UO_2, external gamma radiation field ~3 x 10^3 rad/hour, (a) S/V = 50 m^{-1}; (b) S/V = 5 m^{-1}	3-6	21
Figure 3.3.	Average uranium concentrations vs. time, both S/V ratios, spent fuel test in (a) brine; (b) tuff; and, (c) basalt groundwater leachates	3-7	22
Figure 3.4.	Average uranium concentrations vs. time, all leachates, spent fuel test, (a) S/V = 50 m^{-1}, (b) S/V = 5 m^{-1}	3-9	24
Figure 3.5.	Average cesium-137 concentrations vs. time, both S/V's in (a) brine, (b) tuff, and (c) basalt groundwater leachates	3-11	26
Figure 3.6.	Average cesium-137 concentrations vs. time, all leachates, (a) S/V = 50 m^{-1}, (b) S/V = 5 m^{-1}	3-13	28
Figure 3.7.	Average cesium-134 concentrations vs. time, both S/V's in (a) brine, (b) tuff, and (c) basalt groundwater leachates	3-14	29
Figure 3.8.	Average cesium-134 concentrations vs. time, all leachates, (a) S/V = 50 m^{-1}, (b) S/V = 5 m^{-1}	3-16	31
Figure 3.9.	Average iodine-129 concentrations vs. time, both S/V's in (a) brine, (b) tuff, and (c) basalt groundwater leachates	3-17	32
Figure 3.10.	Average iodine-129 concentrations vs. time, all leachates, (a) S/V = 50 m^{-1}, (b) S/V = 5 m^{-1}	3-19	34
Figure 3.11.	Average strontium-90 concentrations vs. time, both S/V's in (a) brine, (b) tuff, and (c) basalt groundwater leachates	3-20	35

LIST OF FIGURES
(CONTINUED)

		Page	
Figure 3.12.	Average strontium-90 concentrations vs. time, all leachates, (a) S/V = 50 m^{-1}, (b) S/V = 5 m^{-1}	3-22	37
Figure 3.13.	Average americium-241 concentrations vs. time, both S/V's in (a) brine, (b) tuff, and (c) basalt groundwater leachates	3-24	39
Figure 3.14.	Average americium-241 concentrations vs. time, all leachates, (a) S/V = 50 m^{-1}, (b) S/V = 5 m^{-1}	3-26	41
Figure 3.15.	Average curium-244 concentrations vs. time, both S/V's in (a) brine, (b) tuff, and (c) basalt groundwater leachates	3-27	42
Figure 3.16.	Average curium-244 concentrations vs. time, all leachates, (a) S/V = 50 m^{-1}, (b) S/V = 5 m^{-1}	3-29	44
Figure 3.17.	Average plutonium-238 concentrations vs. time, both S/V's in (a) brine, (b) tuff, and (c) basalt groundwater leachates	3-31	46
Figure 3.18.	Average plutonium-238 concentrations vs. time, all leachates, (a) S/V = 50 m^{-1}, (b) S/V = 5 m^{-1}	3-33	48
Figure 3.19.	Average plutonium-239 concentrations vs. time, both S/V's in (a) brine, (b) tuff, and (c) basalt groundwater leachates	3-34	49
Figure 3.20.	Average plutonium-239 concentrations vs. time, all leachates, (a) S/V = 50 m^{-1}, (b) S/V = 5 m^{-1}	3-36	51
Figure 3.21.	Average plutonium-240 concentrations vs. time, both S/V's in (a) brine, (b) tuff, and (c) basalt groundwater leachate	3-37	52
Figure 3.22.	Average plutonium-240 concentrations vs. time, all leachates, (a) S/V = 50 m^{-1}, (b) S/V = 5 m^{-1}	3-39	54
Figure 3.23.	Unleached unirradiated UO_2 pellet surfaces (a) molded surface, pellet type used in Experiment No. 1 and (b) fractured surface, pellet type used in Experiment No. 2	3-41	56
Figure 3.24.	Unirradiated UO_2 pellet surface after leaching in brine, Experiment No. 1, Reaction Vessel No. 3	3-42	57

LIST OF FIGURES
(CONTINUED)

		Page	
Figure 4.1.	Average uranium concentrations versus time for all three experiments in brine at (a) S/V = 5 m^{-1} and (b) S/V = 50 m^{-1}	4-2	60
Figure 4.2.	Average uranium concentrations versus time for all three experiments in synthetic tuff groundwater at (a) S/V = 5 m^{-1} and (b) S/V = 50 m^{-1}	4-3	61
Figure 4.3.	Average uranium concentrations versus time for all three experiments in synthetic basalt groundwater at (a) S/V = 5 m^{-1} and (b) S/V = 50 m^{-1}	4-4	62
Figure 4.4.	Uranium concentrations versus time in all three experiments in deionized water leachate	4-5	63
Figure 5.1.	Calculated total uranium concentration as a function of time for various values of the kinetic exponent n. Solvent is pure water at pe = 2	5-9	81
Figure 5.2.	Calculated uranium dissolution rate as a function of time for various values of the kinetic exponent n. Solvent is pure water at pe = 2	5-9	81
Figure 5.3.	Calculated total uranium concentration as a function of time for various values of the kinetic exponent n. Solvent is synthetic Grande Ronde basalt groundwater at pe = 0	5-10	82
Figure 5.4.	Calculated uranium dissolution rate as a function of time for various values of the kinetic exponent n. Solvent is synthetic Grande Ronde basalt groundwater at pe = 0	5-10	82

f

LIST OF TABLES

		Page	
Table 2.1.	Experimental design for unirradiated UO_2 leach tests	2-2	7
Table 2.2.	Experimental design for spent fuel leach tests	2-2	7
Table 2.3.	Chemical composition of simulated groundwater leachates (mg/L)	2-3	8
Table 3.1.	Average Eh measurement (mV) in each leachate and environment	3-2	17
Table 3.2.	Average pH measurements in each leachate and environment	3-3	18
Table 4.1.	Fraction of cesium-137 and iodine-129 leached relative to total fuel inventory	4-7	65
Table 4.2.	Cs/I ratio in fuel and leachates	4-7	65
Table 4.3.	Sr/U ratio in fuel and leachates at days 27 and 146	4-9	67
Table 4.4.	Pu/U ratio in fuel and leachates at days 27 and 146 (based on Pu-238 data)	4-10	68
Table 4.5.	Pu/U ratio in fuel and leachates at days 27 and 146 (based on Pu-239 data)	4-11	69
Table 4.6.	Am/U ratio in fuel and leachates at days 27 and 146	4-12	70
Table 4.7.	Cm/U ratio in fuel and leachates at days 27 and 146	4-13	71
Table 5.1.	Rate-controlling dissolution kinetics for various minerals measured against their solubility in pure water	5-3	75

CONTRIBUTORS

J. L. Means

A. J. Markworth

J. K. McCoy

M. P. Failey

M. J. Stenhouse

R. Kohli

G. C. Taylor

EXECUTIVE SUMMARY

The Department of Energy (DOE) is conducting a large program for the disposal of high-level radioactive wastes in deep-mined geologic repositories. The Nuclear Regulatory Commission (NRC), being responsible for regulating high-level radioactive waste disposal, will review and determine the adequacy of DOE's application for the construction and operation of the repositories. To assist in evaluating DOE's application, the NRC's Office of Nuclear Regulatory Research is developing an understanding of the long-term performance of geologic repositories. As part of this effort, Battelle has investigated, over a five-year period, the long-term performance of materials used for high-level waste packages. The program, which is now concluded, was conducted in three parallel efforts: waste-form studies, container-material studies, and system performance studies. This report summarizes the final results of experimental and modeling studies performed to evaluate the performance of spent fuel as a waste form. These studies were performed to complement research already performed on waste glass.

The leaching/dissolution characteristics of spent fuel and UO_2 were examined through a series of leaching experiments conducted in the presence and absence of a radiation field. The experiments were specifically designed to account for ambient, long-term conditions in a deep repository where groundwater flow rates are expected to be low and where redox conditions will be influenced and perhaps buffered by the large amount of iron that will be present in the repository environment from canisters, overpacks, and their corrosion products. Surface-area-to-volume ratio was included as a variable because its magnitude in the repository environment depends upon many other parameters and cannot be specified with any confidence. Simulated tuff, basalt, and brine groundwaters were tested to determine whether any differences in dissolution characteristics could be attributed to the composition of these fluids. Isotopes of cesium, iodine, strontium, americium, curium, plutonium, and/or uranium were analyzed in the leachates. Data from the experiments were interpreted in terms of rates and mechanisms of radionuclide release.

The leaching of both cesium and iodine from spent fuel was rapid and linear with the surface-area-to-volume (S/V) ratio. At the higher S/V, concentrations of cesium-137 and iodine-129 in the leachates were in the low mg/L range and several orders of magnitude below saturation with respect to any known common salts of these highly soluble ions. Total amounts of cesium-137 and iodine-129 leached ranged from 0.8 to 1.6 and 0.5 to 0.9 percent, respectively, of their fuel inventories.

Similar to cesium and iodine, strontium release was nearly proportional to S/V. However, unlike cesium and iodine, strontium release was strongly affected by leachate composition, with greater release associated with lower pH. Overall, the results suggest lack of solubility control in any of the leachates and a strong kinetic (nonequilibrium) aspect to strontium release from spent fuel. Because of its short half-life, strontium-90 is not of major concern in licensing a deep geologic repository, but strontium may be a good analog for the much longer-lived isotopes of radium.

Actinides analyzed included plutonium-238 and -239/240, curium-244, americium-241, and total uranium. Actinide concentrations over time in most of the spent fuel leachates showed similar trends, generally decreasing with time. The results are most simply explained as indicating solubility control and equilibration of the actinides during the course of the experiment with phases having lower solubilities than those present in the spent fuel.

The leach and dissolution characteristics of uranium are critical because many of the fission by-products and all of the actinides are dispersed in the UO_2 matrix. Hence, these nuclides should be released congruently with uranium. Uranium release from both unirradiated and irradiated UO_2 appeared to be solubility controlled, with only minor leachate compositional effects on the uranium concentrations.

Some anonamously high uranium concentrations were observed when unirradiated UO_2 was leached in brine exposed to an external radiation field of approximately 3×10^3 R/hr. The elevated uranium concentrations were noted after brine leachates were exposed to a cumulative dose of approximately 10^7 rads. Elevated concentrations of uranium were not observed in the simulated tuff and basalt groundwaters and in the deionized water leachate when exposed to radiation. The two most likely causes are: (1) the gamma radiation produced oxidized species in only the brine which oxidized and dissolved some of the uranium; or (2) the gamma radiation created weaknesses at grain boundaries (causing intergranular attack) which led to the mechanical degradation of the waste form. These experimental data point to the need for additional leach testing of UO_2 or spent fuel in brine and in the presence of an external radiation field.

To develop a predictive model for radionuclide release from spent fuel, a relatively simple, semi-empirical model was used to describe the dissolution kinetics. The model is based on analogous studies that have been conducted in the area of mineral-water interactions. Research focused on evaluating the effects of groundwater chemistry on dissolution kinetics using a Battelle-developed water chemistry model in conjunction with a crystal-dissolution model. The spent fuel dissolution model involves two parameters, a time constant and a kinetic exponent for the dependence of dissolution rate on undersaturation. For fixed values of the time constant and kinetic exponent, the model predicts that the effect of water chemistry on spent fuel dissolution is largely limited to affecting the saturation concentration of uranium in the aqueous solution. This result contrasts sharply with results obtained previously for glass dissolution. The cause of this different behavior is that glass dissolves in sufficient quantities to significantly change the the composition of the groundwater, while spent fuel dissolves in such small quantities that the groundwater composition is barely disturbed.

1. INTRODUCTION

The Waste Policy Act of 1982 delegates to the Department of Energy (DOE) the authority for siting, construction, and operation of deep-mined geologic repositories for the disposal of high-level waste and spent fuel. The Nuclear Regulatory Commission (NRC) has the responsibility to regulate the activities of DOE to assure that the health and safety of the repository workers and of the public are adequately protected. Prior to construction, the DOE will submit a license application to the NRC describing in detail the proposed repository. The DOE has been directed to take a multiple-barrier approach to the isolation of radioactive wastes, with the waste package, the underground facility, and the natural geohydrologic features of the site being the major barriers. Since NRC's compliance assessment requires the technical capability to understand relevant phenomena and processes relating to the long-term performance of the multiple barriers, the NRC's Office of Nuclear Regulatory Research has established this program at Battelle to provide input to the assessment of the waste package. The overall objective of this program was to improve the understanding of the long-term performance of waste-package materials. The principal task areas for the program were waste-form studies, system performance studies, and container-materials studies.

Two waste forms are presently expected to be disposed of in a geologic repository: spent fuel from the commercial nuclear power industry and solidified high-level waste from the reprocessing of spent nuclear fuel. The volume of commercial high-level waste is limited. However, the reprocessing of spent fuel from defense activities has in the past, and will continue in the future, to produce significant volumes of high-level waste. DOE has selected high-level waste solidified in borosilicate glass as the reference waste form. Studies relating to the long-term performance of borosilicate glass conducted under this program are summarized in NUREG/CR-4795, Long-Term Performance of High-Level Glass Waste Forms.

Spent fuel will be the primary high-level waste form available for disposal when a repository is ready for operation; thus, data on its performance will be needed by the NRC. This report summarizes the results of a 2-year experimental program to investigate the leaching/dissolution characteristics of spent fuel in simulated groundwaters. This work was conducted to gain further understanding of spent fuel behavior under anticipated repository conditions.

1.1 Objectives and Approach

The leach/dissolution characteristics of borosilicate glass have been studied extensively; however, much less research has been conducted on spent fuel. This can be partly attributed to the fact that nonradioactive waste glass simulants (that is, glasses that contain nonradioactive metals as substitutes for radioactive species with similar chemical behaviors) have been developed and are readily available. Glass leaching studies can be conducted without special laboratory facilities or nuclear licenses. However, simulants for spent fuel, which has complex physio-chemical characteristics, have not yet been developed, and special requirements must be satisfied for

possessing and handling highly radioactive materials. As a result, few research laboratories have the capability or opportunity to conduct spent fuel research.

When the experiments conducted under this task were designed, it was recognized that many previous studies on unirradiated UO_2 and spent fuel leaching had been conducted in aerobic aqueous environments that were not particularly representative of expected long-term repository conditions. Also, the redox conditions seldom have been defined even semiquantitatively, as redox is a difficult parameter to define in this way. However, because the solubility of UO_2 (the spent fuel matrix) is extremely dependent upon redox, it is difficult to evaluate the applicability of much of the existing spent fuel leach-rate data in terms of predicting spent fuel performance in a geologic repository without this information.

Three different but related leach tests were conducted. The first two experiments evaluated the leaching of unirradiated, depleted UO_2 in simulated groundwaters in the absence (Experiment 1) and presence (Experiment 2) of an external radiation field. The third experiment evaluated the leaching behavior of spent fuel under conditions similar to those of the UO_2 experiments. In all experiments, four different leachate compositions were used, including simulated brine, tuff and basalt groundwaters, and deionized water. Other experimental parameters were surface-area-to-volume ratio (S/V), which varied between approximately 5 and 50 $meter^{-1}$, temperature (90 C), and leachate flow rate, which was adjusted to be equivalent to a one-year contact time. Leachates were collected using pulsed flow at approximately 30-day intervals. In addition, all leachates were equilibrated with ductile iron to simulate contact between the leachate and canister and/or overpack in the repository environment. This procedure was used to scavenge oxygen from the leachate and lower the redox potential. A small amount of iron was also added to the leachate during the process. Experiments 1, 2, and 3 were conducted for approximately 11, 8, and 5 months, respectively.

The primary objectives of Experiment 1 were to: (1) resolve experimental complexities prior to the leach testing of spent fuel in the hot cell where, because of the intense radiation fields, repairs or changes to apparatus would be difficult; and (2) to generate baseline data on the dissolution and solubility of uranium from UO_2 for comparison with the results of Experiments 2 and 3. The primary goal of the second experiment was to evaluate the effect of an external radiation field on the dissolution and solubility of unirradiated UO_2. In the third experiment, spent fuel leachates were analyzed for selected radionuclides (isotopes of cesium, iodine, strontium, plutonium, curium, and americium, in addition to uranium). The principal goal of this last experiment was to generate data that could be interpreted in terms of the rates and mechanisms of radionuclide release, such as congruent versus incongruent leaching, solubility controls, and fuel inventory controls. The effects of time, S/V, and leachate composition were also evaluated. Taken as a whole, the spent fuel and unirradiated UO_2 leach tests were intended to generate data on the leach behavior of UO_2 and various radionuclides in spent fuel under realistic repository environments.

To aid in predicting the dissolution behavior of spent fuel, a simple model describing the effects of water chemistry on dissolution kinetics was developed. The model is based on analogous studies conducted in the area of mineral-water interactions. Research focused on evaluating the effects of groundwater chemistry on dissolution kinetics using a Battelle-developed water chemistry model in conjunction with a crystal-dissolution model.

1.2 Report Organization

This topical report complements other final reports for this program (Long-Term Performance of Container Materials for High-Level Waste, NUREG/CR-4955; Long-Term Performance of High-Level Glass Waste Forms, NUREG/CR-4795; and System Performance of High-Level Waste Package Components, NUREG/CR-4956).

Chapter 2, Leach Testing and Analytical Procedures, outlines the experimental procedures and analysis techniques used for this task. Chapter 3, Analytical Results, presents a discussion of the leach data, Eh and pH trends, and leached UO_2 surface characteristics. Chapter 4, Leaching Mechanisms, provides an interpretation of the leach data, describing possible mechanisms of radionuclide release. Chapter 5, UO_2/Spent-Fuel Dissolution Modeling, describes a model for the dissolution of spent fuel. Finally, the results of these studies are set out in Chapter 6, Conclusions.

Appendix A gives a description of the spent fuel used in the leaching experiments; Appendix B describes the distribution of radionuclides in the spent fuel; Appendix C presents tabulated leach data; Appendix D describes a water chemistry model used in these studies; and Appendix E lists quality assurance procedures for experiments performed in this task.

2. LEACH TESTING AND ANALYTICAL PROCEDURES

2.1 Experimental Methods

As discussed in Section 1.1, three different leaching experiments having similar experimental designs were conducted:

- Experiment No. 1 evaluated the leaching of unirradiated UO_2 in synthetic groundwaters.
- Experiment No. 2 evaluated the leaching behavior of unirradiated UO_2 in synthetic groundwaters exposed to an external radiation field.
- Experiment No. 3 evaluated the leaching behavior of irradiated (spent) fuel in the same synthetic groundwaters as in Nos. 1 and 2 above.

2.1.1 Leachate Composition

The first two experiments consisted of 16 reaction vessels exposed to four different leachate compositions as shown in Table 2.1. The spent fuel leaching experiment was nearly identical in design, except that three sets of conditions previously conducted in triplicate were reduced to duplicate. These conditions are shown in Table 2.2. The chemical compositions of the synthetic groundwaters are shown in Table 2.3. The brine was simulated WIPP (from the Waste Isolation Pilot Plant program) Brine A, which is high in magnesium and potassium, in addition to sodium and chloride, and to a lesser extent in sulfate (Ref. 2.1). The simulated tuff groundwater was based on J-13 well water from the Yucca Mountain area, Nevada, and was a dilute $Na \cdot HCO_3$ solution (Ref. 2.2). The simulated basalt groundwater was based on the Rockwell Hanford formulation, which consists of a dilute $Na \cdot Cl \cdot SO_4$ solution with a pH of approximately 9.7 at 25 C (Ref. 2.3). All leachates were equilibrated with ductile iron prior to being introduced into the reaction vessels. The effect of this procedure, which was intended to simulate contact between leachate and canister and/or overpack in the repository environment, was to scavenge oxygen from the leachate and in turn lower the redox potential (Ref. 2.4). This process also helped to poise the leachate for subsequent Eh measurements (Section 2.2.2) by adding a small amount of iron to the solution. S/V ratio was included as a variable because this parameter may vary widely in the repository setting.

2.1.2 Apparatus Design

Reaction vessels (Figure 2.1) were constructed of carbon steel and ranged in capacity from approximately 500 cm^3 (Experiment Nos. 2 and 3) to 900 cm^3 (Experiment No. 1). Inlet and outlet tubing was 1/8-in stainless steel connected to the reaction vessels via Swage-lock fittings. Reaction vessels for the spent fuel leach tests were similar to those used in the UO_2 experiments except that tubing was plumbed in through the bottom of the reaction vessel. Access to the top of the spent fuel vessels was required so that remote-controlled manipulators could be used during vessel assembly and disassembly. Perforated stainless steel trays were inserted into the reaction

Table 2.1. Experimental design for unirradiated UO_2 leach tests.

Reaction Vessel Number	Synthetic Leachate Composition	S/V (meter^{-1})	Effective Contact Time (years)	Temperature (C)
1	Brine	5	1	90
2	Brine	5	1	90
3	Brine	5	1	90
4	Brine	50	1	90
5	Brine	50	1	90
6	Tuff	5	1	90
7	Tuff	5	1	90
8	Tuff	5	1	90
9	Tuff	50	1	90
10	Tuff	50	1	90
11	Basalt	5	1	90
12	Basalt	5	1	90
13	Basalt	5	1	90
14	Basalt	50	1	90
15	Basalt	50	1	90
16	Deionized Water	5	1	90

Table 2.2. Experimental design for spent fuel leach tests.

Reaction Vessel Number	Synthetic Leachate Composition	S/V (meter^{-1})	Effective Contact Time (years)	Temperature (C)
1	Brine	5	1	90
2	Brine	5	1	90
3	Brine	50	1	90
4	Brine	50	1	90
5	Tuff	5	1	90
6	Tuff	5	1	90
7	Tuff	50	1	90
8	Tuff	50	1	90
9	Basalt	5	1	90
10	Basalt	5	1	90
11	Basalt	50	1	90
12	Basalt	50	1	90
13	Deionized Water	5	1	90

7

Table 2.3. Chemical composition of simulated groundwater leachates (mg/L).

Chemical Species	Brine[a]	Tuff[b]	Basalt[c]
Na	42,000	46	358
Ca	600	12	2.8
Mg	35,000	1.7	0.03
K	30,000	5.5	3.4
Sr	5	--	--
Cl	190,000	6.4	312
SO_4	3,500	19.2	173
HCO_3	700	121	55[e]
Br	400	--	--
I	10	--	--
BO_3	1,200	--	--
F	--	1.9	33.4
NO_3	--	12.4	--
SiO_2	--	64.2	76.2
pH[d]	6.5 ± 0.1	7.0 ± 0.2	9.77

(a)WIPP Brine A (Ref. 2.1).

(b)J-13 Well Water (Ref. 2.2).

(c)Grande Ronde Formation (Ref. 2.3).

(d)at 25 C.

(e)Total inorganic carbon species as bicarbonate.

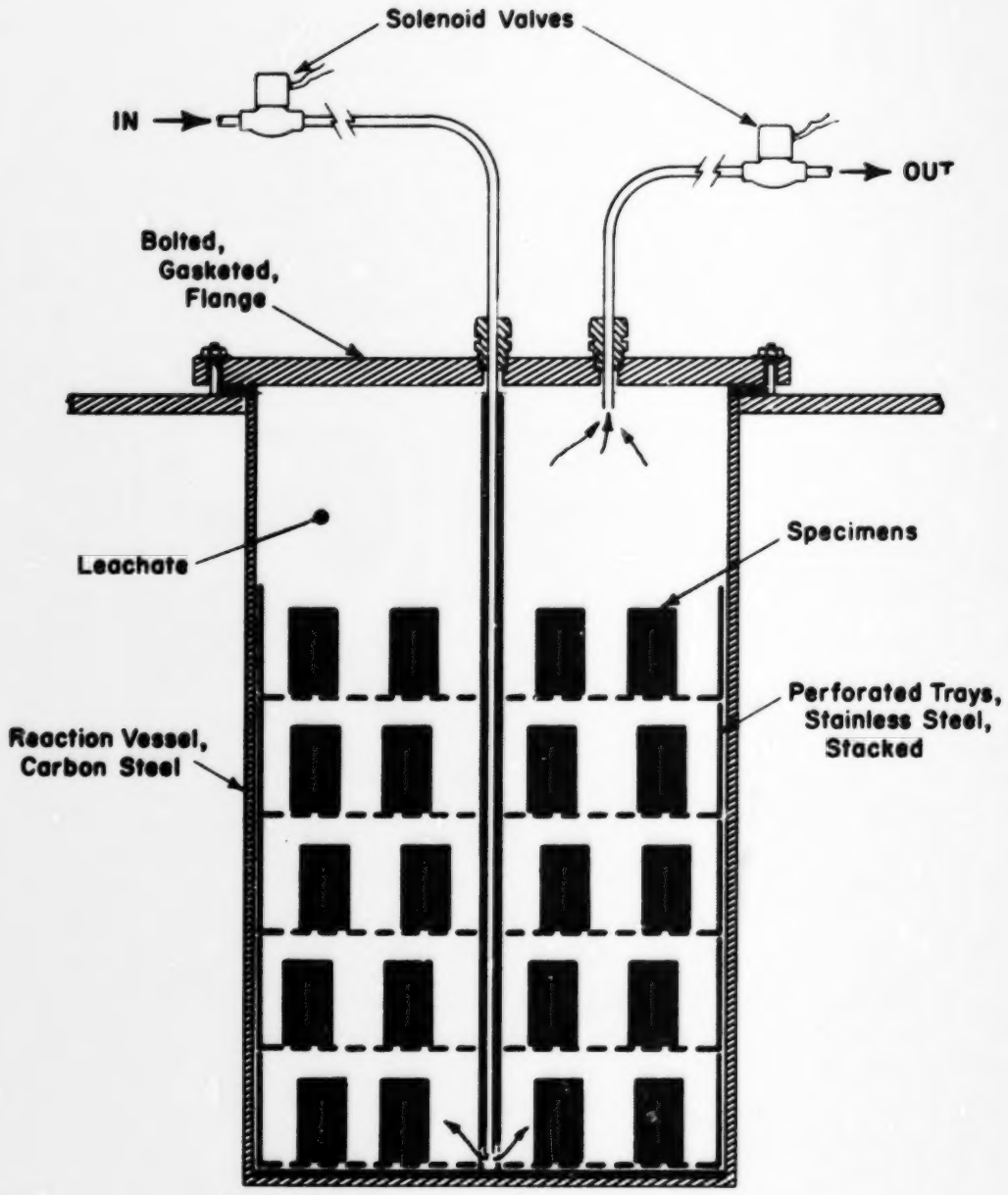

Figure 2.1. Schematic of reaction vessel used for UO_2 and spent fuel pulsed-flow leach tests.

BEST COPY AVAILABLE

vessels to accommodate the large number of fuel pieces required for the high-S/V-ratio experiments. For example, approximately 35 cylindrical UO_2 pellets approximately 0.85 cm in diameter by 0.32 cm in length are necessary to achieve an S/V ratio of 50 m^{-1} in a reaction vessel having a total volume of 500 cm^3. The reaction vessels were placed in a thermostatically controlled oven at 90 C for the duration of the experiments.

The unirradiated UO_2 samples were obtained from Combustion Engineering and were cylindrical, hot-pressed pellets. The spent fuel consisted of approximately 1/4- to 1/3-in-long slices of irradiated fuel retaining its Zircaloy cladding around the circumference but completely exposed on the round faces. We assumed that the fuel/cladding gap would allow leachate to come in contact with the fuel underlying the cladding when calculating experimental S/V ratios. Detailed characteristics of the spent fuel used in this set of experiments are given in Appendix A, and a general summary of the distribution of radionuclides in spent fuel is provided in Appendix B.

2.1.3 Test Procedures

At the outset of each experiment and after UO_2 or spent fuel specimens were placed in their holders, the reaction vessels were sealed, purged with nitrogen gas for several minutes, and then filled to capacity (via peristaltic pump) with the appropriate leachate pretreated with ductile iron. The contents of the reaction vessels were then isolated from the external environment by solenoid valves located at both the inlet and outlet. Thereafter, leachate samples were collected at intervals of approximately 20 to 30 days for the duration of the experiments, which were 328, 238, and 146 days, respectively, for Experiment Nos. 1, 2, and 3. Leachate samples were collected by displacing a small volume of old leachate with fresh leachate (always equilibrated with carbon steel chips). The old leachate was collected outside of the oven in glass sample jars and immediately acidified to pH <1 with ultrapure HNO_3. At each sampling event, a volume equivalent to that needed to simulate a contact time of 1 year was collected. That is, if 30 days had passed since the last sample was collected, then approximately 1/12 (or 30/365) of the total volume of leaching in that vessel would be displaced by an identical volume of fresh leachate and collected for analysis.

As discussed above, the only significant difference between Experiment Nos. 1 and 2 was that the specimens in Experiment No. 2 were exposed to an external gamma radiation field of approximately 3 $x10^3$ R/hr. This field was provided by 2- to 3-foot-long sections of spent fuel hung around the circumference of the oven containing the reaction vessels. Since this experiment was conducted for 238 days, the average cumulative gamma dose to leachates in each of the 16 reaction vessels was 1.7 x 10^7 rads. An external radiation field was not used with the spent fuel leaching experiment. In that experiment, the average gamma dose rate was approximately 1 x 10^3 R/hr, the sole source being the spent fuel pieces contained within the 13 reaction vessels. Cumulative dose rate was approximately 3.5 x 10^6 rads at the conclusion of this 146-day experiment.

2.2 Analytical Methods

2.2.1 Radionuclide Analyses

2.2.1.1 Uranium

Prior to analysis, the uranium in leachate samples was separated from potential interference by extraction into ethyl acetate. A small aliquot of ethyl acetate extract was pipetted onto a NaF/Na_2CO_3 pellet (flux) on the platinum disc. This pellet was then fused at high temperature using a Rotary Fusion Burner (Model RFB-400 by EDA Instru. Inc.) and analyzed by fluorometry (Jarrell Ash Model 26-000, 27-100, or 17-010) using procedures adapted from Price et al. (Ref. 2.5) and Centanni et al. (Ref. 2.6). Samples spiked with a known concentration of uranium (standard additions) were included with each analysis to permit an evaluation of quenching (analytical interface); samples having high quench factors were then reanalyzed. Blanks and standards were analyzed simultaneously with the unknowns and spiked unknowns. Precision is approximately $\pm$ 20 percent and the detection limit is 0.01 mg/L. This method represented a distinct improvement over the one used to collect preliminary data reported in NUREG/CR-4379, Tables 2.9 and 2.10.

2.2.1.2 Cesium-134 and Cesium-137

Cesium-134 and Cs-137 emit high-energy gamma rays with good intensity. As such, it is possible to measure both radionuclides using gamma-ray spectroscopy. In the case of the present UO_2 fuel experiments, the radionuclides were determined by counting aliquots of the sampled solutions in energy- and efficiency-calibrated gamma-ray detector geometries. The detection system consisted of a high-resolution intrinsic germanium detector capable of a peak resolution of 2.0 keV full-width half maximum, or better, at the primary gamma-ray energies of both Cs-134 and Cs-137. The data obtained were analyzed using standard gamma-ray spectrum analysis procedures.

2.2.1.3 Iodine-129

Simulated groundwater solutions in contact with irradiated fuel will leach a variety of radionuclides which may include I-129. Because I-129 emits a low intensity gamma ray, the radionuclide is difficult to measure in the presence of other radionuclides unless the specific activity of I-129 is very great relative to the combined activities of all other radionuclides.

The condition of high I-129 specific activity does not exist in the case of the present UO_2 fuel experiments. Therefore, to detect and measure I-129, it was necessary to separate it from all other activities.

The I-129 separation begins with the addition of inactive iodine carrier followed by absorption of radioiodine, with carrier, on an ion exchange column. Interfering cation activities were eluted from the column and discarded as waste. The retained iodine was eluted from the column and further purified using solvent extraction, precipitation, and filtration. The dried precipitate was X-ray and gamma-ray counted using a low energy

photon spectroscopy system. The I-129 was measured by detecting xenon X-rays from the internal conversion, de-excitation of the xenon product nuclide formed from the I-129 parent.

2.2.1.4 Strontium-90

Fresh irradiated reactor fuel contains a variety of radioactive strontium isotopes, the longest lived of which is Sr-90 with a half life of 29 years. However, after decay periods of approximately 3 years, all radioactive isotopes of strontium with the exception of Sr-90 have decayed to stable species. The irradiated fuel experiments conducted in this study used irradiated fuel that was at least 12 years old. Because of the length of the decay period, all radioisotopes of strontium other than Sr-90 have been removed from the fuel radionuclide inventory. Simulated groundwater in contact with the irradiated fuel leaches Sr-90 and a variety of other isotopes. Because Sr-90 is a pure beta emitter and is difficult to measure in the presence of other fission products, it is necessary to radiochemically separate Sr-90 from all other activities. The separation is performed by adding carriers to precipitate the majority of interfering activities. Then, in another separation step, the strontium fraction is precipitated as a carbonate. The $SrCO_3$ is purified and the Sr-90 activity measured using liquid scintillation counting.

2.2.1.5 Actinides

The actinides were separated from the bulk of the beta/gamma emitters according to the method of Holm and Fukai (Ref. 2.7) by anion exchange using a 93 percent methanol-7 percent nitric acid ($\equiv$1) mixture. Univalent and bivalent cations remained in solution, while the actinides were retained on the column. After several washings, the actinides were regenerated using 0.5M nitric acid. Following anion exchange, the actinides were electroplated using the classical procedure of Talvitie (Ref. 2.8). Overall yields were typically better than 60 percent; in any case two isotope spikes (Am-243 and U-234) were used as yield monitors.

Each electroplated disk was counted using alpha spectrometry and also gamma-ray spectrometry to aid in the interpretation of the alpha spectra, some of which were complex. Gamma-ray spectrometry was performed using a Ge(Li) detector coupled to a computerized data acquisition system. Alpha spectrometry was achieved using a surface-barrier detector coupled to a multichannel analyzer.

The actinides detected using the above procedure were Am-241, Am-243,* Pu-238, Pu-239/240, Pu-241, Cm-243/244, and U-234.* Neptunium-237 was not detected, having an MDA of 140 pCi (~0.2 µg) using gamma-ray spectrometry. Europium (Eu-154, Eu-155) was electroplated with the actinides, and Ce-144 was detected in several samples.

---

*Not quantified.

2.2.2 Eh and pH Measurements

Leachates were analyzed for both Eh and pH as soon as possible after collection. A small aliquot (several mL) of leachate was cooled to room temperature and then analyzed for pH using a small-bore combination pH electrode. In-line Eh measurements were obtained using an Eh cell designed especially for this purpose. Leachate samples were collected in-line into the inert environment of the Eh cell, and measurements were taken without external exposure. The Eh cell design is shown in Figure 2.2.

The cell includes one large septum-lined cap at the top through which the electrode is inserted. A platinum/Ag·AgCl combination electrode was used. A thermometer was inserted through the top septum for monitoring the temperature, which slightly affects the numerical conversion of measured potential to Eh. Three smaller arm-like glass ports extend out from the glass body of the cell and also have septum-lined caps.

Through one of the three arms a continuous, low-level flow of argon gas is maintained; through another arm excess gas flows out and bubbles through water for indicating positive pressure and for preventing air from entering the cell. Through the third arm, samples can be introduced in-line directly from the outlet tubing from the reaction vessel. At the bottom of the cell a Teflon* stop-cock allows for simple discharge of the sample and rinsing of the cell. Using this cell, sample introduction, measurements, removal, and cell rinsing were accomplished in a matter of a few minutes for each sample. Platinum electrode/Ag·AgCl reference potential measurements were calibrated using the Zobell solution; these measurements were then converted to Eh using the procedures described by Langmuir (Ref. 2.9).

2.2.3 UO_2 Surface Analysis

Leached UO_2 surfaces were analyzed by scanning electron microscopy/energy-dispersive X-ray analysis (SEM/EDAX), X-ray diffraction (XRD), and X-ray photoelectron spectroscopy (XPS), more commonly known as electron spectroscopy for chemical analysis (ESCA). Examination of the spent fuel specimens was not possible because of their intense radioactivities.

After leaching, the UO_2 pellets were air-dried and then carbon-coated by vacuum evaporation. The samples were mounted on conductive paint on a copper SEM holder, then examined by scanning electron microscopy in a JEOL JEM100B scanning transmission electron microscope equipped with a Kevex 7000 energy-dispersive spectrometer. Particular attention was given to examining the leached UO_2 surfaces for morphology and elemental composition.

The XRD equipment consisted of a Philips vertical diffractometer fitted with a theta-compensating divergence slit, in-plane sample spinner, and diffracted-beam monochromator. Unknowns were identified by comparison with the Powder Diffraction File (PDF), which contains over 30,000 standard patterns in the inorganic section of the file. Samples were prepared for analysis in two ways. First, surface deposits were gently scraped from the leached UO_2 pellets with a stainless steel microspatula and collected on double-stick tape. Second, tape softened with acetone was pressed onto the

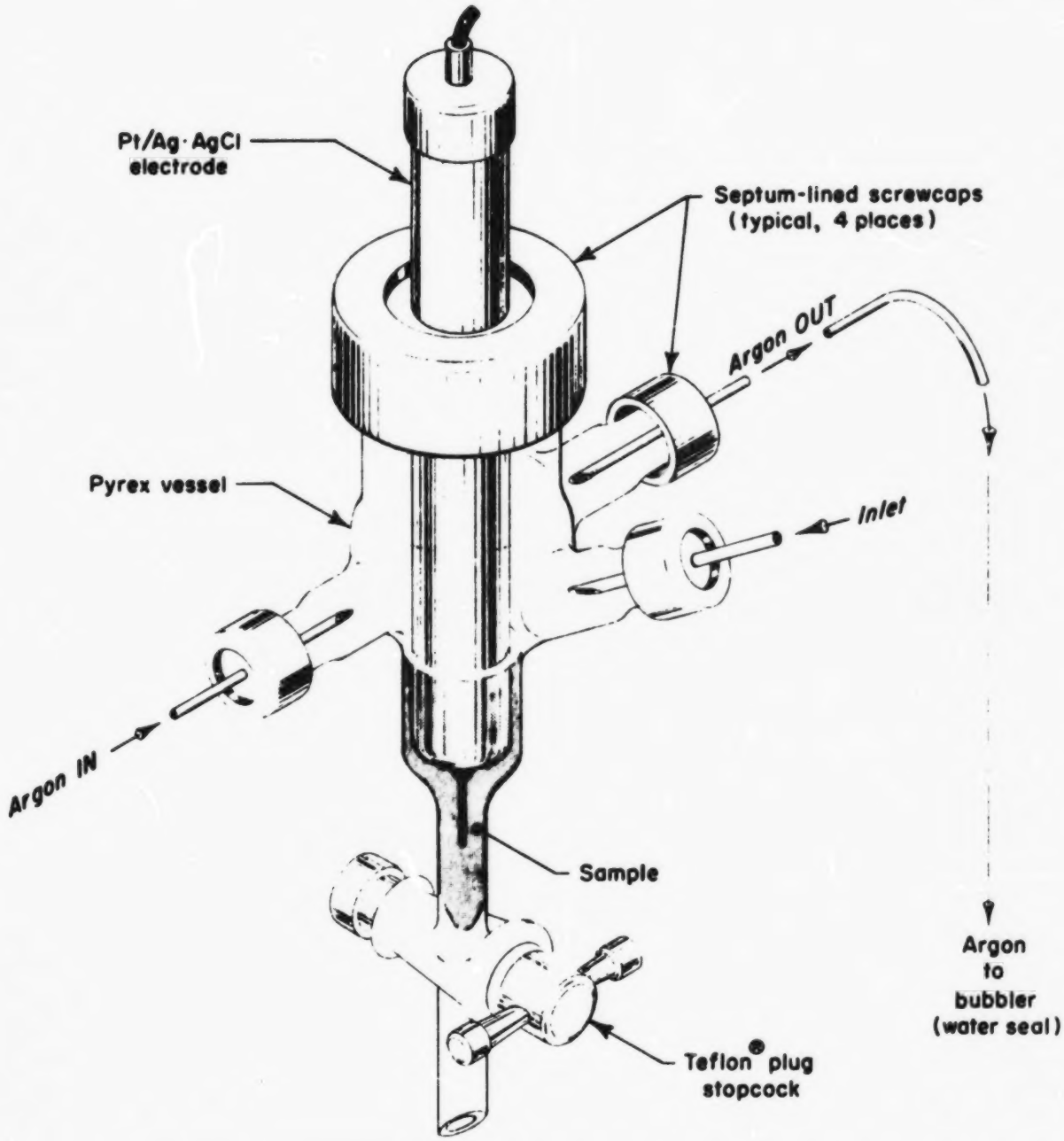

Figure 2.2. Schematic of cell designed for in-line Eh (platinum electrode) measurement in leachates.

BEST COPY AVAILABLE

surface of a pellet and then stripped off after drying. The process was repeated on different samples from the same reaction vessel to increase the amount of sample for analysis.

XPS was used to help identify alteration products in the leached UO_2 surface layer and to analyze the valence state of uranium. A typical analysis detects only those elements in the upper 30 angstroms in a circular area of 1.0 cm^2, although depth profiles down to several hundred angstroms can be generated by analyzing for several hours or more. The XPS system at Battelle is a Leybold Heraeus Model LHS-10. The XPS utilizes the characteristic X-rays from a magnesium or aluminum anode to ionize electrons from the sample. The binding energies are characteristic quantities for a certain shell of the element, and are slightly different for elements in their atomic state and in chemical compounds. All of the valence states that are present can usually be resolved.

2.3 References for Chapter 2

(2.1) M. A. Molecke, "A Comparison of Brines Relevant to Nuclear Waste Experimentation", SAND83-0516, Sandia National Laboratories (1983).

(2.2) A. E. Ogard and J. F. Kerrisk, "Groundwater Chemistry Along Flow Paths Between a Proposed Repository Site and the Accessible Environment", LA-10188-MS (November 1984).

(2.3) T. E. Jones, "Reference Material Chemistry--Synthetic Groundwater Formulation", RHO-BW-ST-37P (April 1982).

(2.4) C. M. Jantzen, "Methods for Simulating Low Redox Potential (Eh) for a Basalt Repository", in: Scientific Basis for Nuclear Waste Management VII, Material Research Society Symposia Proceedings Volume 26, G. M. McVay (ed.) (North Holland, NY, 1984).

(2.5) G. R. Price, R. J. Ferretti, and S. Schwartz, "Fluorometric Determination of Uranium", Anal. Chem. 25 (2), 322-331 (1953).

(2.6) F. A. Centanni, A. M. Ross, and M. A. DeSesa, "Fluorometric Determination of Uranium", Anal. Chem. 28(11), 1651-1657 (1956).

(2.7) E. Holm and R. Fukai, "Method for Multi-element Alpha Spectrometry of Actinides and Its Application to Environmental and Radioactivity Studies", Talanta 24, 659-664 (1977).

(2.8) N. A. Talvitie, "Electrodeposition of Actinides for Alpha Spectrometric Determination", Anal. Chem. 44, 280-283 (1972).

(2.9) D. Langmuir, "Eh-pH Determination", in: Procedures in Sedimentary Petrology, R. E. Carver (ed.), pp. 597-632 (1971).

3. ANALYTICAL RESULTS

3.1 Eh/pH Trends

3.1.1 Eh

As discussed in Section 2.2, Pt/Ag·AgCl electrode measurements were made on leachates in a glass cell under inert gas. Statistical analysis of these data showed no apparent trends in the Eh measurements over time for a given reaction vessel. Also, there was no variability that could be attributed to S/V ratio. Thus, the data were averaged for a given leachate composition in each of the three experiments (Table 3.1), and 95-percent confidence intervals (C.I.) for Eh were computed as follows:

$$\hat{Eh} = \sum Eh/n \qquad (3\text{-}1)$$

where n was the number of reaction vessels sampled on a particular day, for each leachate and environment. Also,

$$\overline{Eh} = \sum Eh/d \qquad (3\text{-}2)$$

where d is the number of days over which $\overline{Eh}$ (average Eh) was computed. Therefore,

$$95\%\ \text{C.I.} = \overline{Eh} \pm 2s/\sqrt{d} \qquad (3\text{-}3)$$

where s was the standard deviation of $\hat{Eh}$. This process eliminates one source of variability by using the mean values for each particular day. Since these mean values are known fairly well, the day-to-day variation can be reasonably determined, and the resulting confidence intervals should be relatively accurate.

Based on the information given in Table 3.1, no definite overall environmental effects were apparent. However, with some leachates, the following significant differences in Eh means between environments appeared: (1) $Eh_s < Eh_r$ in the tuff leachates; and (2) $Eh_s < Eh_r < Eh_n$ in the basalt leachates, where s, r, and n designate spent fuel, radiation field, and nonradiation field environments, respectively.

Also, there were no definite overall leachate effects. However, in the radiation and nonradiation environments, the following significant differences in Eh means between leachates appeared: (1) $Eh_b < Eh_t, Eh_{bs}$ in radiation; and (2) $Eh_b < Eh_t < Eh_{bs}$ in nonradiation, where b, t, and bs designate the brine, tuff, and basalt leachates, respectively.

Table 3.1. Average Eh measurement (mV) in each leachate and environment.

Leachate	Nonradiated Environment Eh Mean[a]	Radiated Environment Eh Mean[b]	Spent Fuel Environment Eh Mean[c]
Brine	-221 (-347 to -95)[d]	-113 (-173 to -53)	-106 (-126 to -86)
Tuff	-24 (-78 to 30)	21 (-21 to 63)	-129 (-229 to -29)
Basalt	114 (78 to 150)	55 (13 to 97)	-152 (-208 to -96)
Deionized Water	35 (-67 to 137)	-85 (-185 to 15)	-132 (-204 to -60)

[a]Experiment No. 1.
[b]Experiment No. 2.
[c]Experiment No. 3
[d]95-percent confidence intervals in parentheses.

We acknowledge that platinum electrode measurements do not necessarily yield an exact measure of the redox potential of a system. Leachates were pretreated with iron in part to make the systems better poised for the Eh measurements; as a result, measurements were generally stable and did not drift substantially during analysis. Leachates not treated with iron gave Eh readings from +161 to +400 mV and exhibited more drift. The data in Table 3.1 indicate near-neutral to moderately reducing conditions, which are reasonable in terms of the expected repository environments. A more precise quantitative designation of the redox potentials of these systems is probably not warranted because of the limitations associated with platinum electrode measurements and redox disequilibria (Ref. 3.1).

3.1.2 pH

As with Eh, pH did not vary systematically with time or S/V. Averages and 95-percent confidence intervals (calculated as in Section 3.1.1) are presented in Table 3.2. The leachate pH prior to contact with UO_2 or spent fuel is given in Table 2.3.

The pH of the simulated brine and basalt groundwaters changed only slightly during leaching, and radiation appeared to cause a slight pH decrease. Simulated tuff groundwater and deionized water both increased in pH as a result of interaction with UO_2 or spent fuel. For the deionized water leachate, the pH increase was greater in the presence of radiation (Experiments No. 2 and No. 3).

Table 3.2. Average pH measurements in each leachate and environment.

Leachate	Nonradiated Environment pH Mean[a]	Radiated Environment pH Mean[b]	Spent Fuel Environment pH Mean[c]
Brine	6.6 (6.5 to 6.7)[d]	6.3 (6.2 to 6.4)	6.1 (6.0 to 6.2)
Tuff	8.7 (8.5 to 8.9)	8.9 (8.8 to 9.0)	8.7 (8.3 to 9.1)
Basalt	9.7 (9.6 to 9.8)	9.6 (9.5 to 9.7)	9.4 (9.3 to 9.5)
Deionized H_2O	7.3 (6.6 to 8.0)	8.6 (8.4 to 8.8)	9.0 (8.5 to 9.5)

[a]Experiment No. 1.
[b]Experiment No. 2.
[c]Experiment No. 3.
[d]95-percent confidence intervals in parentheses.

3.2 Leach Data

The radionuclide release results from the three leaching experiments are presented below. Uranium was the only analyte in the unirradiated UO_2 leach tests. The radionuclides analyzed in the spent fuel leachates included cesium-134 and -137, iodine-129, strontium-90, americium-241, curium-244, and plutonium-238, -239, and -240, in addition to total uranium. Some surface characteristics of the leached unirradiated UO_2 pellets are shown and evaluated in Section 3.3. The surface characteristics of the leached spent fuel specimens were not examined.

Raw radionuclide concentration data are tabulated in Appendix C. The radionuclide concentrations versus time are shown in Figures 3.1 through 3.22. In these figures, the concentrations have been averaged for replicate reaction vessels (see Tables 2.1 and 2.2). Circles represent brine data, triangles represent tuff, squares represent basalt, and stars represent deionized water. Radionuclide distributions at 12.1 and 12.4 years after removal from the reactor were estimated for the spent fuel used in Experiment No. 3, based on its burn-up history using an ORIGEN code calculation. These distributions are tabulated for the radionuclides analyzed in these leachates in Appendix A (Table A.1). The ORIGEN code calculations are helpful in evaluating leaching mechanisms, which are the subject of Chapter 4. Radionuclide concentration trends with time and the influences of leachate composition and S/V are discussed.

3.2.1 Uranium

3.2.1.1 Unirradiated UO_2, No External Radiation Field

Total uranium concentrations range from approximately 10 to 150 µg/L, most falling in the range of 20 to 50 µg/L (Table C.1). Increasing the S/V ratio by a factor of 10 did not significantly increase the concentration of uranium (Figure 3.1). Also, uranium concentrations were fairly uniform over time and were not significantly affected by leachate composition.

3.2.1.2 Unirradiated UO_2, External Radiation Field

Uranium concentrations for the tuff and basalt ground waters (Figure 3.2) were analogous to those observed when there was no external radiation field (Figure 3.1). Some elevated uranium concentrations in the deionized water and brine leachates in the S/V = 5 m^{-1} experiments were observed (Figure 3.2b) but showed no apparent trend over time. The most notable results are some very elevated uranium concentrations in the high S/V brine leachates at days 126, 156, 182 and 238. The peak at days 156 and 182 was followed by a return to ambient concentrations at day 213, then was followed by another increase. Both of the increases as well as the decrease at day 213 were observed in both high S/V reaction vessels, Nos. 4 and 5 (Table C.2). These data have been confirmed by numerous replicate analyses of the same leachates and cannot be the result of analytical interference or be an artifact. Unfortunately, the experiment had to be discontinued at day 238; thus, continued collection of data was impossible. This anomalous behavior of uranium in brines exposed to radiation is discussed further in Section 4.1.

3.2.1.3 Spent Fuel Uranium

In brine, uranium concentrations in the higher S/V experiments were approximately two to four times higher than those observed in the low S/V experiments (Figure 3.3a). In tuff and basalt, high S/V uranium concentrations started high (~0.4 to 0.5 mg/L) and decreased to about the value of the low S/V experiments (~0.03 to 0.04 mg/L) by the conclusion of the experiment at day 146 (Figures 3.3b, c). Uranium concentrations were especially high at the first sampling point in the deionized water leachate (Figure 3.4b). The strong leachate composition effect early in the experiments gradually disappeared, and by the conclusion of the experiment uranium concentrations in all four leachates at both S/V ratios were within approximately a factor of two (Figure 3.4). By far the dominant isotope (by more than 99 percent) of uranium in spent fuel is uranium-238, followed by -235, -236, and -234 (as shown in Table A.1). The analyses discussed above reflect total uranium concentrations and did not discriminate between isotopes. The analyses discussed in the following sections do apply to specific isotopes.

3.2.2 Cesium

Two isotopes of cesium, cesium-137 (half-life 30 years) and -134 (half-life 3.1 years) were quantitated in the leachates. Cesium-134 is present in only minor amounts (Table A.1), but is easily quantitated because of its distinct gamma spectrum. The spent fuel also contains significant amounts of stable

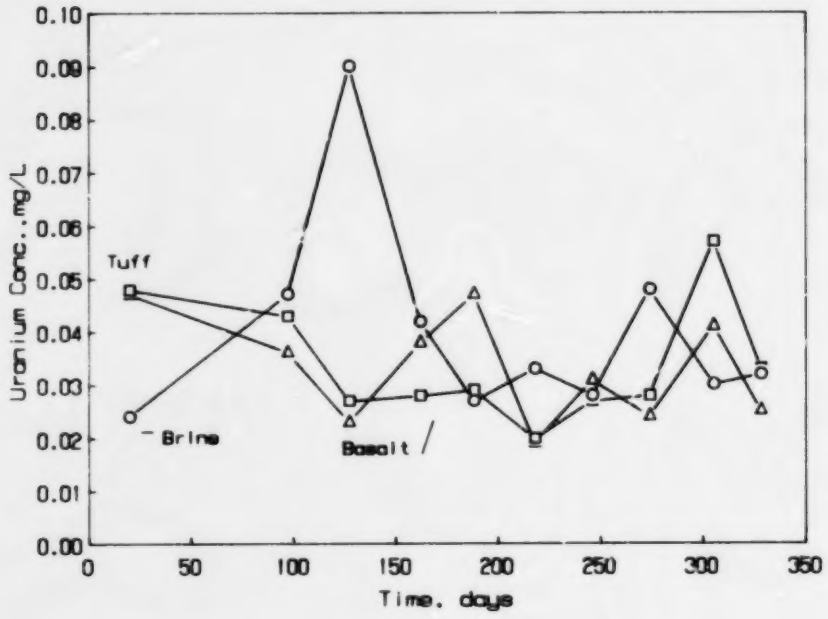

(a)

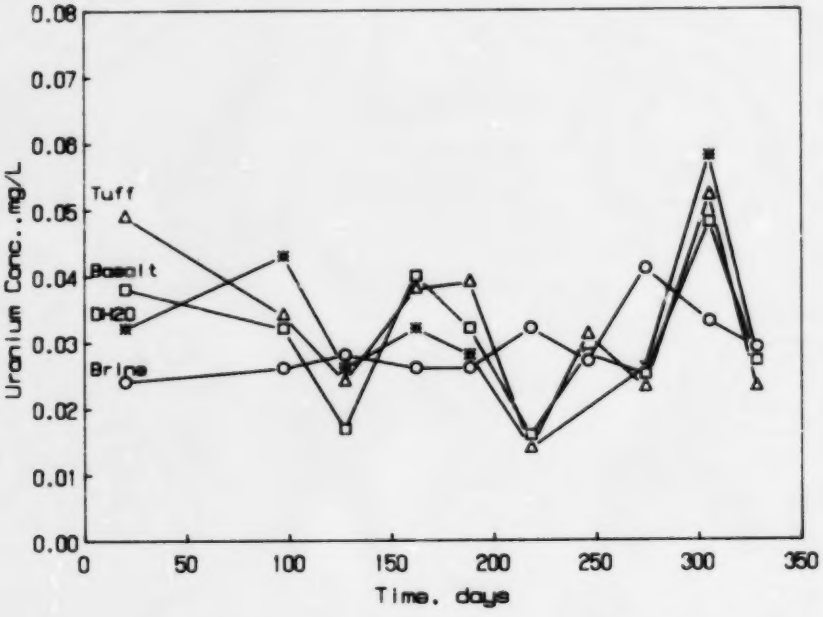

(b)

Figure 3.1. Average uranium concentrations vs. time for all leachates, unirradiated UO_2, no external radiation field, with (a) S/V = 50 m^{-1} and (b) S/V = 5 m^{-1}.

BEST COPY AVAILABLE

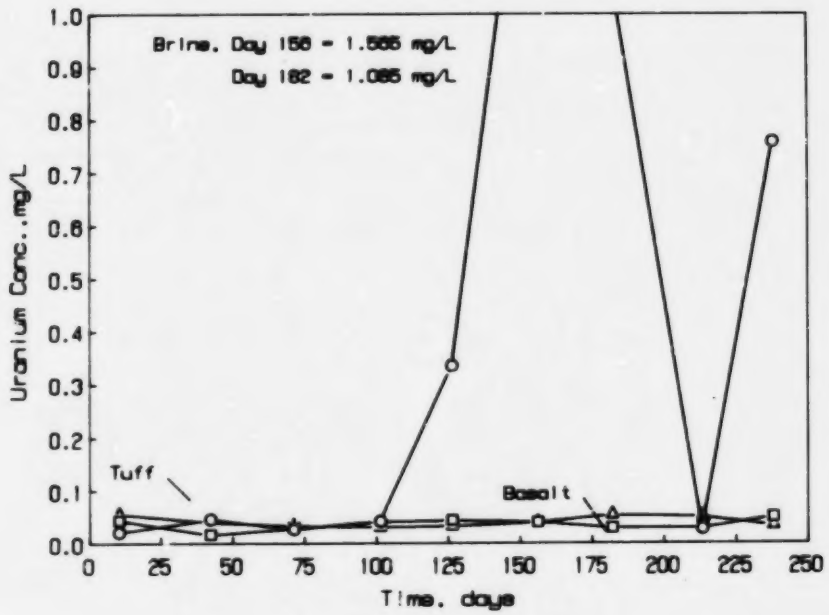

(a)

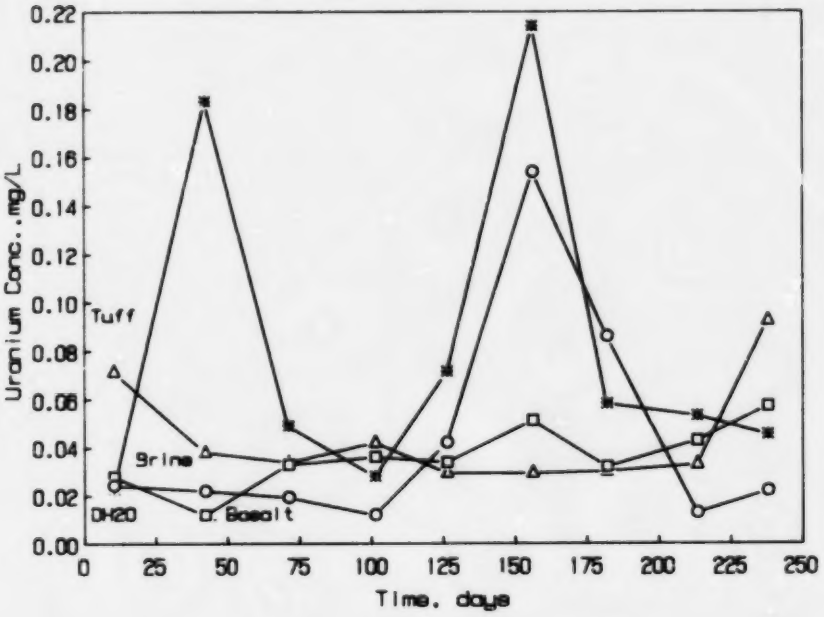

(b)

Figure 3.2. Average uranium concentrations vs. time, all leachates, unirradiated UO_2, external gamma radiation field ~3 x 10^3 rad/hour, (a) S/V = 50 m^{-1}; (b) S/V = 5 m^{-1}.

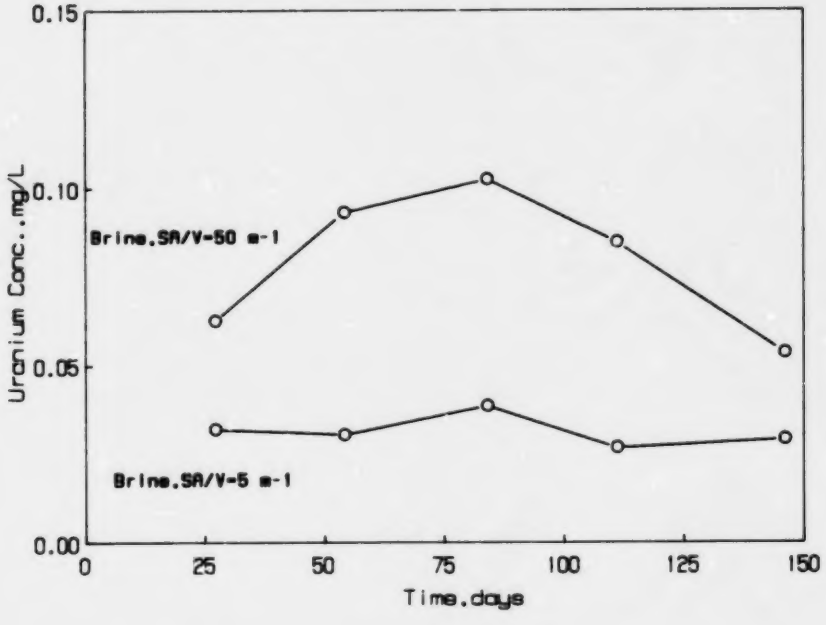

(a)

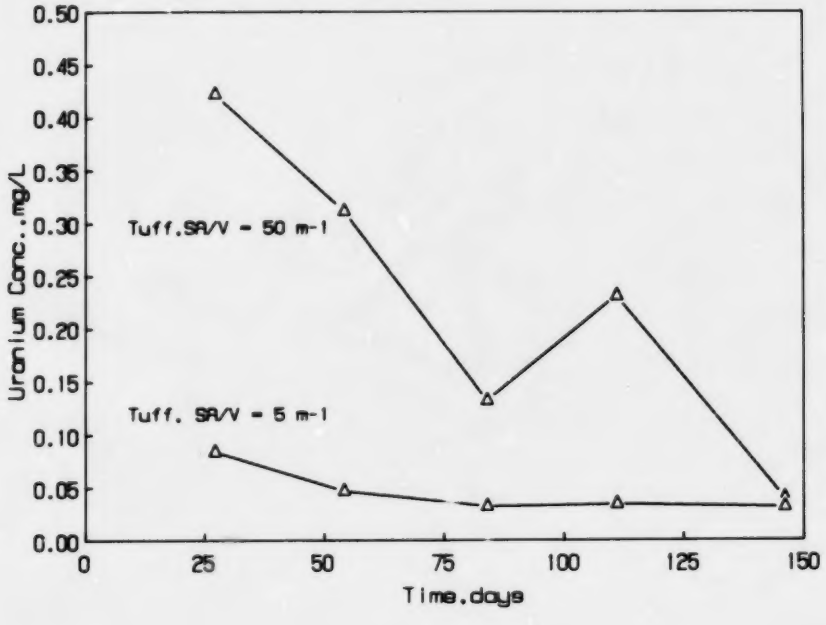

(b)

Figure 3.3. Average uranium concentrations vs. time, both S/V ratios, spent fuel test in (a) brine; (b) tuff; and, (c) basalt groundwater leachates.

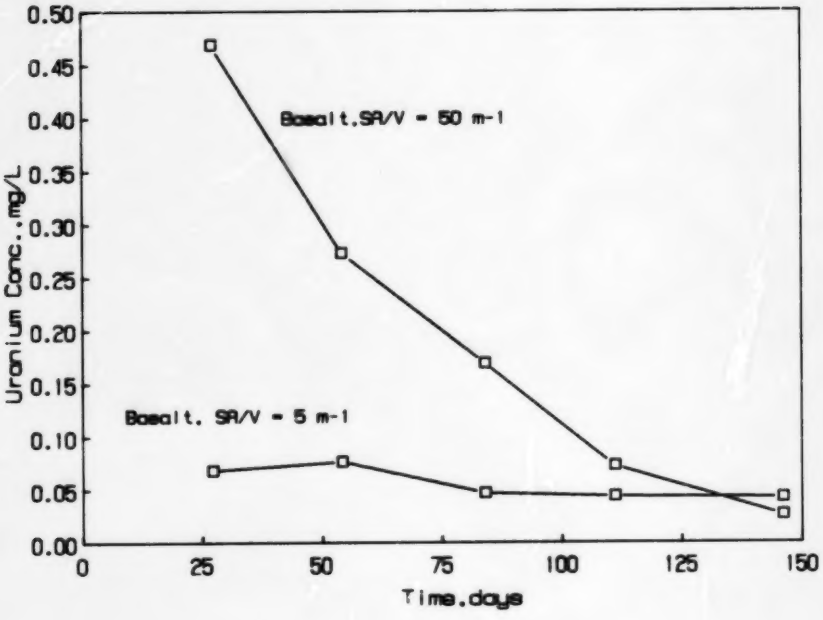

(c)

Figure 3.3. Continued.

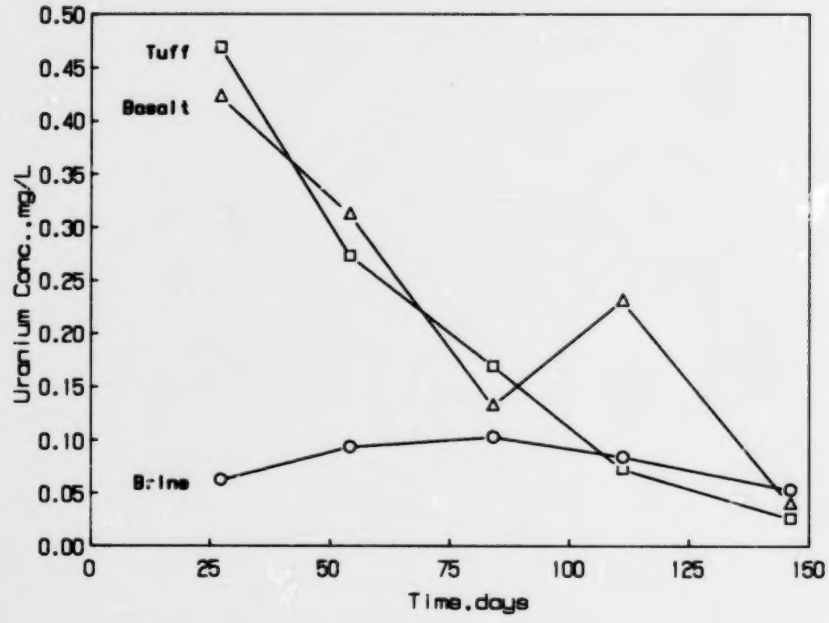

(a)

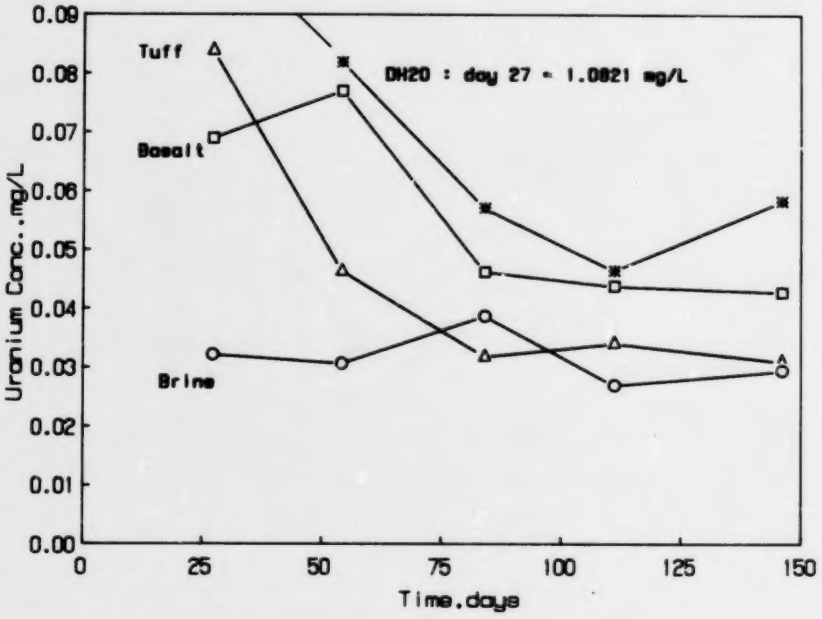

(b)

Figure 3.4. Average uranium concentrations vs. time, all leachates, spent fuel test, (a) S/V = 50 m^{-1}, (b) S/V = 5 m^{-1}.

cesium-133 and long-lived cesium-135 (half-life 2 x 10^6 years, see Table A.1). The chemical behavior of cesium-135 is undoubtedly analogous to that of its shorter-lived counterparts.

Cesium-137 concentrations ranged from approximately 3.0 to 4.4 mg/L at the onset of the high S/V experiments to 1.7 to 2.6 mg/L at their conclusion. Lowering the S/V ratio to 5 m^{-1} resulted in a cesium-137 concentration reduced by approximately a factor of 10 (Figure 3.5 and Table C.4). The decrease in concentration of cesium-137 during the course of the experiment reflects the dilution that occurs during sampling. As discussed in Section 2.1.3, approximately 10 to 15 percent of spent leachate is collected by introducing an equivalent volume of fresh leachate at each sampling. From the data in Figure 3.5, it appears that cesium leaches rapidly (or at least some component of the total cesium in the fuel leaches very rapidly), and that the leach rate of cesium subsequent to the first sampling at day 27 is negligible compared to the removal rate of cesium from the reaction vessel during sampling. Had the experiment continued for an additional several hundred days, and the trend continued, the concentration of cesium in both the higher and lower S/V experiments would have asymptotically approached zero. The release behavior of cesium is discussed further in Section 4.2. Leachate compositional effects on cesium-137 dissolution are minor (Figure 3.6). The behavior of cesium-134 basically paralleled that of cesium-137 (Figures 3.7 and 3.8).

3.2.3 Iodine

The results for iodine-129 (half-life 1.6 x 10^7 years) are plotted in Figures 3.9 and 3.10. Spent fuel also contains a small amount of stable iodine-127 (Table A.1). The behavior of iodine is similar to that of cesium; that is, a strong S/V effect and rapid leaching followed by subsequent dilution (Figure 3.9). The dilution curves are not as well defined as those for cesium (Figures 3.5 through 3.8), and this is attributed to the experimental and statistical error associated with the iodine-129 analysis as compared with the radiocesium analyses. The two isotopes of cesium were easily quantitated because of the activity of the isotopes and the ease of analysis. The activity of iodine-129 was represented by only a few tens or hundreds of disintegrations per minute. Associated counting statistics were not nearly as good as for the isotopes of cesium. There is a slight indication of a leachate compositional effect, with the total iodine-129 release in brine being greater than that in tuff or deionized water, which in turn was greater than that in basalt water.

3.2.4 Strontium

The release behavior of strontium-90 (half-life 28 years) over time is shown in Figures 3.11 and 3.12. Spent fuel also contains a small amount of stable strontium-88 (Table A.1). Because of its relatively short half-life, it is unlikely that Sr-90 will be an issue of concern during licensing; however, it may be a good analogue for the longer-lived isotopes of radium. Similar to cesium and iodine, strontium release was nearly proportional to S/V (Figure 3.11). However, unlike results for cesium and iodine, a very strong leachate compositional effect was also observed (Figure 3.12). Comparison

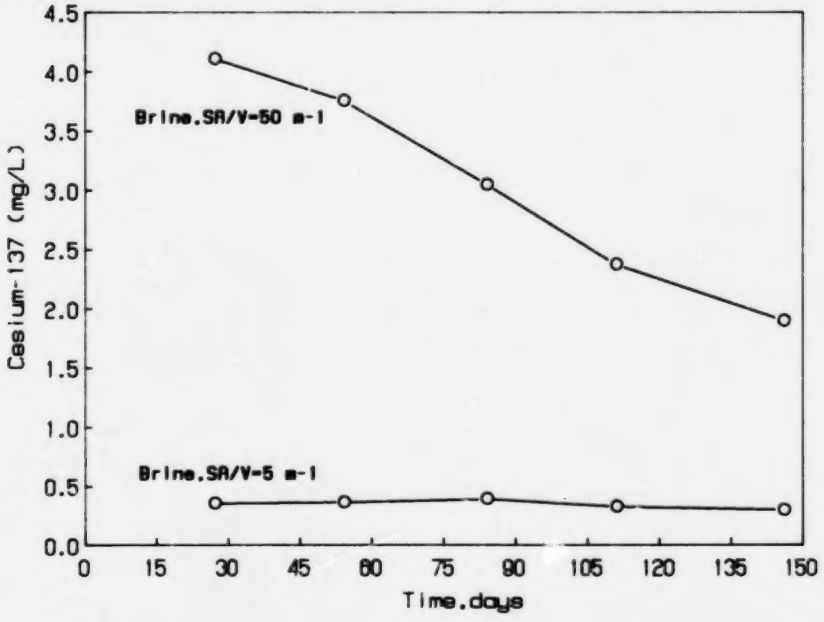

(a)

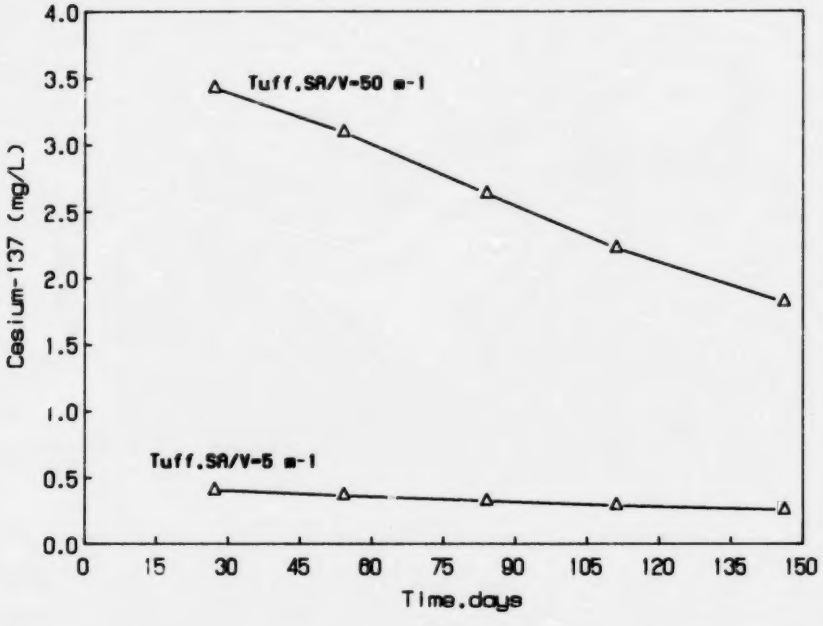

(b)

Figure 3.5. Average cesium-137 concentrations vs. time, both S/V's in (a) brine, (b) tuff, and (c) basalt groundwater leachates.

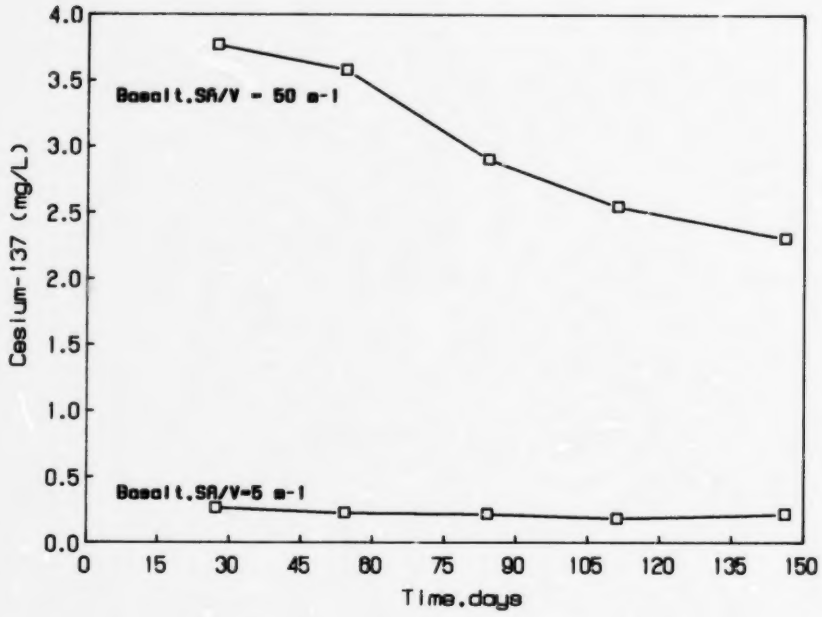

(c)

Figure 3.5. Continued.

27

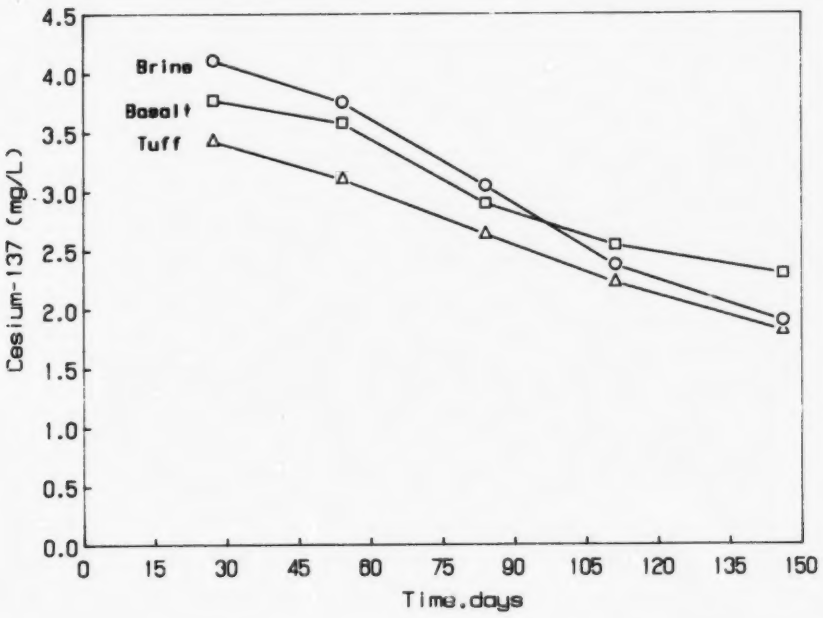

(a)

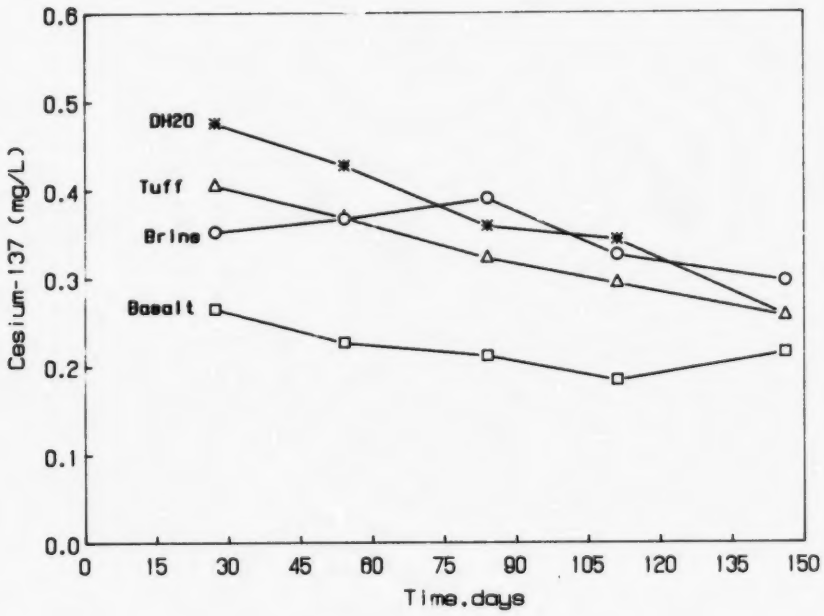

(b)

Figure 3.6. Average cesium-137 concentrations vs. time, all leachates, (a) S/V = 50 m^{-1}, (b) S/V = 5 m^{-1}.

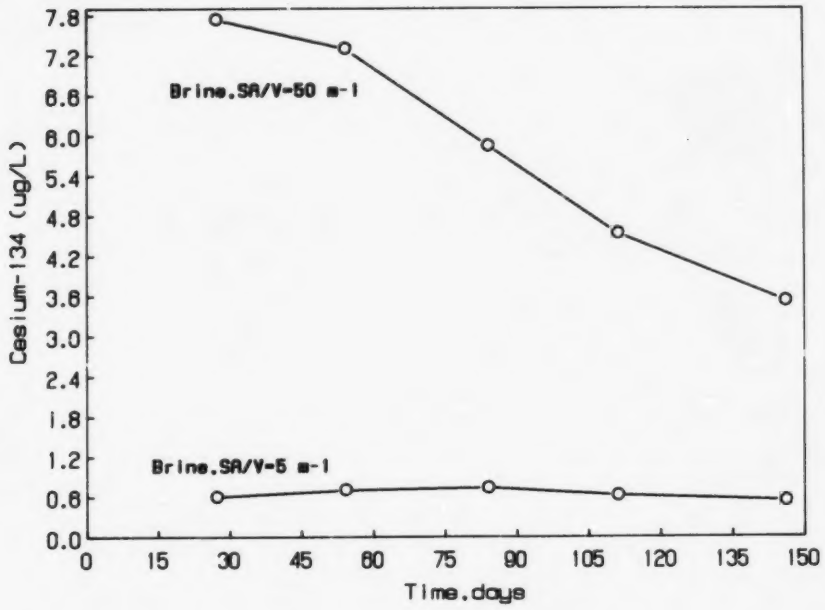

(a)

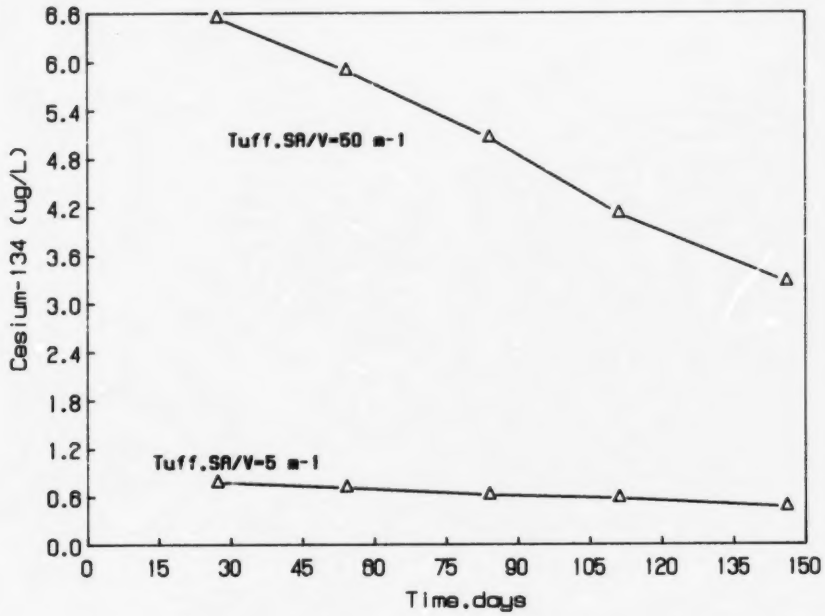

(b)

Figure 3.7. Average cesium-134 concentrations vs. time, both S/V's in (a) brine, (b) tuff, and (c) basalt groundwater leachates.

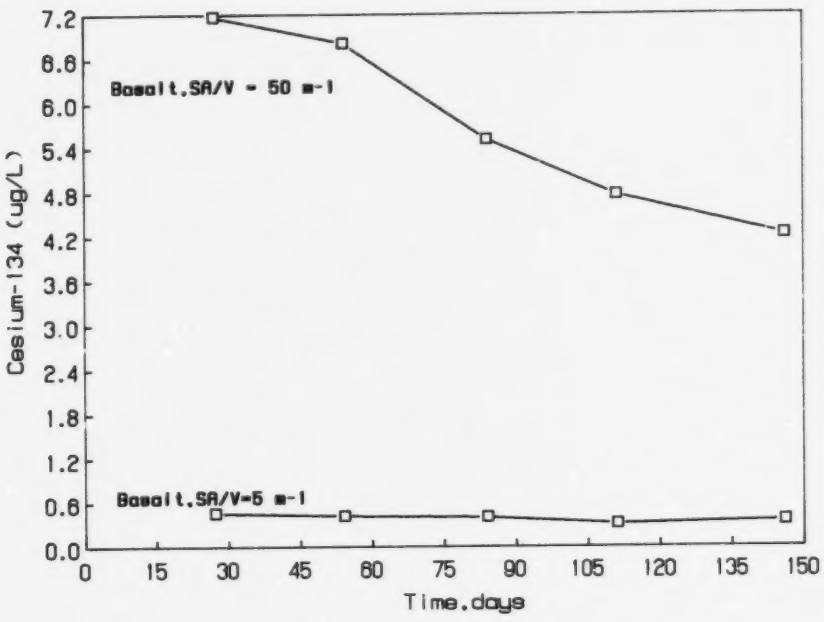

(c)

Figure 3.7. Continued.

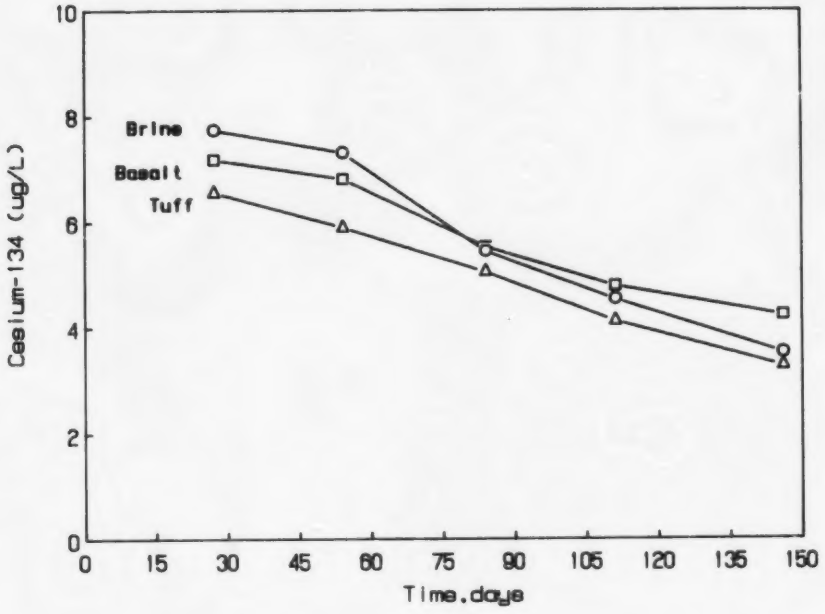

(a)

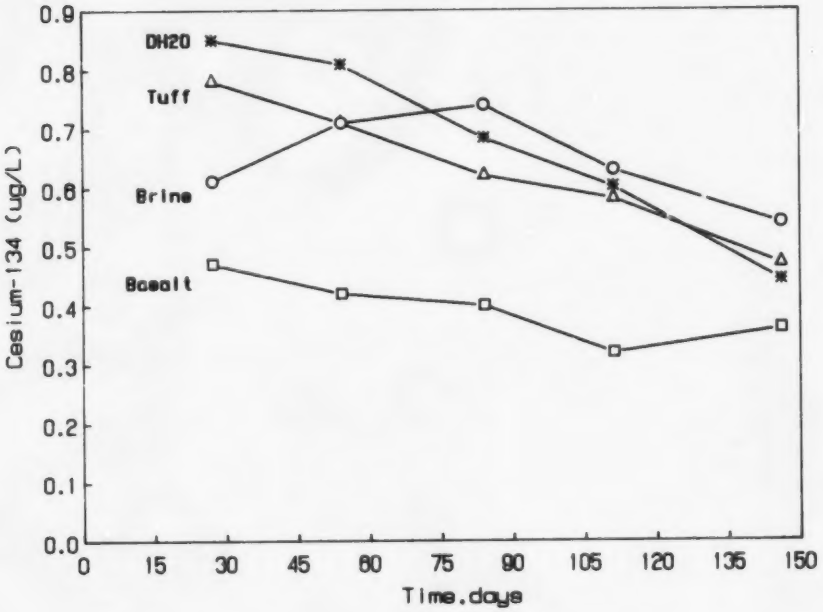

(b)

Figure 3.8. Average cesium-134 concentrations vs. time, all leachates, (a) S/V = 50 m^{-1}, (b) S/V = 5 m^{-1}.

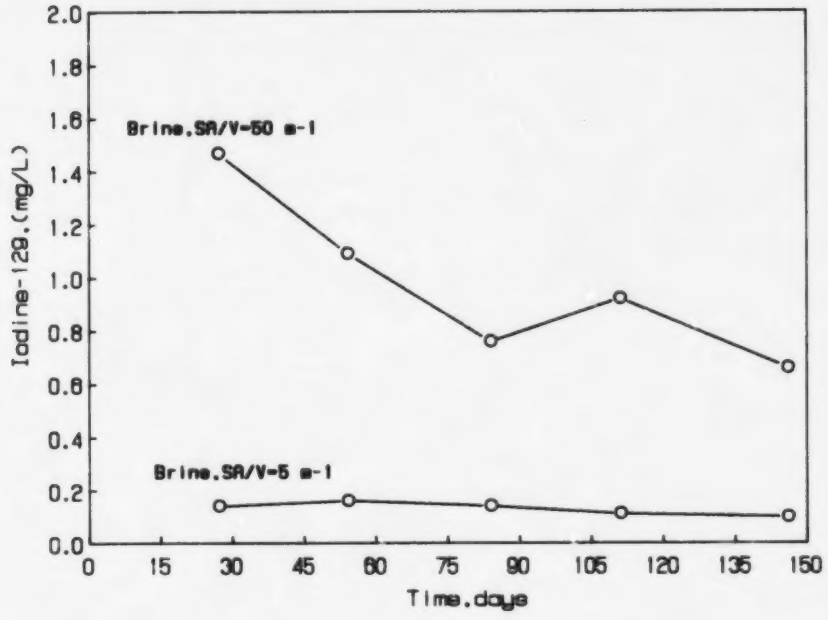

(a)

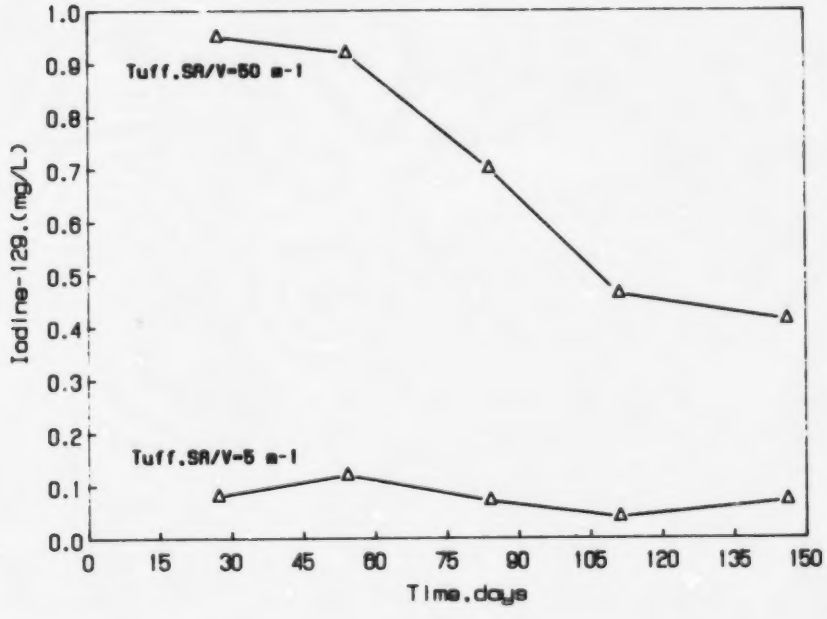

(b)

Figure 3.9. Average iodine-129 concentrations vs. time, both S/V's in (a) brine, (b) tuff, and (c) basalt groundwater leachates.

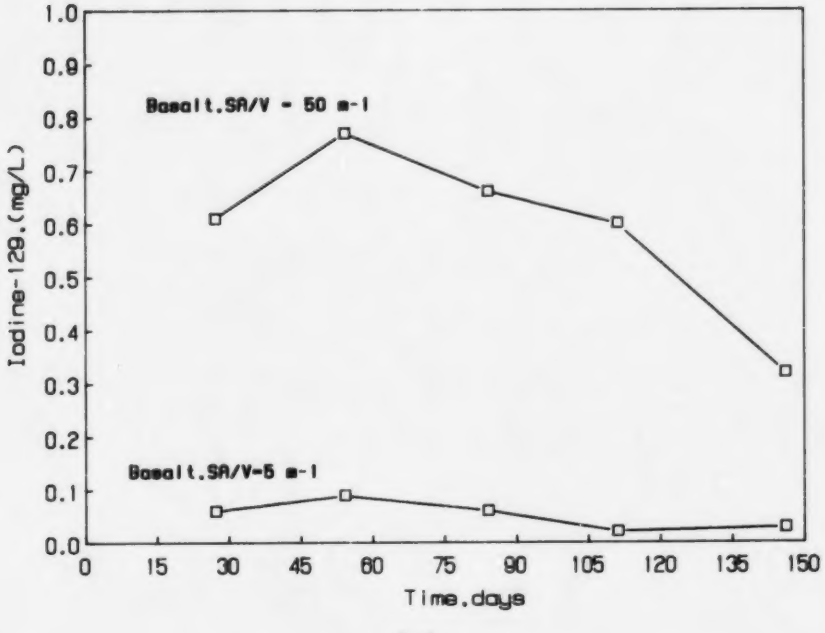

(c)

Figure 3.9. Continued.

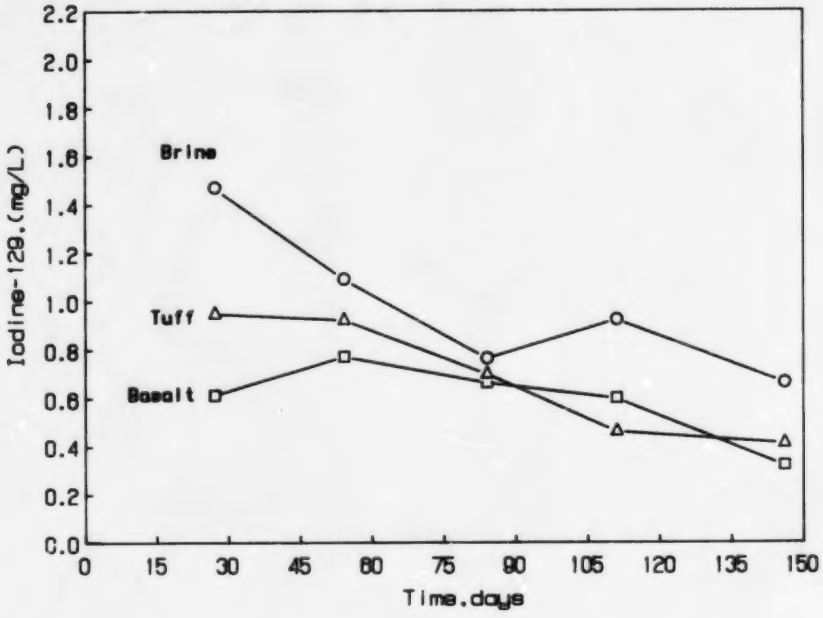

(a)

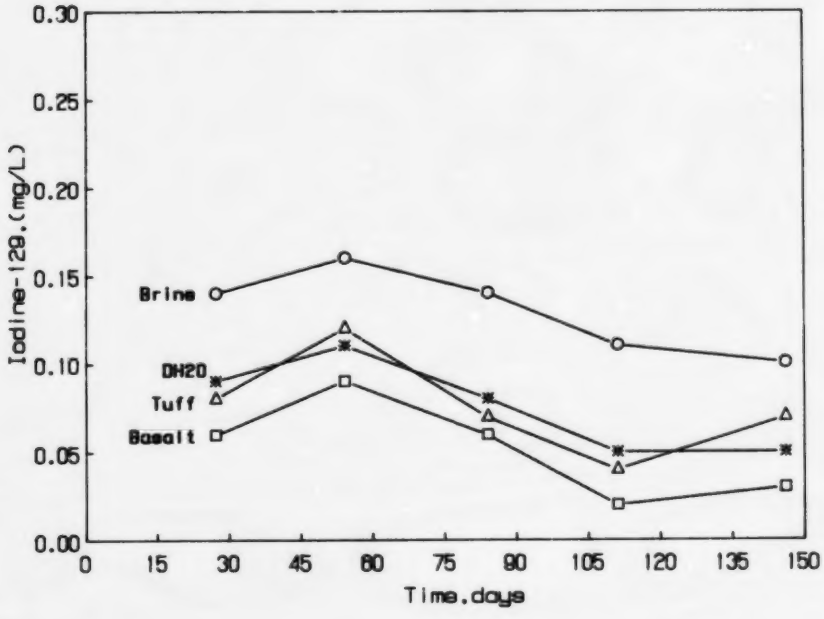

(b)

Figure 3.10. Average iodine-129 concentrations vs. time, all leachates, (a) S/V = 50 m^{-1}, (b) S/V = 5 m^{-1}.

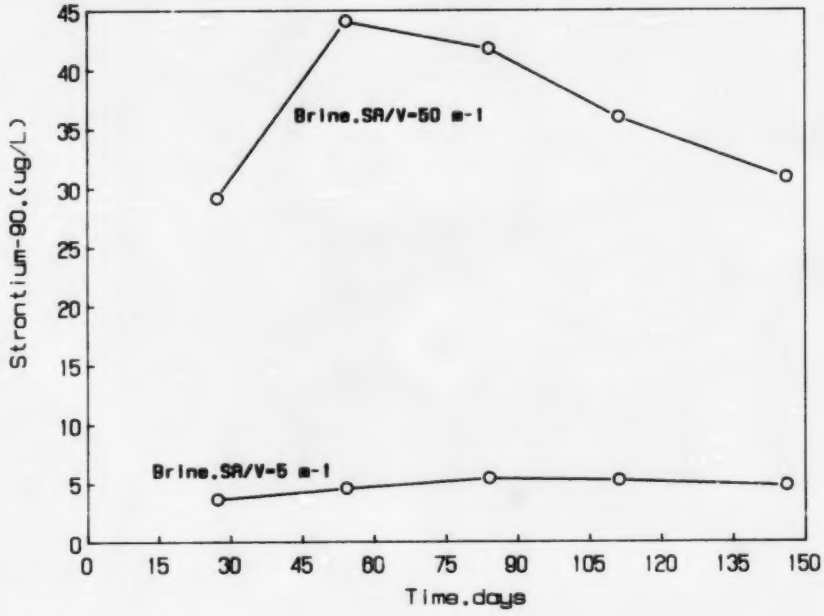

(a)

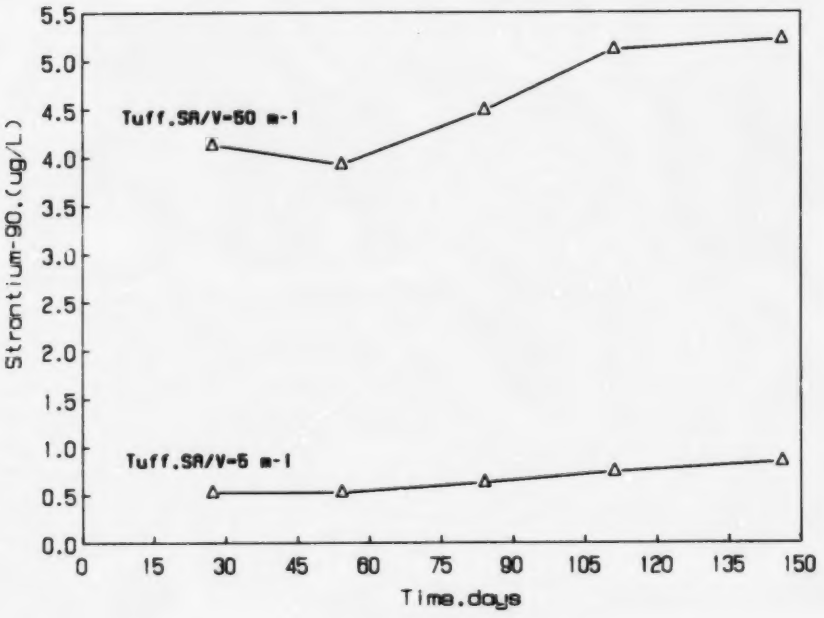

(b)

Figure 3.11. Average strontium-90 concentrations vs. time, both S/V's in (a) brine, (b) tuff, and (c) basalt groundwater leachates.

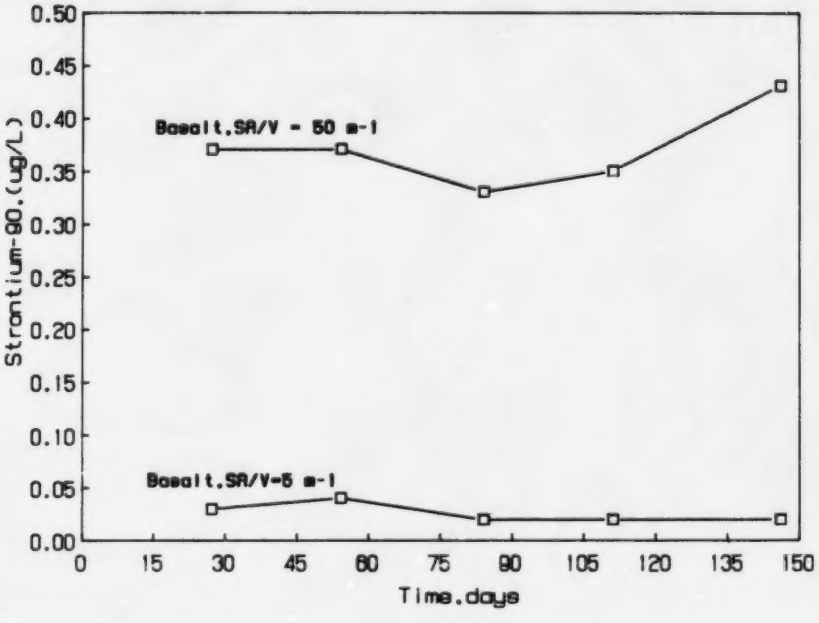

(c)

Figure 3.11. Continued.

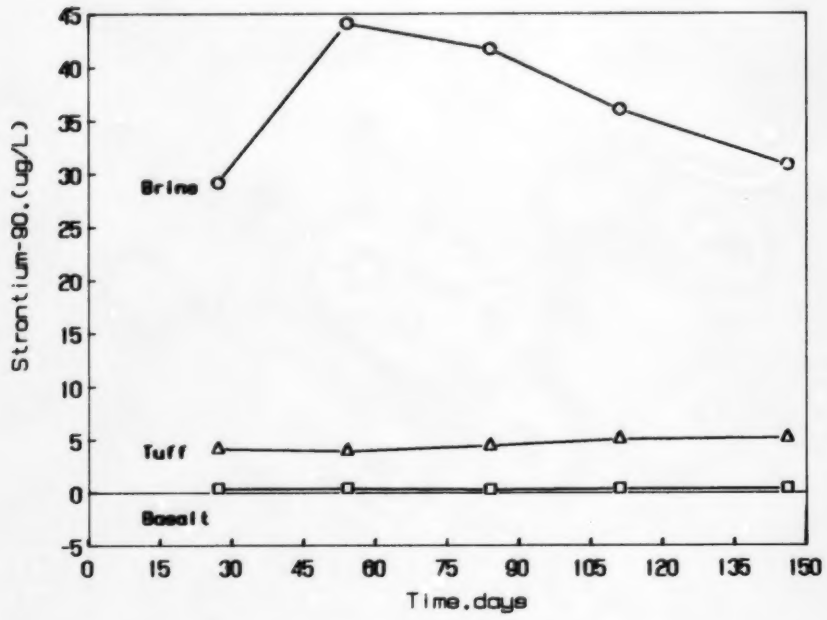

(a)

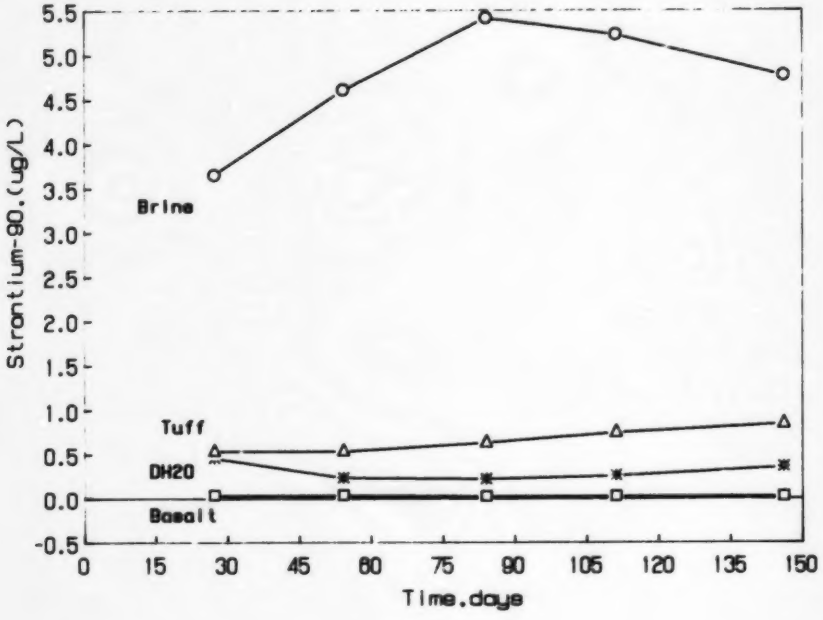

(b)

Figure 3.12. Average strontium-90 concentrations vs. time, all leachates, (a) S/V = 50 m^{-1}, (b) S/V = 5 m^{-1}.

of leachate compositions in Table 2.3 reveals that strontium-90 concentrations correlate only with pH, with higher releases occurring at lower pH. These two coexisting effects indicate a nonequilibrium situation because the leachate compositional effect (Figure 3.12) suggests that strontium-90 concentrations in the basalt, tuff, and deionized water leachates are suppressed by pH, while the S/V effect (Figure 3.11) implies that all three simulated groundwater leachates are undersaturated with respect to strontium. In fact, WIPP Brine A includes 5 mg/L strontium in its formulation (Table 2.3), hence it is unlikely that an additional 30 to 45 µg/L has caused this solution to saturate. If solubility control is absent, then the strong compositional effect in Figure 3.12 must be explained by kinetics.

The dilution curve concentration trends that were exhibited for cesium and iodine (Figures 3.5 to 3.10) are conspicuously absent for strontium. Considering that leachates are diluted by about 10 to 15 percent at sampling, the trends of increasing or nearly constant strontium concentrations over time (Figures 3.11 and 3.12) indicate continued strontium release during the almost 5-month experiments. Also, the release rates were higher in the first 27 days than during the last 119 days.

3.2.5 Americium

The two principal isotopes of americium in spent fuel are americium-241 (half-life 458 years) and americium-243 (half-life 7,650 years). Americium-241 is more easily measured because of its shorter half-life and higher concentrations in fuel within several thousand years after burn-up (Table A.1).

Americium-241 concentrations ranged up to only ~0.5 µg/L in the high S/V tuff and basalt leachates (Figures 3.13b,c). Initially, much higher americium concentrations in the high S/V experiments were followed by significant decreases over time, and by the conclusion of the 146-day test, the S/V effect had essentially vanished (Figure 3.13).

The leachate compositional effect over time was similar to that for S/V, that is, significant effect early in the experiment followed by rapid lessening, in fact almost disappearance, of the effect with time (Figure 3.14). The americium-241 concentration in synthetic brine was lower than that of the lower ionic strength leachates at the onset but nearly equal at the conclusion (Figure 3.14). Deionized water dissolved comparatively more americium-241 in the short-term, but most of that initially dissolved was lost from solution by day 54 (Figure 3.14b).

3.2.6 Curium

Curium-243 (half-life 28.5 years) and curium-244 (half-life 18.1 years) are analytically indistinguishable using alpha spectroscopy. The total curium concentrations in Figures 3.15 and 3.16 can be viewed as curium-244 because the curium-243/-244 ratio in this spent fuel is less than 0.005. Total curium concentrations in the fuel at 12.1 years after burnup are approximately 38 times lower than those of americium (Table A.1).

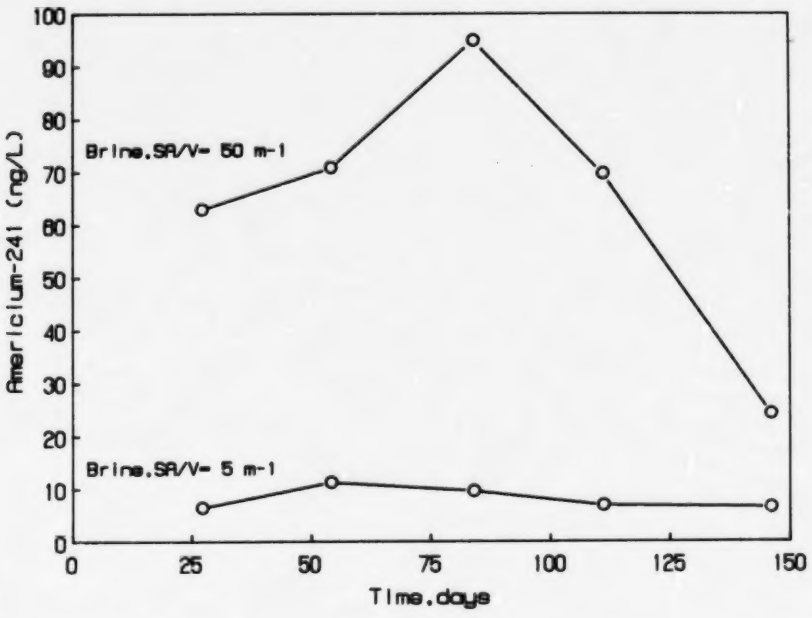

(a)

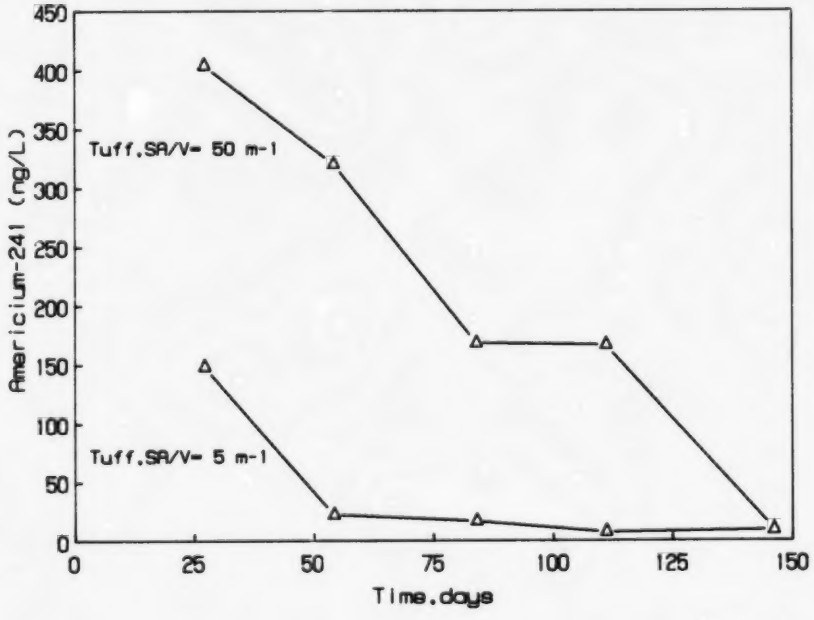

(b)

Figure 3.13. Average americium-241 concentrations vs. time, both S/V's in (a) brine, (b) tuff, and (c) basalt groundwater leachates.

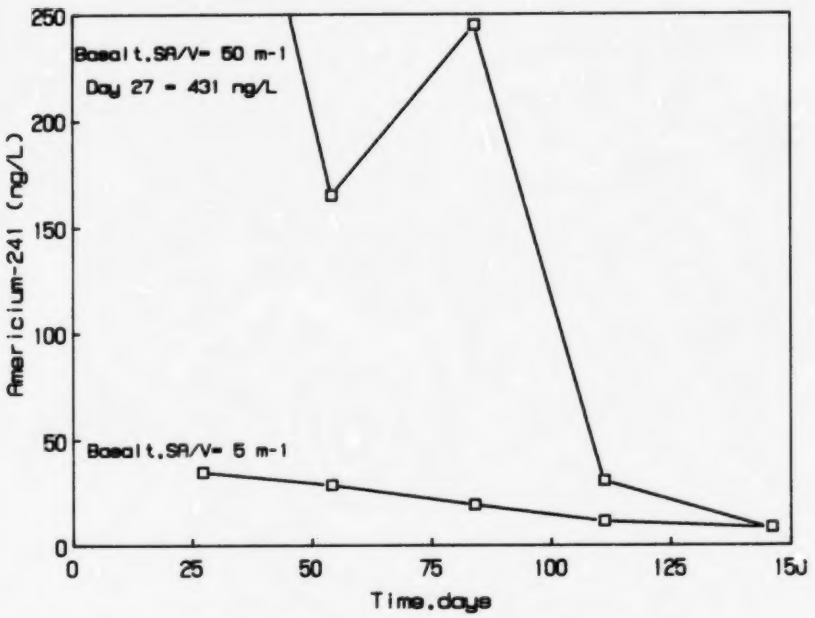

(c)

Figure 3.13. Continued.

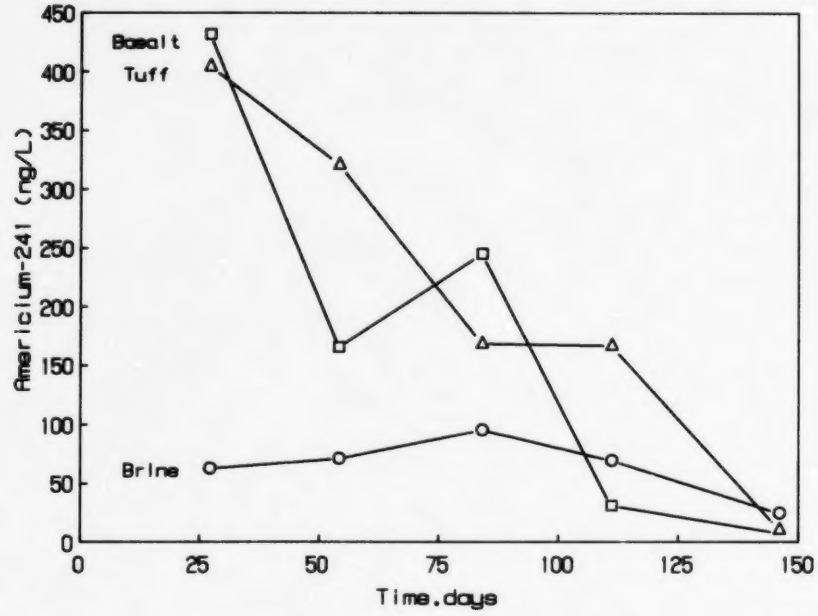

(a)

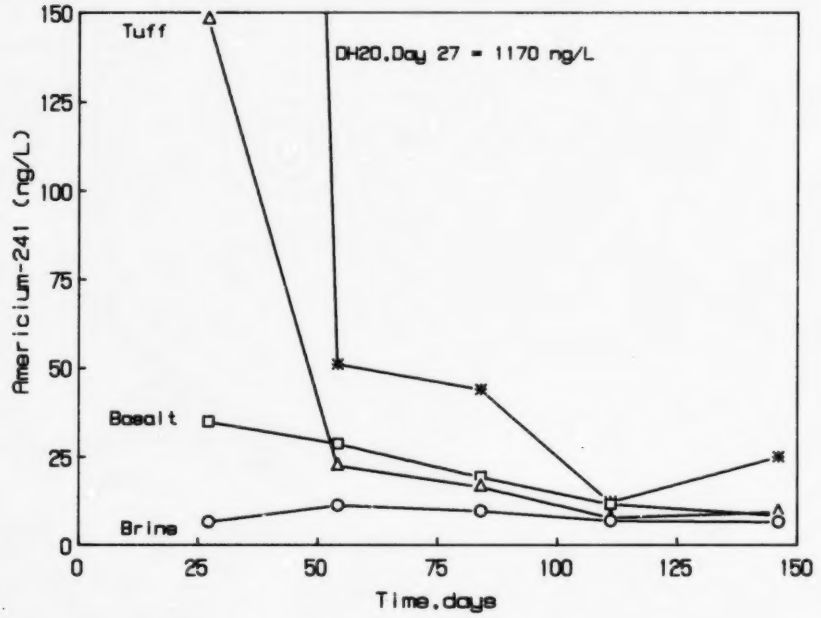

(b)

Figure 3.14. Average americium-241 concentrations vs. time, all leachates, (a) S/V = 50 m^{-1}, (b) S/V = 5 m^{-1}.

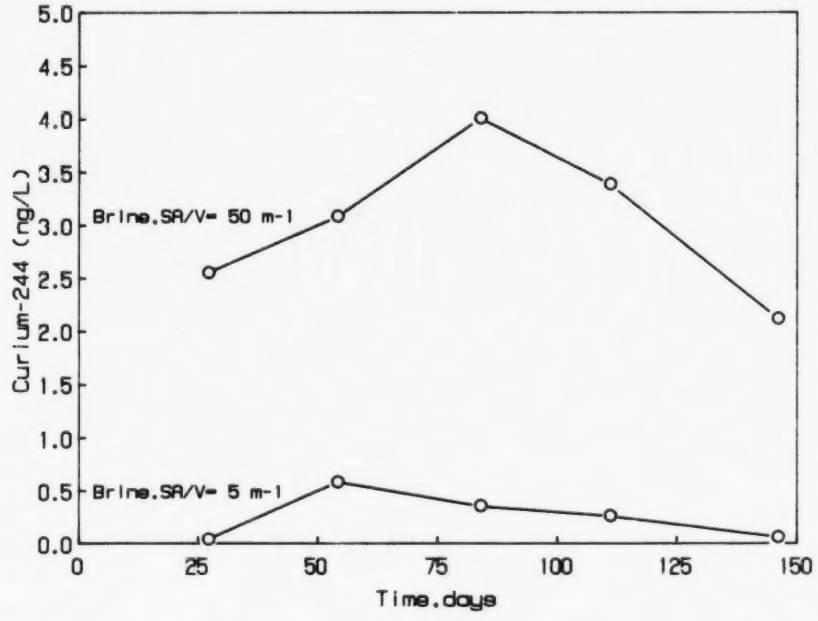

(a)

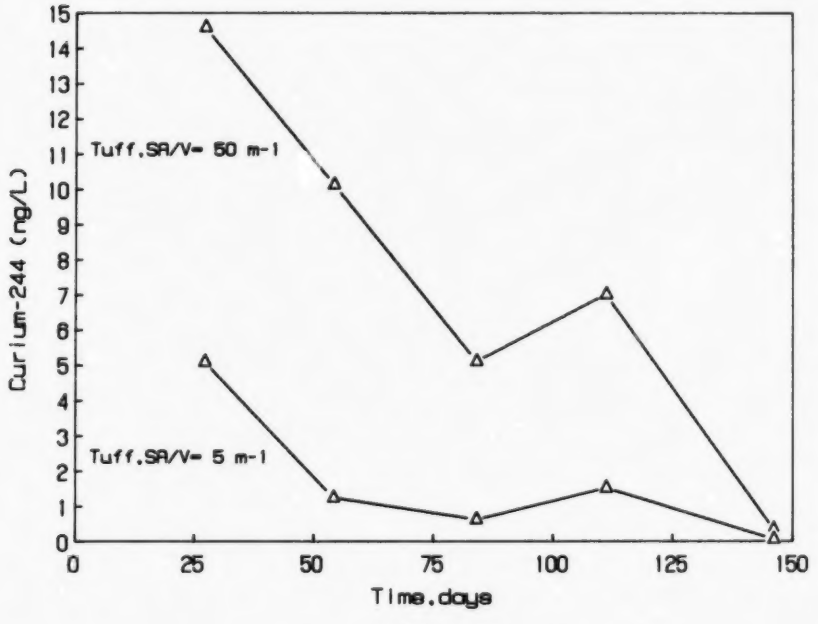

(b)

Figure 3.15. Average curium-244 concentrations vs. time, both S/V's in (a) brine, (b) tuff, and (c) basalt groundwater leachates.

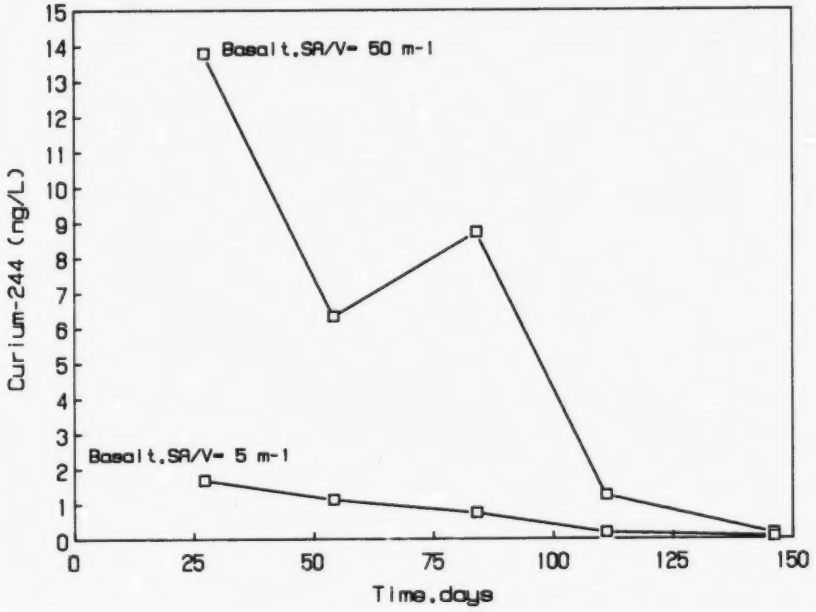

(c)

Figure 3.15. Continued.

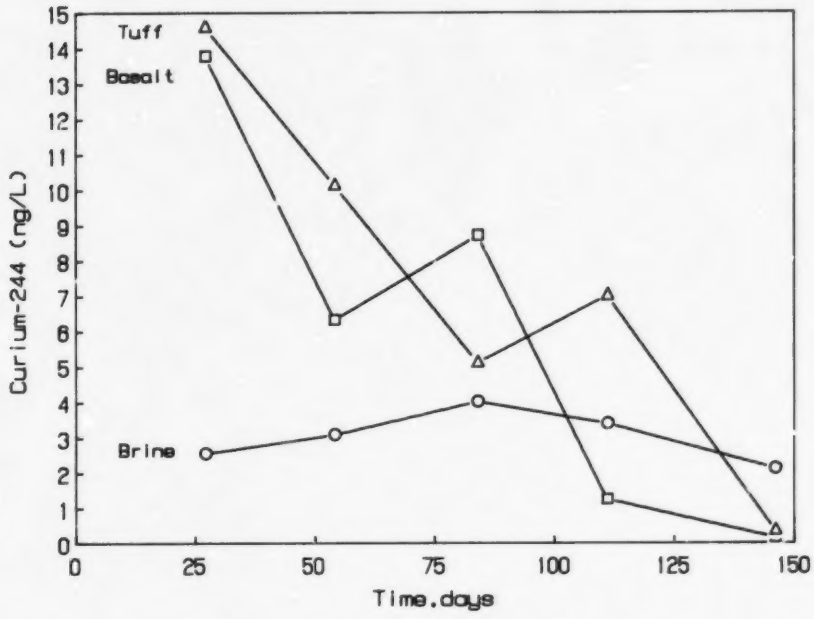

(a)

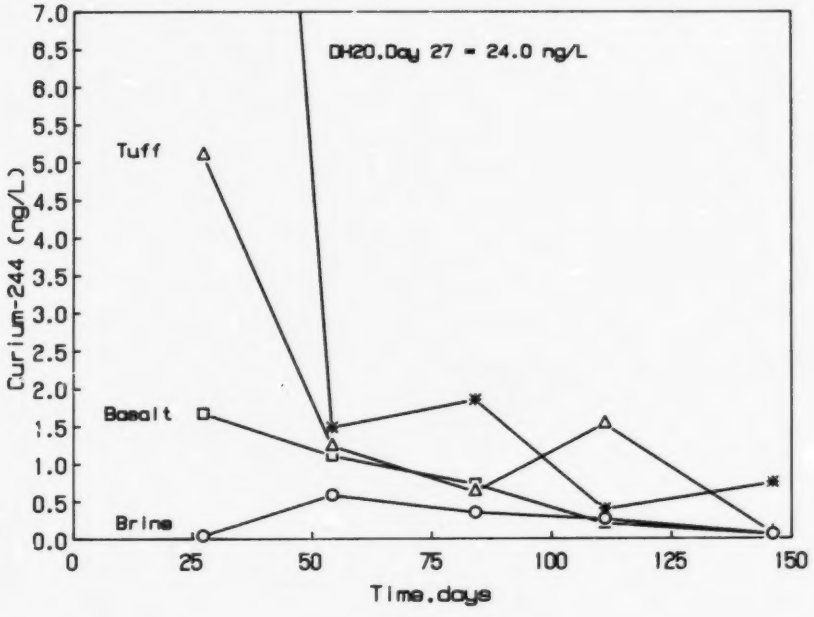

(b)

Figure 3.16. Average curium-244 concentrations vs. time, all leachates, (a) S/V = 50 m^{-1}, (b) S/V = 5 m^{-1}.

Curium behavior paralleled that of americium. Note that the highest curium-244 concentration observed was only 24 ng/L (day 27, deionized water leachate, Figure 3.16b); most values were in the range of 0 to 5 ng/L. The S/V effect was initially present for all three leachates but, by day 146, had disappeared for tuff and basalt groundwater (Figure 3.15). A significant leachate compositional effect (deionized water > tuff and basalt > brine) was apparent only early in the experiments and largely vanished by the conclusion (Figure 3.16).

3.2.7 Plutonium

Five isotopes of plutonium are present in spent fuel, with atomic weights ranging from 238 to 242. Three were quantitated in the leachate from these experiments: plutonium-238 (half-life 89 years), plutonium-239 (half-life 24,360 years), and plutonium-240 (half-life 6,760 years). The latter two are indistinguishable based on alpha spectroscopy, but these were quantitated by gross alpha counts for their corresponding alpha particle energy level and their 12.1-year elemental ratios, according to the ORIGEN code calculation (Table A.1). Plutonium-241 has a relatively short half-life (13 years) and thus is not a concern with respect to the long-term isolation of radioactive waste. Plutonium-242 has a very long half-life (3.79×10^5 years), and its chemical behavior is presumably analogous to that of the other plutonium isotopes. It is reassuring that the temporal concentration trends of plutonium-238 and plutonium-239/-240, measured by independent analytical techniques, are nearly identical (Figures 3.17 through 3.22). It is principally their concentrations that differ; for example, the ORIGEN code predicts a 38:1 ratio of plutonium-239 to plutonium-238 at 12.1 years after burn-up (see Table A.1).

Concentration trends for plutonium are very similar to those of the other actinides, uranium, americium, and curium. The major trends are: (a) a strong S/V effect for the brine leachates which is apparent throughout the 146-day test (Figures 3.17a, 3.19a, and 3.21a); (b) an initially strong S/V effect for tuff and basalt leachates which disappears by day 146, the plutonium concentrations in the high S/V experiments having decreased to the values observed in the low S/V experiments (Figures 3.17b,c; 3.19 b,c; and 3.21 b,c); and (c) a strong leachate compositional effect early in the experiment (deionized water > tuff ~ basalt > brine), which is gone by day 146 (Figures 3.18, 3.20, and 3.22). The only anomaly in the data for plutonium, relative to the other actinides, are some systematically elevated day-111 values for the tuff leachate. Day-146 values for the same reaction vessels have returned to the low levels expected based on analogy with the other actinides.

Based on ORIGEN code extrapolations of the plutonium-239 data, the highest total plutonium (isotopes-238 through -242) concentration observed was at day 27 for the deionized water leachate and was approximately 6.8 µg/L (Figure 3.20b). For tuff and basalt the highest total plutonium concentrations were also observed at day 27, that is, 2.8 and 2.3 µg/L, respectively (Figure 3.19b, c). Total plutonium in the high S/V brine ranged from several tenths of a microgram per liter to 1 µg/L throughout the duration of the experiment.

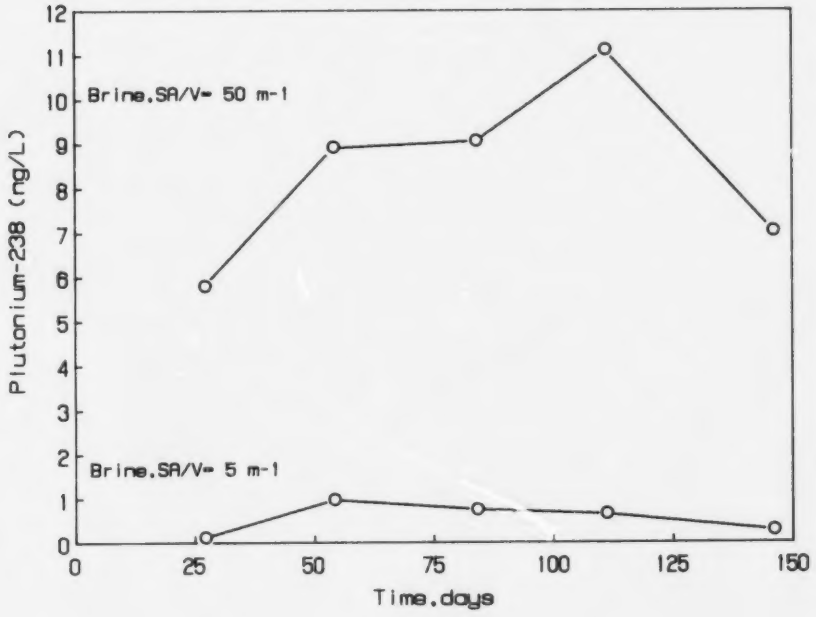

(a)

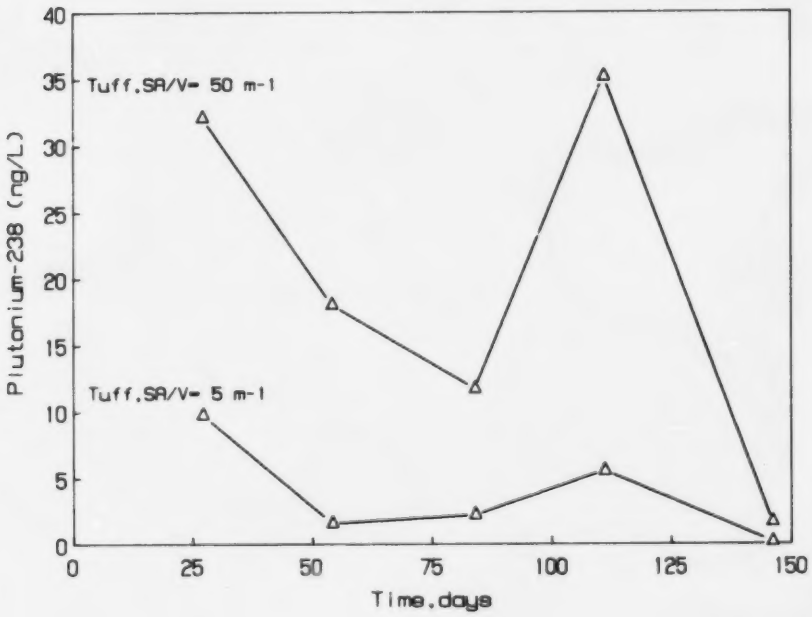

(b)

Figure 3.17. Average plutonium-238 concentrations vs. time, both S/V's in (a) brine, (b) tuff, and (c) basalt groundwater leachates.

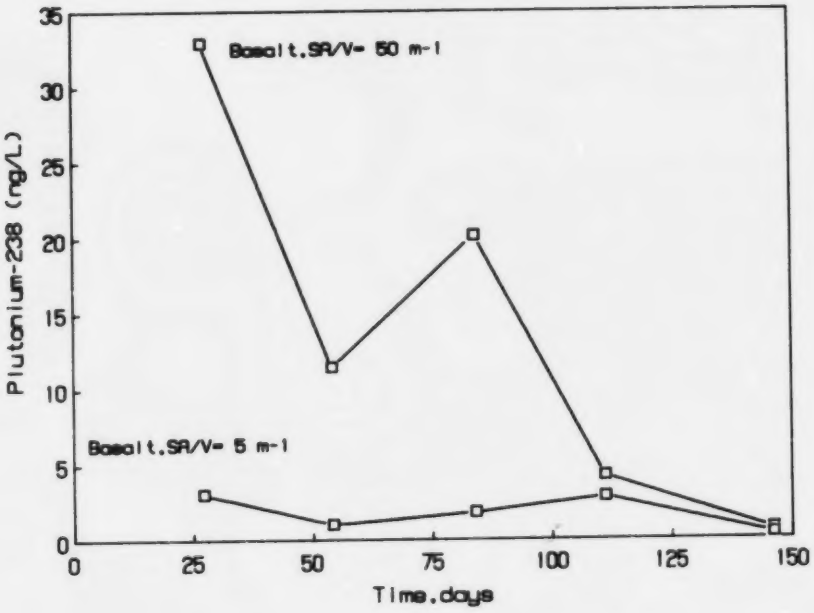

(c)

Figure 3.17. Continued.

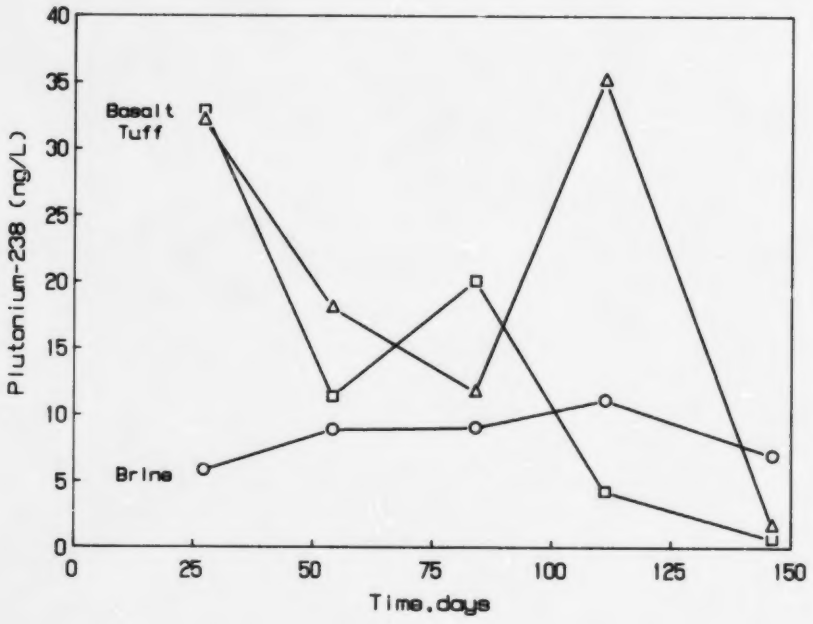

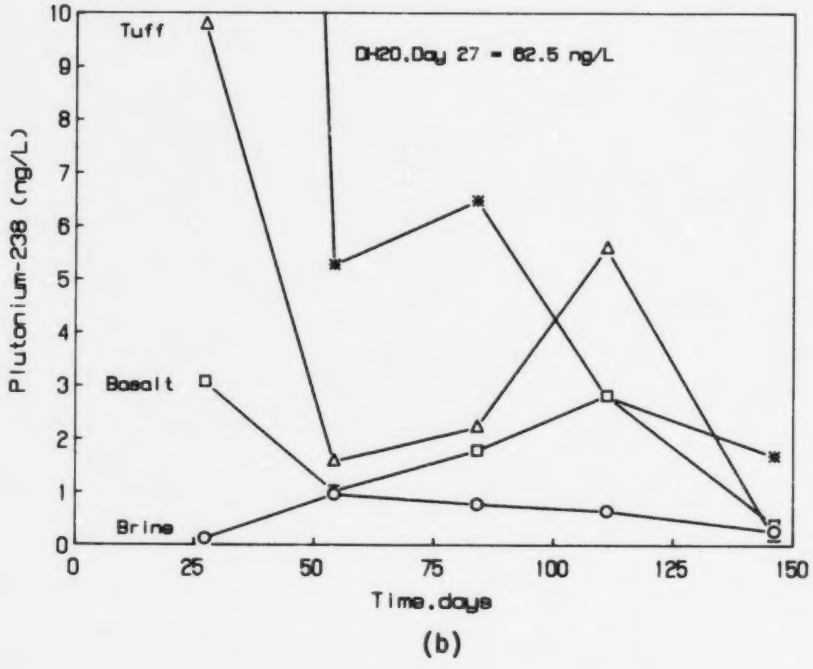

Figure 3.18. Average plutonium-238 concentrations vs. time, all leachates, (a) S/V = 50 m^{-1}, (b) S/V = 5 m^{-1}.

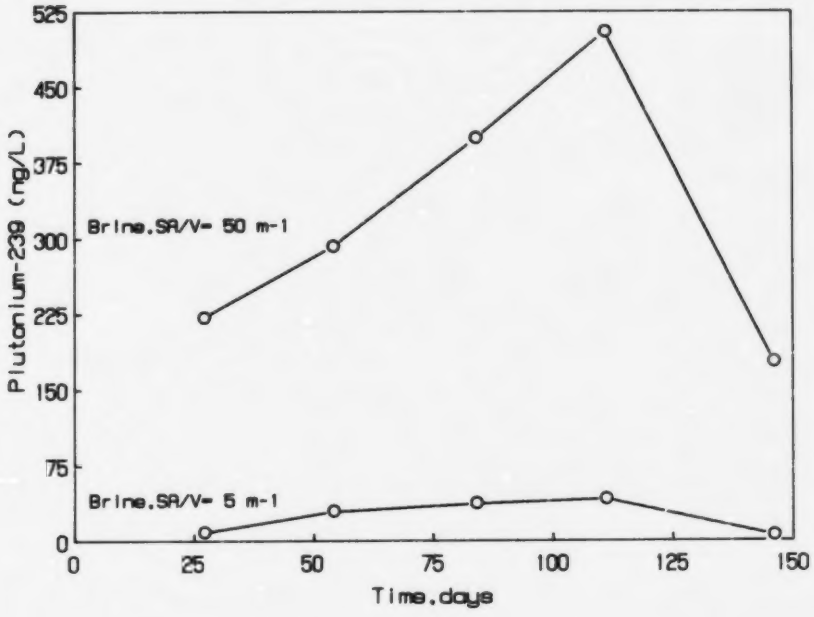

(a)

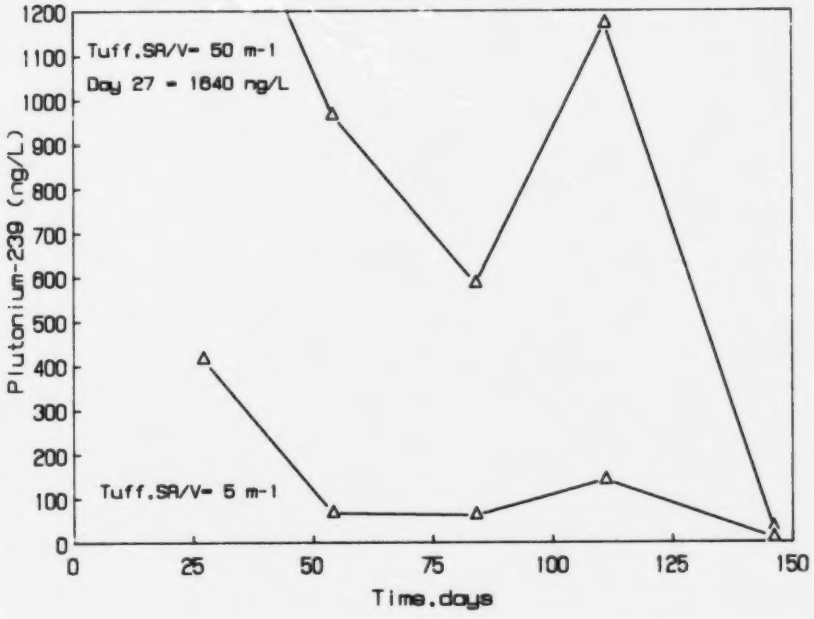

(b)

Figure 3.19. Average plutonium-239 concentrations vs. time, both S/V's in (a) brine, (b) tuff, and (c) basalt groundwater leachates.

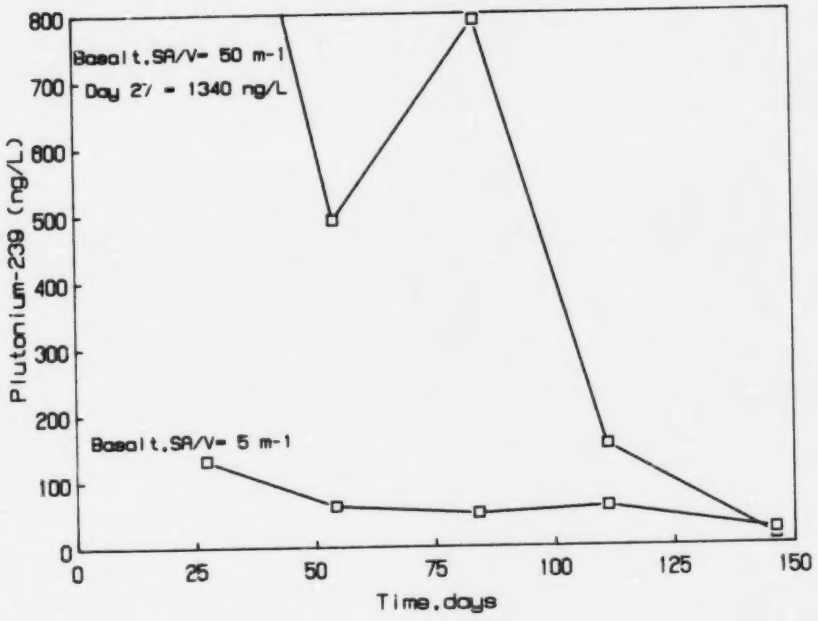

(c)

Figure 3.19. Continued.

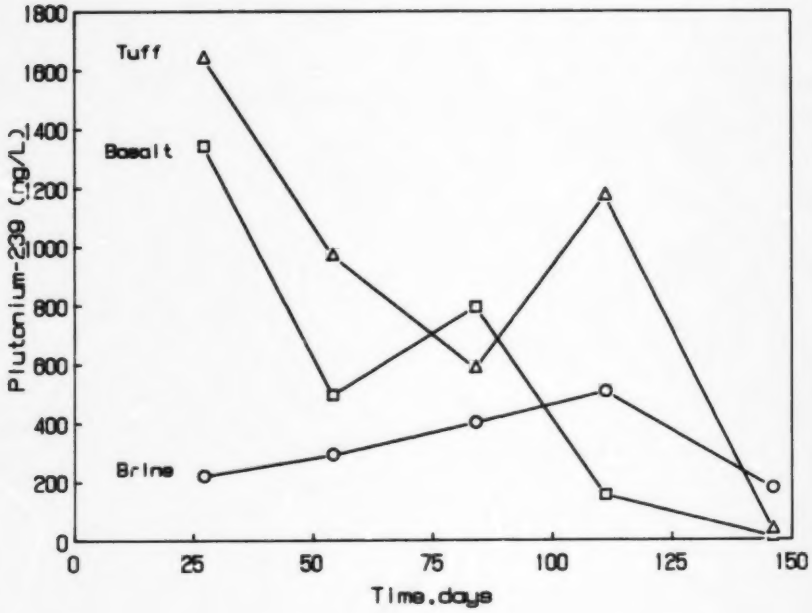

(a)

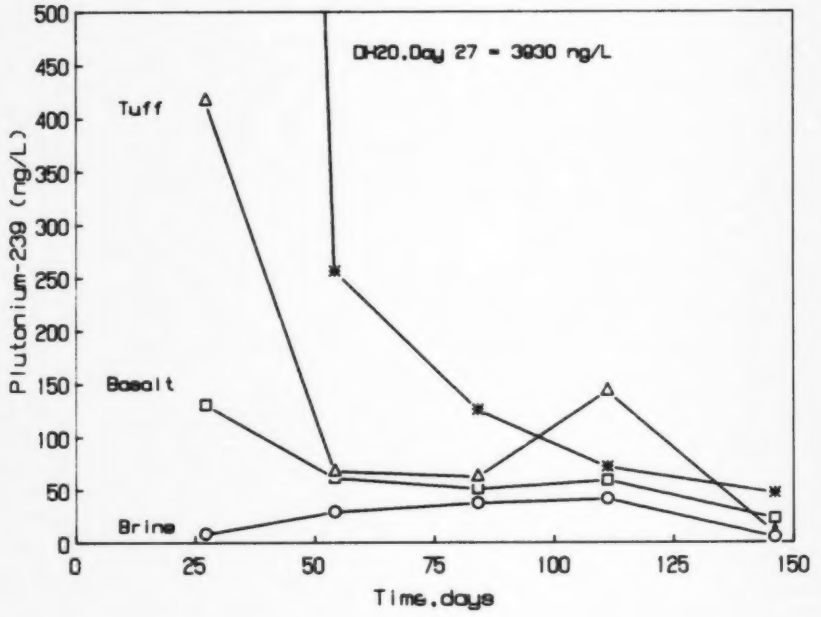

(b)

Figure 3.20. Average plutonium-239 concentrations vs. time, all leachates, (a) S/V = 50 m^{-1}, (b) S/V = 5 m^{-1}.

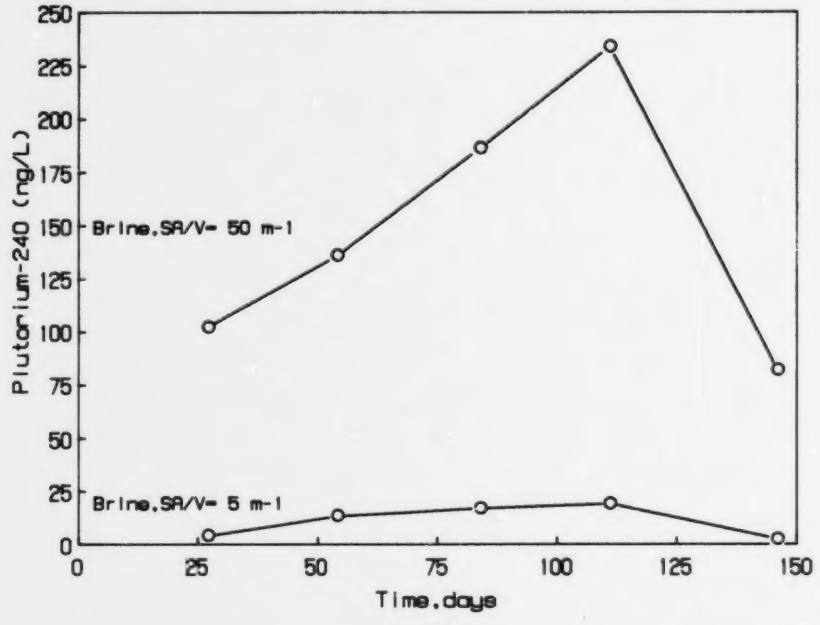

(a)

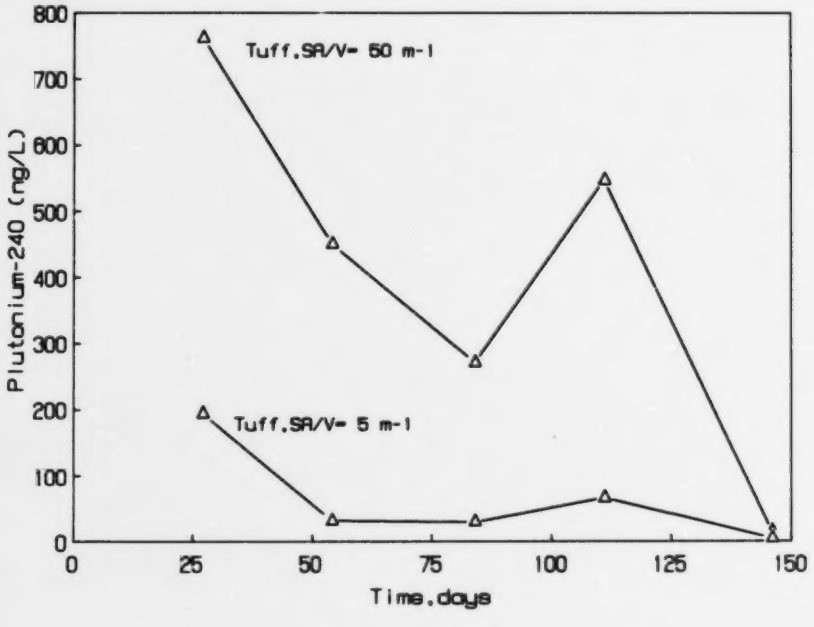

(b)

Figure 3.21. Average plutonium-240 concentrations vs. time, both S/V's in (a) brine, (b) tuff, and (c) basalt groundwater leachate.

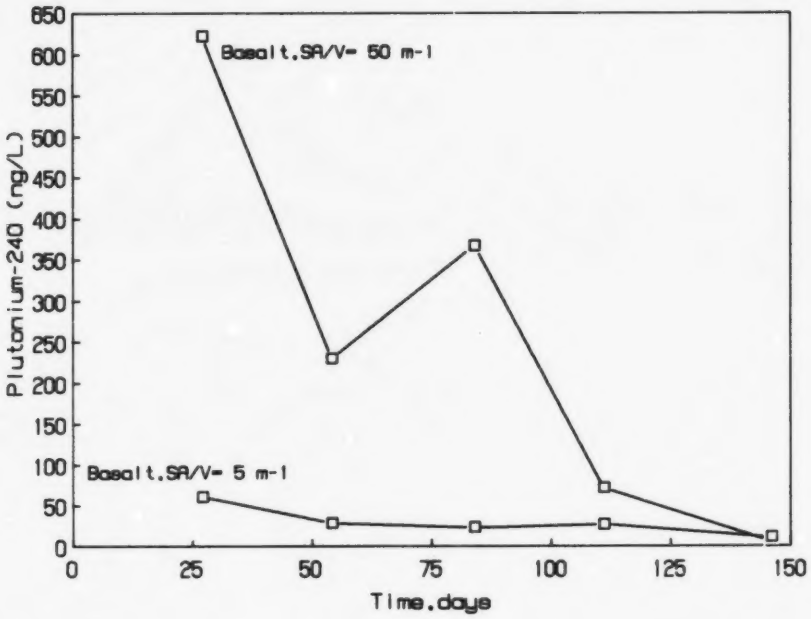

(c)

Figure 3.21. Continued.

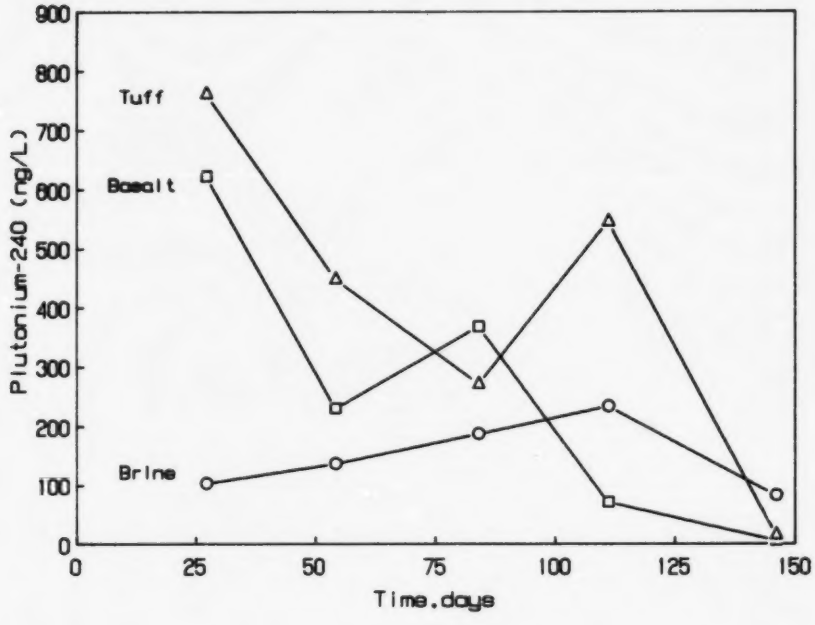

(a)

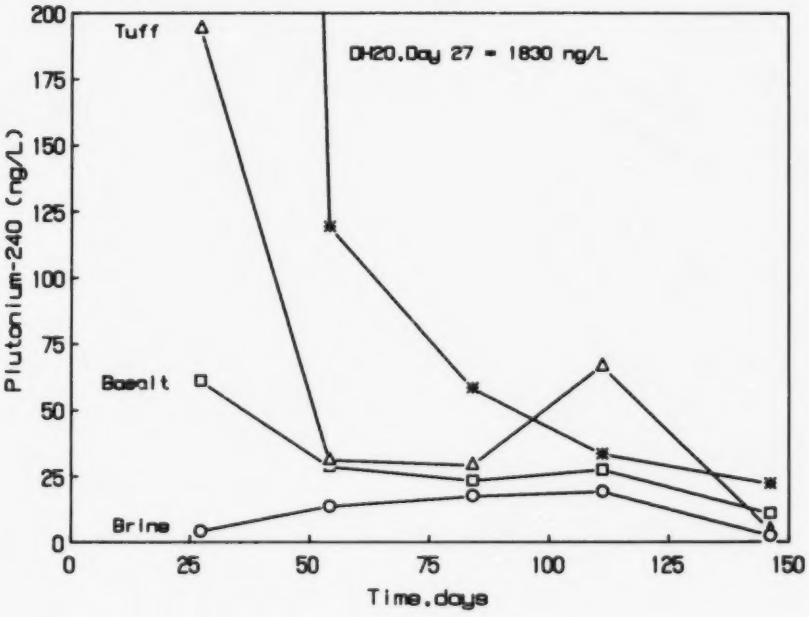

(b)

Figure 3.22. Average plutonium-240 concentrations vs. time, all leachates, (a) S/V = 50 m^{-1}, (b) S/V = 5 m^{-1}.

3.3 Leached UO_2 Surface Characteristics

Unirradiated UO_2 surfaces were photographed using scanning electron microscopy (SEM) before and after leaching. Precipitates that formed on the surface during leaching were chemically analyzed by energy-dispersive X-ray analysis (EDAX), X-ray diffraction (XRD), and electron spectroscopy for chemical analysis (ESCA). The morphological and chemical characterizations of the UO_2 surfaces were intended to aid in the evaluation of uranium leaching mechanisms, discussed further in Section 4.1.

Typical unleached UO_2 pellet surface morphology is shown in Figure 3.23. Figure 3.23a is a molded surface from Experiment No. 2; and Figure 3.23b is a fractured surface from Experiment No. 1. Note the granular structure of the depleted UO_2 pellets and the pores that are introduced during pellet fabrication.

Precipitates formed on essentially all pellets that were leached in both unirradiated UO_2 experiments. The most common precipitates in the tuff and basalt leachates were iron silicates. Both of these synthetic groundwaters contain silica in their formulation (Table 2.3), and iron is present as both an additive to simulate canister corrosion products and in the carbon steel reaction vessels. Iron silicates are commonly observed in borosilicate glass leaching experiments (Refs. 3.2, 3.3, 3.4). It appears that these phases are very stable and commonly form when significant amounts of both ferrous iron and silica are present in the same aqueous system.

Precipitates forming during the brine leach tests were more complex. Figure 3.24 shows typical deposits that formed during the 328-day leach test in the absence of an external radiation field (Experiment 1). EDAX analysis showed they were primarily enriched in magnesium and iron. XRD analyses identified the following:

- magnesite ($MgCO_3$)
- pyroaurite ($Mg_6Fe_2CO_3(OH)_{16}\cdot 4H_2O$)
- β-$Fe_2(OH)_3Cl$
- geothite (α-FeO(OH)).

The carbonates, magnesite and pyroaurite, were the dominant phases. Similar precipitates formed on UO_2 leached in brine in the presence of a radiation field (Experiment No. 2). No uranium-bearing alteration products were detected. If the UO_2 surfaces become completely passivated with such precipitates, then the leach rates of the UO_2 would be expected to decrease because of the lack of contact between leachate and fuel. However, such an effect was not observed in these experiments, as no significant reduction in uranium concentrations over time was observed (Figures 3.1 and 3.2).

A small number of UO_2 surfaces, both before and after leaching, were also analyzed by ESCA. The purpose was to characterize the oxidation state of

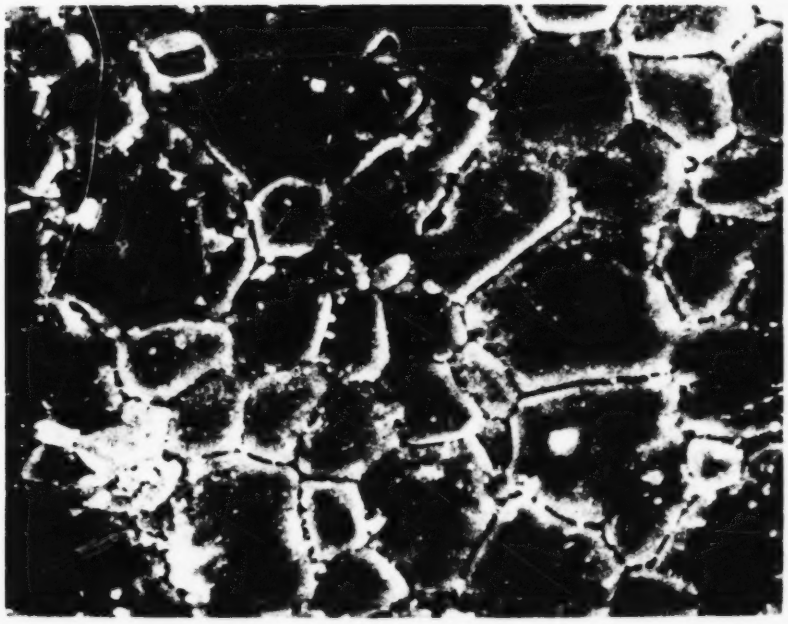

(a) 2000X

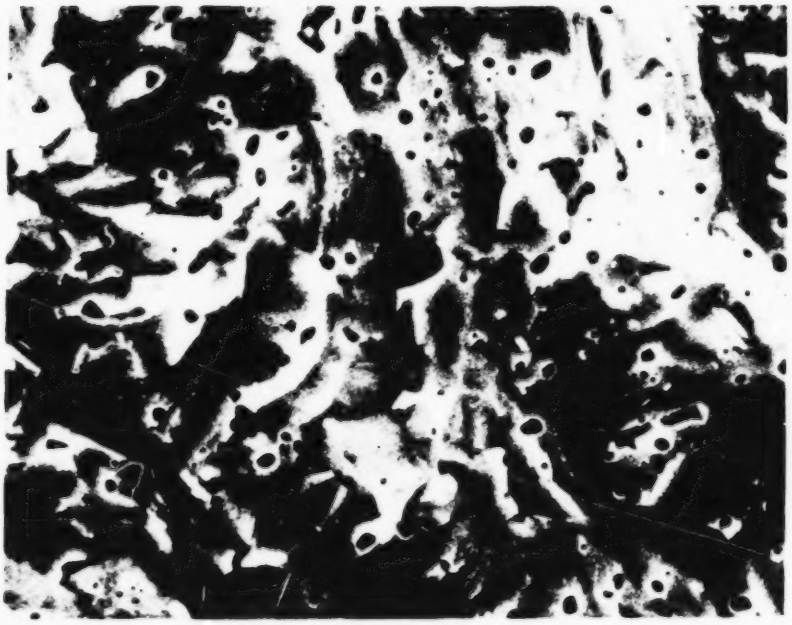

(b) 5000X

Figure 3.23. Unleached unirradiated UO_2 pellet surfaces (a) molded surface, pellet type used in Experiment No. 1 and (b) fractured surface, pellet type used in Experiment No. 2.

BEST COPY AVAILABLE

3600X

3600X

Figure 3.24. Unirradiated UO_2 pellet surface after leaching in brine, Experiment No. 1, Reaction Vessel No. 3.

BEST COPY AVAILABLE

uranium in the pellet surface to determine if tetravalent UO_2 was oxidized to U(VI) during leaching. A trace amount of hexavalent uranium was detected in only the outermost layer (~10 to 20 angstroms) of the UO_2 pellet surface; and the percentage of hexavalent uranium in the surfaces of the leached pellets was no greater than that in the unleached specimens. Hence, it was concluded that the leaching mechanism of uranium in these two experiments did not include the oxidation of U(IV) to U(VI) and subsequent precipitation of films containing hexavalent uranium back onto the UO_2 surface, as has been reported by Wang and Katayama (Ref. 3.5) for other experimental systems.

3.4 References for Chapter 3

(3.1) Lindberg, Ralph D., and Donald D. Runnells, "Ground Water Redox Reactions: An Analysis of Equilibrium State Applied to Eh Measurements and Geochemical Modeling", Science, 225, 925-927 (1984).

(3.2) G. L. McVay and C. Q. Buckwalter, "Effect of Iron on Waste-Glass Leaching", Jour. Amer. Ceram. Soc. 66 (3), 170-174 (1983).

(3.3) C. M. Jantzen, "Effects of Eh (Oxidation Potential) on Borosilicate Waste Glass Durability", in Advances in Ceramics, Vol. 8, Nuclear Waste Management, G. G. Wicks and W. A. Ross, Eds., pp. 385-393. The American Ceramics Society (Columbus, Ohio, 1984).

(3.4) C. M. Jantzen, "Methods for Simulating Low Redox Potential (Eh) for a Basalt Repository". Scientific Basis for Nuclear Waste Management VII, Material Research Society Symposia Proceedings Volume 26, G. M. McVay, ed. (North Holland, New York, 1984).

(3.5.) R. Wang and Y. B. Katayama, "Dissolution Mechanisms for UO_2 and Spent Fuel", Nuclear and Chemical Waste Management, Vol. 3, pp 83-90 (1982).

4. LEACHING MECHANISMS

The distribution of radionuclides in spent fuel (Appendix B) is complex, and different leaching mechanisms may be operative for different radionuclides. Some portion of certain radionuclides (for example, cesium and iodine) has migrated to the fuel/cladding gap and UO_2 grain boundaries during burn-up. That component of those radionuclides is readily released upon contact with leachate. Other radionuclides such as the actinides are primarily dissolved in the UO_2 matrix. Therefore, the UO_2 must be dissolved before the leachate can come in contact with these radionuclides. Other discrete phases may exist in spent fuel; for example, strontium zirconate. Subsequent to leaching, radionuclides may equilibrate with and form other discrete phases, such as oxides and hydroxides, that are not originally present in the irradiated fuel. The geochemistry of certain radionuclides (for example, the actinides) is complex even in simple systems. Significant progress must be made before the behavior of actinides in complex systems such as spent fuel can be accurately predicted or modeled.

Chapter 3 of this report presented radionuclide concentrations in the leachates as a function of time and identified some of the major experimental dependencies, such as the effects of S/V ratio and leachate composition. This chapter discusses the results of simple calculations that provide additional insights on the mechanisms of radionuclide release and behavior subsequent to release. For the volatile fission by-products iodine and cesium, total amounts dissolved in the leachates were compared with total inventory in the fuel. For strontium, americium, curium, and plutonium, radionuclide concentrations in the leachates were ratioed with respect to leachate uranium concentrations at the onset and conclusion of the experiments. When compared to their respective radionuclide/uranium ratios in the fuel, these calculations provide insights as to whether the leaching of radionuclides disseminated in the UO_2 matrix is congruent or incongruent with the leaching of uranium.

4.1 Uranium

Section 3.2.1 illustrated the uranium concentration trends with time for each of the three experiments. Figures 4.1 through 4.4 show the trends for all experiments as a function of S/V ratio and leachate composition. The main result was that uranium concentrations in leachates from all three of these very different experiments were remarkably similar, with two major exceptions:

(1) Uranium concentrations in the spent-fuel leachates were much higher at the onset of the experiments in the low-ionic-strength leachates (tuff, basalt, and deionized water--Figures 4.2 to 4.4). This is attributed to the presence of hexavalent and readily soluble uranium on the spent-fuel surface. Either the hexavalent uranium was initially present (it may have formed during cutting) or it formed as a result of interaction with slightly oxidized day-27 leachates. The data do not permit differentiation. That the elevated uranium concentrations were not observed in the day-27 brine leachates is attributed to the lower and

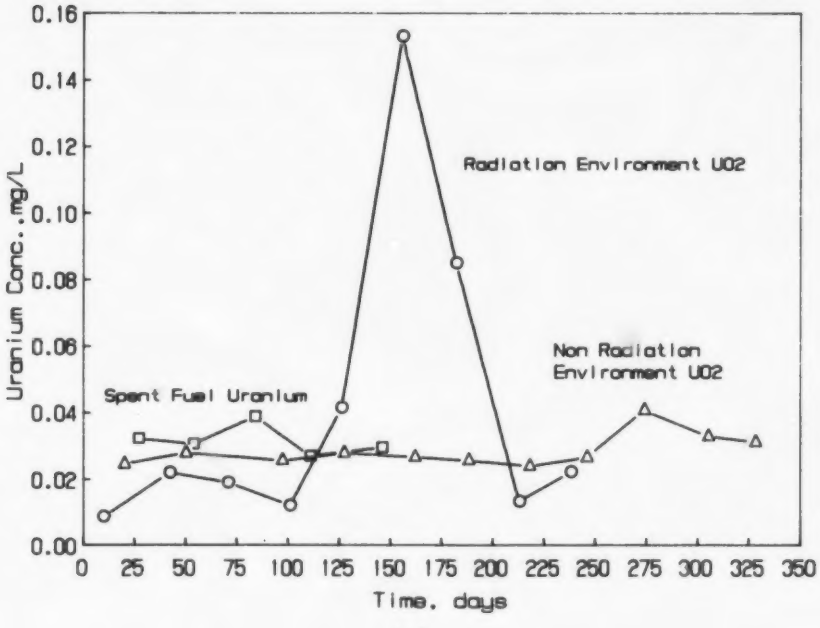

(a)

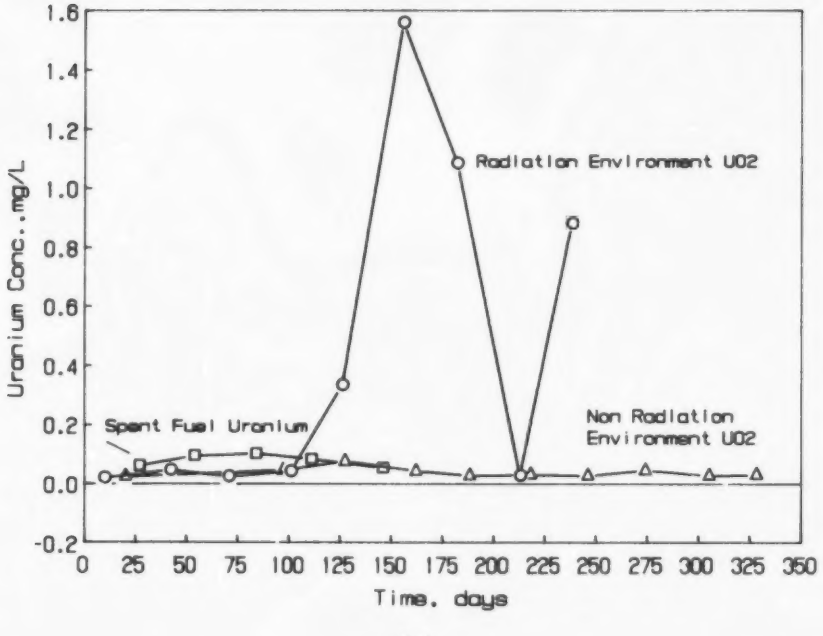

(b)

Figure 4.1. Average uranium concentrations versus time for all three experiments in brine at (a) S/V = 5 m^{-1} and (b) S/V = 50 m^{-1}.

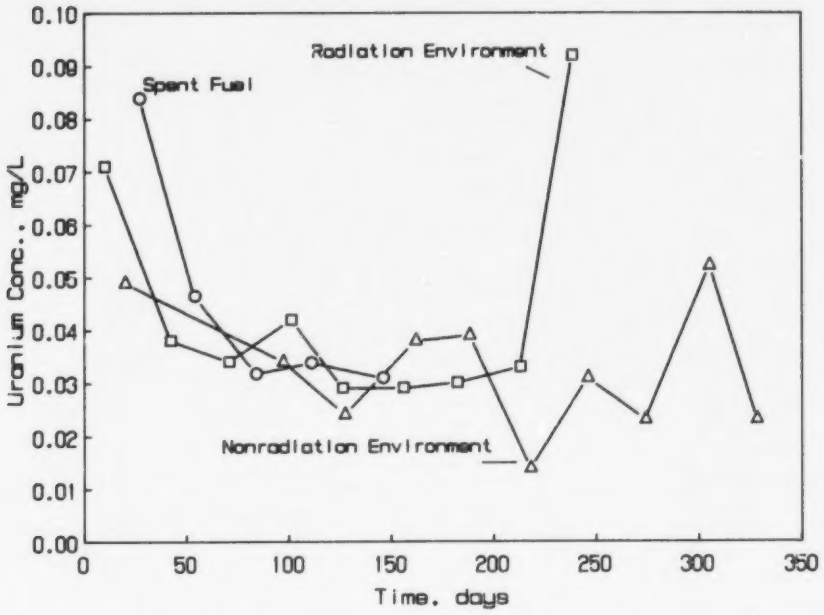

(a)

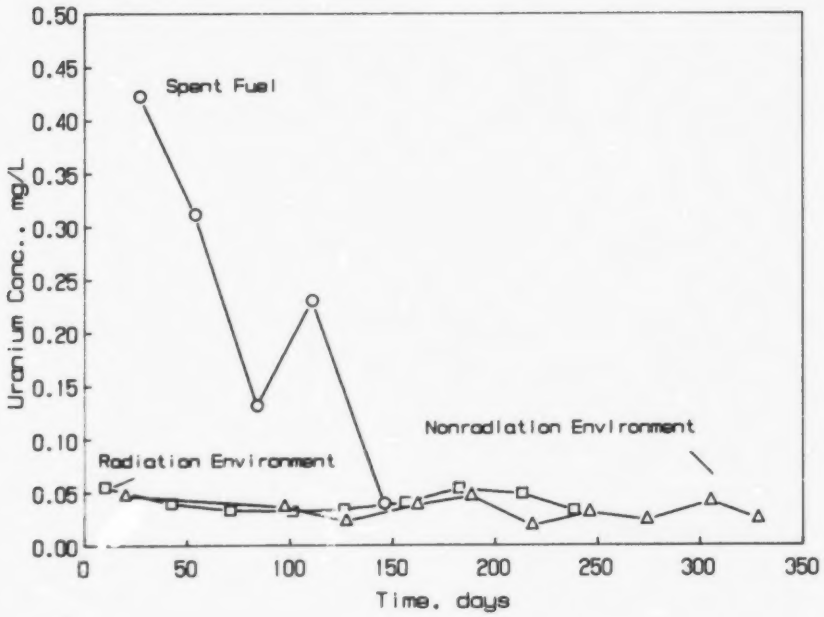

(b)

Figure 4.2. Average uranium concentrations versus time for all three experiments in synthetic tuff groundwater at (a) S/V = 5 m^{-1} and (b) S/V = 50 m^{-1}.

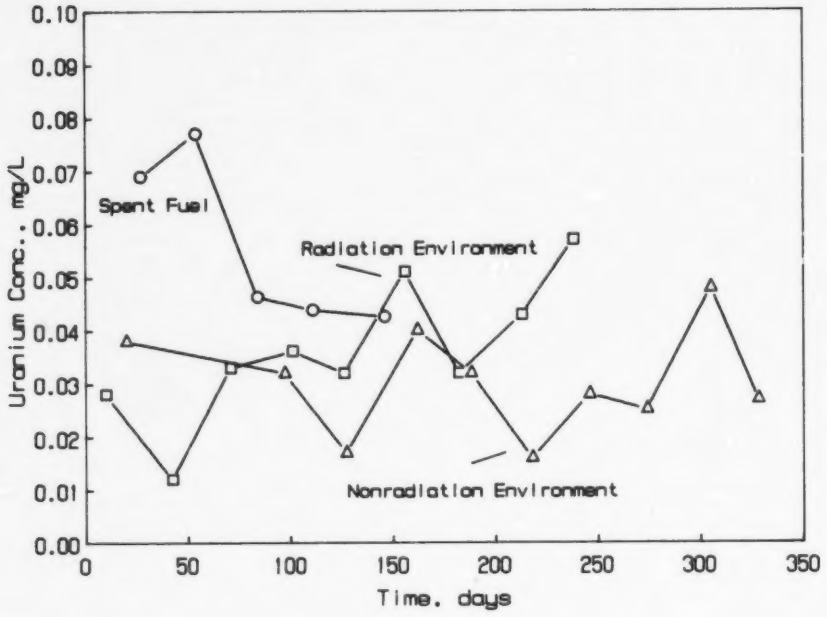

(a)

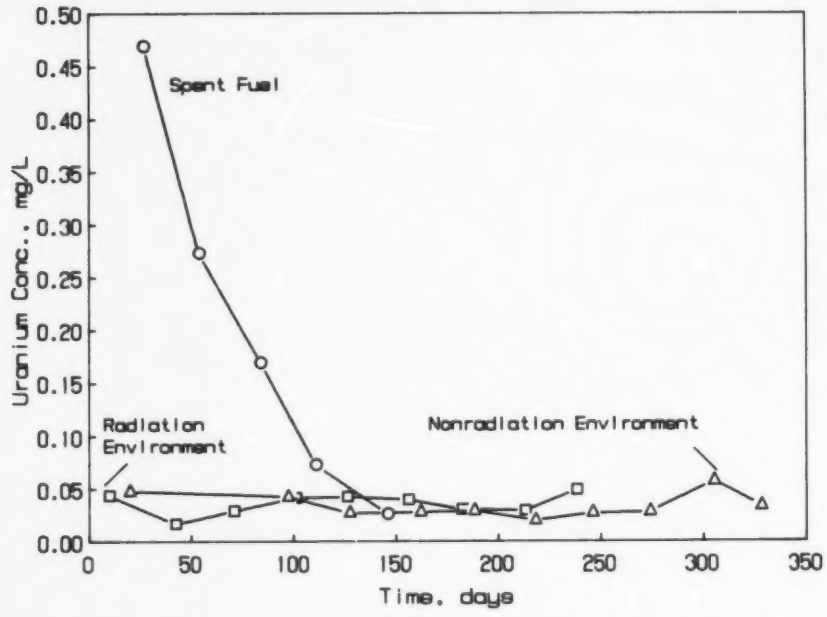

(b)

Figure 4.3. Average uranium concentrations versus time for all three experiments in synthetic basalt groundwater at (a) S/V = 5 m^{-1} and (b) S/V = 50 m^{-1}.

better-buffered redox potential of the brine, caused by the larger amount of ferrous iron that it dissolved during the carbon steel equilibration step. Any hexavalent uranium present on the spent-fuel surface was apparently reduced to its relatively insoluble tetravalent form prior to day 27.

(2) As discussed in Section 3.2.1, there was an anomalous increase in uranium concentrations in brine in the presence of an external radiation field, as shown in Figure 4.1. There appear to be two possible causes. One is that the interaction between gamma radiation and brine produced oxidized solution species that oxidized some of the uranium. The second is that the gamma radiation created weaknesses at grain boundaries (that is, intergranular attack), which led to mechanical degradation of the waste form. A difficulty shared by both hypotheses is the return of uranium concentrations at day 213 to ambient levels, which is not readily explained. That elevated concentrations were not similarly observed in the low ionic strength leachates also argues against the second hypothesis. Hence, the preferred interpretation is brine radiolysis. These data point to the need for additional leach testing of UO_2 or spent fuel in brine and in the presence of an external radiation field.

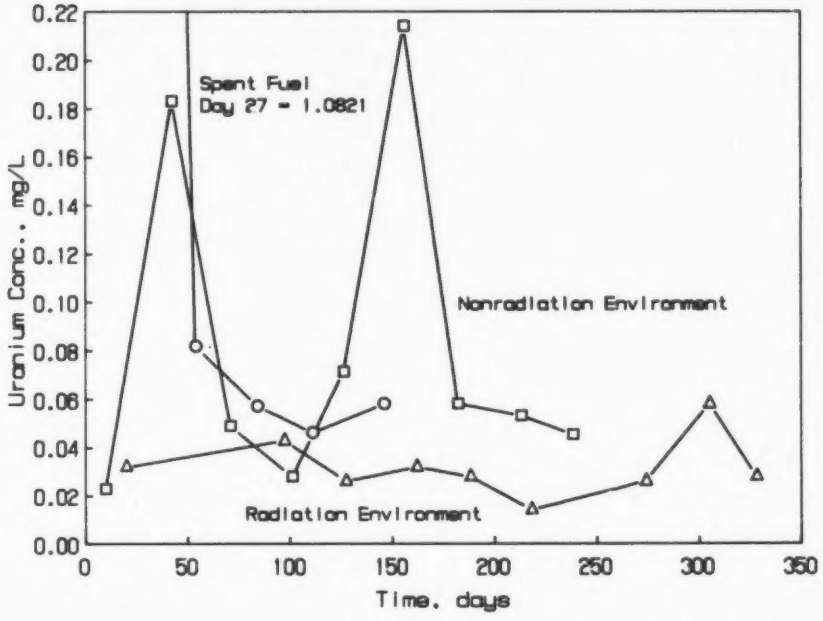

Figure 4.4. Uranium concentrations versus time in all three experiments in deionized water leachate.

In conclusion, apart from the exceptions cited above, the release of uranium from UO_2 and spent fuel clearly appears to be controlled by the solubility of UO_2. This is similar to the findings of Forsyth et al. (Ref. 4.1), who observed solubility-controlled behavior of uranium in spent-fuel leachates and rapid UO_2 dissolution kinetics. Uranium concentrations observed in this particular set of experiments were largely unaffected by the presence of inorganic anions and pH (from approximately 6 to 9) and ranged mostly between 0.02 to 0.06 mg/L, regardless of whether the waste form was unirradiated or irradiated UO_2. This is in contrast with the results of Gray et al. (Ref. 4.2), who found that the release of uranium from spent fuel was approximately 100 times greater than that from unirradiated UO_2. Based on the known geochemical properties of uranium and the results of these experiments, it would appear that redox potential is the single most important parameter affecting UO_2 solubility.

4.2 Cesium and Iodine

Cesium and iodine behaved similarly in the leaching experiments and are thus discussed together. Both leached rapidly and linearly with S/V. At S/V = 50 m^{-1}, cesium-137 and iodine-129 concentrations were only in the low mg/L range, many orders of magnitude below saturation with respect to most known salts of these highly soluble ions.

In that results indicate that the readily available forms of these isotopes will leach rapidly, it is of interest to determine what fraction of the fuel these isotopes comprise relative to the total cesium-137 and iodine-129 inventories. Eklund and Forsyth (Ref. 4.3) observed that the cesium-137 leached from spent fuel constituted from 0.03 to 0.7 percent of the total fuel inventory and correlated with burn-up rating. The rationale is that the higher the fuel burn-up, the greater the movement of volatile radionuclides to the gap, grain boundaries, and peripheral cracks where they are more accessible to leachate. Results from this experiment congregate around the high end of that range for cesium-137 and from about 0.8 to 1.6 percent total fuel inventory for iodine-129, as shown in Table 4.1.

Because cesium and iodine have nearly identical molecular weights, the results in Table 4.1 suggest some preferential leaching of iodine relative to cesium. This was examined by calculating Cs/I molar ratios in the leachates and comparing them with that of the fuel. The results in Table 4.2 refer to total cesium and iodine, not just the specific isotopes in Table 4.1, since the behavior of the elements (calculated from the radiochemistry data and ORIGEN output) and not the individual isotopes is of interest here. The Cs/I ratio in the fuel is 9:1, and current understanding is that iodine occurs completely as cesium iodide. However, this means that 8/9 of the cesium must occur as some other phase, the composition of which is not clear, perhaps a uranate (Ref. 4.4). It is not surprising that Cs/I ratios in the leachates are somewhat lower than that of the fuel, indicating preferential removal of the iodine, caused most likely by the lesser solubility of the cesium not associated with iodine.

Table 4.1. Fraction of cesium-137 and iodine-129 leached relative to total fuel inventory.

Leachate	S/V (m^{-1})	Fuel Inventory Leached, Percent	
		Cesium-137	Iodine-129
Brine	5	0.77	1.54
	50	0.92	1.60
Tuff	5	0.80	1.15
	50	0.77	1.03
Basalt	5	0.53	0.86
	50	0.85	0.84
Deionized H_2O*	5	0.94	1.06

Table 4.2. Cs/I ratio in fuel and leachates.

Sample	S/V (m^{-1})	Cs/I
Spent fuel		9.0
Brine leachate	5	4.5
Brine leachate	50	4.8
Tuff leachate	5	6.3
Tuff leachate	50	6.7
Basalt leachate	5	5.5
Basalt leachate	50	9.1
H_2O** leachate	5	8.0

*Molar ratio of total cesium (includes cesium-133 plus -134 plus -135 plus -137) to total iodine (includes iodine-127 plus -129).
**Deionized.

Thus, two of the important controls of cesium and iodine release from spent fuel are SA/V ratio and fuel burn-up. Cesium-137 and iodine-129 concentrations were well below saturation with respect to any common solid phase, even in a moderate burn-up fuel such as this and at a relatively high S/V ratio of 50 m^{-1}. Iodine appears to be somewhat more leachable than cesium, and one possible explanation for this is that iodine occurs completely as highly soluble cesium iodide, but cesium, which is 9 times more abundant than iodine in spent fuel, occurs primarily as uranates and/or other phases that are not completely soluble.

4.3 Strontium

Strontium-90 concentrations do not appear to be solubility-controlled, as illustrated by the strong S/V effect in Figure 3.11. Strontium-90 concentrations are less than 0.1 mg/L, while concentrations at saturation with respect to carbonate or sulfate phases would likely be much higher (Refs. 4.5, 4.6). In fact, the WIPP Brine A recipe contains 5 mg/L strontium, and an additional few tenths of mg/L is unlikely to cause supersaturation. The complexity is that strontium-90 release was also very dependent upon leachate composition, apparently correlated with pH, as shown in Figure 3.12. The coexistence of the leachate compositional effect and the S/V effect indicates nonequilibrium behavior. In fact, Figures 3.11 and 3.12 show that, in several cases, strontium-90 concentrations continued to climb with time regardless of the dilution that was occurring at each sampling.

The Sr/U ratios in leachates are consistently higher than the Sr/U ratio of the fuel, and they increased during the course of the experiment, indicating incongruent and preferential release of strontium relative to uranium, as shown in Table 4.3. Forsyth et al. (Ref. 4.1) also observed that strontium was released faster than uranium during leaching of spent fuel.

We conclude that the release of strontium-90 from spent fuel is strongly affected by pH, but that it also exhibits a kinetic dependency. Future study is needed on the physio-chemical form of strontium-90 in spent fuel.

4.4 Other Actinides

Plutonium, americium, and curium behaved similarly; thus, they are discussed together in this section. Their absolute concentrations were somewhat different, with plutonium > americium > curium. It would be premature to speculate that this solely reflects the lower solubility of curium relative to americium and plutonium because it is not clear that true solubility was established in all the reaction vessels (although this appears to have been the case in at least a few) during the time frame of this experiment. The different concentrations probably also reflect nuclide inventories in the fuel.

Table 4.3. *Sr/U ratio in fuel and leachates at days 27 and 146.

Sample	*Sr/U	
	Day 27	Day 146
Spent Fuel	1.8×10^{-3}	
Vessel No. 1	4.8×10^{-1}	1.1×10^{0}
Vessel No. 2	6.6×10^{-1}	6.3×10^{-1}
Vessel No. 3	2.0×10^{0}	2.7×10^{0}
Vessel No. 4	2.7×10^{0}	3.2×10^{0}
Vessel No. 5	3.9×10^{-2}	1.6×10^{-1}
Vessel No. 6	2.5×10^{-2}	1.2×10^{-1}
Vessel No. 7	7.4×10^{-2}	1.0×10^{0}
Vessel No. 8	3.8×10^{-2}	3.9×10^{-1}
Vessel No. 9	2.7×10^{-3}	2.0×10^{-3}
Vessel No. 10	1.7×10^{-3}	1.8×10^{-3}
Vessel No. 11	9.8×10^{-3}	6.1×10^{-2}
Vessel No. 12	3.5×10^{-3}	1.1×10^{-1}
Vessel No. 13	2.1×10^{-3}	3.1×10^{-2}

*Molar ratio of total strontium (includes strontium-88 plus -90 but excludes 5 mg/L strontium in WIPP Brine A recipe) to total uranium (primarily uranium-238).

As mentioned in Sections 3.2.5 through 3.2.7, actinide concentrations in the leachates generally decreased with time. Forsyth et al. (Ref. 4.7) also reported this type of behavior for plutonium concentrations in synthetic groundwater leachates from low burn-up spent fuel and speculated that it reflected the crystallization of amorphous plutonium oxide hydrate to the lower solubility PuO_2 with time. Relative to uranium, leachate actinide concentrations were also dominantly lower at the conclusion of the experiment (day 146) than near the onset (day 27), as shown in Tables 4.4 through 4.7. Plutonium/uranium ratios were calculated twice, once based on the plutonium-238 data (Table 4.4) and then based on plutonium-239 (Table 4.5). The ratios are remarkably similar, with the exception of two plutonium-238 data points (reaction vessel 2, day 27 and reaction vessel 10, day 146), which are probably spurious. For plutonium, americium, and curium the ratios for reaction vessels 3 through 13 tend to indicate initial dissolution that was congruent with uranium, as witnessed by the similarities between day 27 leachate ratios and ratios calculated from the ORIGEN code data for the spent fuel. By the conclusion of the experiment, actinide/uranium ratios were generally (and in some cases almost two orders of

67

Table 4.4. *Pu/U ratio in fuel and leachates at days 27 and 146 (based on Pu-238 data).

Sample	*Pu/U	
	Day 27	Day 146
Spent Fuel	9.1×10^{-3}	
Vessel No. 1	3.8×10^{-4}	7.3×10^{-4}
Vessel No. 2	6.6×10^{-5}	4.6×10^{-4}
Vessel No. 3	7.3×10^{-3}	9.8×10^{-3}
Vessel No. 4	4.9×10^{-3}	7.3×10^{-3}
Vessel No. 5	8.1×10^{-3}	2.7×10^{-4}
Vessel No. 6	7.2×10^{-3}	4.0×10^{-4}
Vessel No. 7	6.5×10^{-3}	2.5×10^{-3}
Vessel No. 8	4.3×10^{-3}	2.9×10^{-3}
Vessel No. 9	3.3×10^{-3}	1.0×10^{-3}
Vessel No. 10	2.5×10^{-3}	1.3×10^{-4}
Vessel No. 11	4.1×10^{-3}	2.1×10^{-3}
Vessel No. 12	4.7×10^{-3}	1.2×10^{-3}
Vessel No. 13	3.8×10^{-3}	1.9×10^{-3}

*Molar ratio of total plutonium (includes plutonium-238 plus -239 plus -240 plus -241 plus -242) to total uranium (primarily uranium-238).

Table 4.5. *Pu/U ratio in fuel and leachates at days 27 and 146 (based on Pu-239 data).

Sample	*Pu/U	
	Day 27	Day 146
Spent Fuel	9.1×10^{-3}	
Vessel No. 1	3.8×10^{-4}	4.8×10^{-4}
Vessel No. 2	5.5×10^{-4}	2.2×10^{-4}
Vessel No. 3	8.0×10^{-3}	6.6×10^{-3}
Vessel No. 4	3.7×10^{-3}	4.6×10^{-3}
Vessel No. 5	9.1×10^{-3}	5.4×10^{-4}
Vessel No. 6	8.0×10^{-3}	5.1×10^{-4}
Vessel No. 7	7.0×10^{-3}	8.6×10^{-4}
Vessel No. 8	6.5×10^{-3}	1.8×10^{-3}
Vessel No. 9	3.6×10^{-3}	5.6×10^{-4}
Vessel No. 10	3.0×10^{-3}	1.3×10^{-3}
Vessel No. 11	4.8×10^{-3}	1.3×10^{-3}
Vessel No. 12	4.9×10^{-3}	3.5×10^{-4}
Vessel No. 13	6.3×10^{-3}	1.4×10^{-3}

*Molar ratio of total plutonium (includes plutonium-238 plus -239 plus -240 plus -241 plus -242) to total uranium (primarily uranium-238).

Table 4.6. *Am/U ratio in fuel and leachates at days 27 and 146.

Sample	*Am/U	
	Day 27	Day 146
Spent Fuel	7.3×10^{-4}	
Vessel No. 1	$<1.8 \times 10^{-4}$	$<2.5 \times 10^{-4}$
Vessel No. 2	$<2.8 \times 10^{-4}$	$<2.6 \times 10^{-4}$
Vessel No. 3	1.6×10^{-3}	5.5×10^{-4}
Vessel No. 4	6.0×10^{-4}	$<4.9 \times 10^{-4}$
Vessel No. 5	2.5×10^{-3}	$<2.9 \times 10^{-4}$
Vessel No. 6	1.7×10^{-3}	$<3.9 \times 10^{-4}$
Vessel No. 7	1.0×10^{-3}	$<4.1 \times 10^{-4}$
Vessel No. 8	1.2×10^{-3}	$<2.0 \times 10^{-4}$
Vessel No. 9	8.0×10^{-4}	$<2.0 \times 10^{-4}$
Vessel No. 10	3.8×10^{-4}	$<2.6 \times 10^{-4}$
Vessel No. 11	8.2×10^{-4}	$<3.4 \times 10^{-4}$
Vessel No. 12	1.1×10^{-3}	$<3.8 \times 10^{-4}$
Vessel No. 13	1.3×10^{-3}	5.0×10^{-4}

*Molar ratio of total americium (includes americium-241 plus -243 to total uranium (primarily uranium-238).

Table 4.7. *Cm/U ratio in fuel and leachates at days 27 and 146.

Sample	*Cm/U	
	Day 27	Day 146
Spent Fuel	2.1×10^{-5}	
Vessel No. 1	1.8×10^{-6}	2.4×10^{-6}
Vessel No. 2	7.3×10^{-7}	1.8×10^{-6}
Vessel No. 3	5.5×10^{-5}	4.7×10^{-5}
Vessel No. 4	2.3×10^{-5}	3.2×10^{-5}
Vessel No. 5	6.0×10^{-5}	2.5×10^{-6}
Vessel No. 6	6.1×10^{-5}	2.0×10^{-6}
Vessel No. 7	5.3×10^{-5}	8.2×10^{-6}
Vessel No. 8	2.6×10^{-5}	9.0×10^{-6}
Vessel No. 9	3.2×10^{-5}	2.4×10^{-6}
Vessel No. 10	1.6×10^{-5}	5.0×10^{-7}
Vessel No. 11	2.5×10^{-5}	7.3×10^{-6}
Vessel No. 12	3.0×10^{-5}	3.7×10^{-6}
Vessel No. 13	2.2×10^{-5}	1.3×10^{-5}

*Molar ratio of curium-244 (which approximates total curium) to total uranium (primarily uranium-238).

magnitude) lower than the corresponding ratio for the spent fuel, suggesting that the actinides equilibrated with a phase having a lower solubility and precipitated from solution. There appear to be reasonable geochemical explanations for the two exceptions. The low S/V brines (reaction vessels 1 and 2) possessed day 27 actinide/uranium ratios consistently lower than that of the fuel; this suggests more rapid equilibration of the actinide in the brine with the geochemical environment of the reaction vessel, caused perhaps by the brine's lower and better-poised redox potential, which was due to its having complexed more iron during the carbon steel chip equilibration step. The second exception was the day 146 actinide/uranium ratios in reaction vessels 3 and 4, corresponding to the higher S/V brines. Contrary to the other day 146 ratios, the high S/V brines were not very much lower than those at day 27 and in fact were very similar to those of the spent fuel. A reasonable explanation is the complexation characteristics of the brine. The high anion content of the brine kept both the uranium and other actinides from reprecipitating as the less-soluble phases that appear to have been stable in the lower-ionic-strength leachates.

4.5 References for Chapter 4

(4.1) R. S. Forsyth, L. O. Werme, and J. Bruno, The Corrosion of Spent UO_2 Fuel in Synthetic Groundwater, SKB Technical Report 85-16, Swedish Nuclear Fuel and Waste Management Co., Box 5864, S-102 48 Stockholm, Sweden (1985).

(4.2) W. J. Gray, G. L. McVay, J. O. Barner, J. W. Shade, and R. W. Cote, "Evaluation of Spent Fuel as a Waste Form in a Salt Repository," Mat. Res. Soc. Symp. Proc. 26, 437-444 (1984).

(4.3) U. Eklund and R. Forsyth, Leaching of Irradiated UO_2 Fuel, KBS Technical Report 70 (English translation) (1978).

(4.4) L. H. Johnson, S. S. Stroes-Gascoyne, J. D. Chen, M. E. Attas, D. M. Sellinger, and H. G. Delaney, "The Relationship between Fuel Element Power and the Leaching of ^{137}Cs and ^{129}I from Irradiated UO_2 Fuel," Proceedings of the Topical Meeting on Fission Product Behavior and Source Term Research, Snowbird, UT (1984).

(4.5) E. J. Reardon and D. K. Armstrong, "Celestite ($SrSO_4(s)$) Solubility in Water, Seawater and NaCl Solution," Geochimica et Cosmochimicia Acta 51, 63-72 (1987).

(4.6) W. Stumm and J. J. Morgan, Aquatic Chemistry, J. Wiley and Sons, NY, p. 243 (1981).

(4.7) J. Bruno, R. S. Forsyth, and L. O. Werme, "Spent UO_2 - Fuel Dissolution. Tentative Modeling of Experimental Elemental Solubilities," Mat. Res. Soc. Symp. Proc. 44, 413-420 (1985).

5. UO_2/SPENT-FUEL DISSOLUTION MODELING

The development of predictive models for radionuclide release from spent nuclear fuels within a repository environment is, at best, in the earliest stage. This has been pointed out recently by Stephens et al. (Ref. 5.1). The research summarized below reflects this fact in the sense that a relatively simple, semi-empirical model is used to describe the dissolution kinetics. This model is based on analogous studies that have been conducted in the more advanced geochemical area of mineral-water interactions. Our research focused on evaluating the effects of groundwater chemistry on dissolution kinetics by using a Battelle-developed water chemistry model in conjunction with the above-mentioned crystal-dissolution model. Effects of groundwater flow were also included in this model. The results of these studies are presented following a brief review of some general but pertinent concepts of mineral dissolution as well as of past studies of UO_2 and spent-fuel modeling.

5.1 Previous Studies in Mineral-Dissolution Modeling

5.1.1 General Concepts

The dissolution of UO_2 or spent fuel in the presence of an aqueous medium is actually an example of the more general subject of "chemical weathering" of minerals, the latter being a topic of major importance to geochemists. As pointed out by Lasaga (Ref. 5.2), the accumulation of sufficient experimental data in the general area of weathering has made it possible to begin the formulation of truly quantitative descriptions of the process. However, even prior to the publication of Lasaga's comment, various models of mineral dissolution had been formulated. In his review of weathering, Berner (Ref. 5.3) noted that most theoretical descriptions of the process (at least up to that time) had been based on "equilibrium or irreversible, quasi-equilibrium models", and that the application of chemical kinetics to the process was a relatively recent occurrence. However, some theoretical studies of mineral-water interactions, based on detailed chemical-kinetics principles, have been carried out. One of the most notable is the study by Dibble and Tiller (Ref. 5.4), who applied well-known concepts of crystal-growth theory to develop a comprehensive theoretical description of nonequilibrium mineral-water interactions.

Much of the theoretical and experimental work in mineral dissolution has been carried out for systems of aqueous suspensions of finely dispersed particles. The dissolution kinetics for such mineral systems would, in general, be different from that for more monolithic mineral specimens, for which the surface area exposed to the solution would be smaller. Nevertheless, considerable information on dissolution kinetics that is of general value is now available.

5.1.2 Rate-Controlling Processes in Mineral Dissolution

When a mineral (including UO_2/spent fuel) dissolves into an aqueous solution, a number of processes can contribute to the dissolution. First, an interface-reaction mechanism that takes place results in a transfer of

mineral species from the surface of the solid into the solution--the actual dissolution process. This overall process actually may consist of a number of different contributing processes, depending upon the availability of interface free energy to drive the detachment process (Ref. 5.4). Second, the dissolved mineral undergoes chemical diffusion away from the region of the solid/liquid interface into the bulk of the solution. (We do not consider possible electromigration of charged chemical species through the solution [Ref. 5.5].) Third, if the aqueous solution is flowing past the solid mineral, it carries away the dissolved species; thus, solution flow also affects the rate of dissolution. Finally, if the dissolved species precipitate from solution as more stable minerals (for example, as colloids or some other crystalline form), this too reduces their content in solution and correspondingly affects the dissolution rate. The overall dissolution rate may be affected by a combination of these processes in a complex manner. However, if one of the processes occurs very slowly, then, depending on how the various processes are coupled, that process may be rate-limiting and it alone would determine the net rate of dissolution.

Detailed studies have been conducted on mineral-dissolution kinetics related to the competition between interface-reaction kinetics and diffusion (assuming no flow of the bulk liquid). In one early study, Nielsen (Ref. 5.6) concluded that crystal dissolution usually would be diffusion controlled because the layer-by-layer breakdown of crystals does not require such processes as surface nucleation or the growth of spiral steps, the layers being readily attacked at edges and corners. However, other investigators, for example, Berner (Refs. 5.3, 5.7) and Dibble and Tiller (Ref. 5.4), have developed models that illustrate the characteristics of mineral-dissolution kinetics under competing interface-reaction and diffusion kinetics. The last work (Ref. 5.4) is particularly detailed, and it includes an assessment of rate-laws for various types of interfacial-dissolution processes.

One particularly interesting study was that reported by Berner (Ref. 5.7), who constructed a correlation between solubility and rate-controlling reaction based on dissolution information for a number of minerals. His results are summarized in Table 5.1. He concluded that interface-reaction kinetics is dominant below a solubility of 10^{-4} mol/L. Within the range of 10^{-4} to 10^{-3} mol/L, either interface-reaction kinetics or solution transport (with diffusion into a liquid that is not flowing being the slowest form of transport) will dominate, depending on the mineral. With one mineral ($PbSO_4$), the dominant mechanism was also dependent upon undersaturation level and temperature. Above 2×10^{-3} mol/L, transport control is dominant. As pointed out by Berner (Ref. 5.7), exceptions do exist (for example, with AgCl).

The results tabulated in Table 5.1 can be applied, with caution, to other minerals. As Berner indicated (Ref. 5.7), more minerals should be included in such a tabulation; moreover, the majority of the results presented in the table are for pure salt solutions. More complex chemical compositions may alter the kinetics, for example, by causing "surface poisoning" and changing otherwise transport-controlled kinetics to interface-reaction-controlled kinetics. Nevertheless, it is interesting to place UO_2 into this ranking

Table 5.1. Rate-controlling dissolution kinetics for various minerals measured against their solubility in pure water (after Berner [Ref. 5.7]).

Mineral	Solubility* (mol/L)	Dissolution Kinetics
$KAlSi_3O_8$	3×10^{-7}	Interface reaction control
$NaAlSi_3O_8$	6×10^{-7}	Interface reaction control
$BaSO_4$	1×10^{-5}	Interface reaction control
$SrCO_3$	3×10^{-5}	Interface reaction control
$CaCO_3$	6×10^{-5}	Interface reaction control
Ag_2CrO_4	1×10^{-4}	Interface reaction control
$SrSO_4$	9×10^{-4}	Interface reaction control
Opaline SiO_2	2×10^{-3}	Interface reaction control
$PbSO_4$	1×10^{-4}	Mixed Control
AgCl	1×10^{-5}	Transport Control
$Ba(IO_3)_2$	8×10^{-4}	Transport Control
$CaSO_4 \cdot 2H_2O$	5×10^{-3}	Transport Control
$Na_2SO_4 \cdot 10H_2O$	2×10^{-1}	Transport Control
$MgSO_4 \cdot 7H_2O$	3×10^{0}	Transport Control
$Na_2CO_3 \cdot 10H_2O$	3×10^{0}	Transport Control
KCl	4×10^{0}	Transport Control
NaCl	5×10^{0}	Transport Control
$MgCl_2 \cdot 6H_2O$	5×10^{0}	Transport Control

*See Berner (Ref. 5.7) for explanation of how these data were obtained.

by solubility level. In a study that supports this concept, Forsyth et al. (Ref. 5.8) measured a tentative value for the saturation concentration of uranium, dissolved from spent UO_2 fuel, of about 5×10^{-5} g/L or less in deionized water. This value is smaller than the lowest solubility shown on Table 5.1 and hence strongly suggests that UO_2 dissolution kinetics is interface-reaction controlled.

It must be emphasized that the rate-controlling mechanism can change as time progresses and conditions that influence dissolution kinetics (for example, water chemistry) change. Moreover, for interface-reaction-controlled

dissolution, the mechanism at the interface (which can include diffusion-dominated processes [Ref. 5.4]) can likewise change. In their discussion of these changes, Dibble and Tiller (Ref. 5.4) cite the examples of quartz (Refs. 5.9, 5.10) and feldspar (Ref. 5.11), although these studies were concerned with systems in which the dissolving crystals existed in finely divided form, which may have affected the measured kinetics.

The effect of solution bulk flow is to increase dissolution by removing dissolved species from the vicinity of the mineral as they are produced. Since the mineral is thus exposed to fresh solution, the species dissolve at a higher rate than would occur otherwise. This phenomenon has been modeled by Berner (Ref. 5.7) for mineral dissolution and by researchers at Battelle under this program (Refs. 5.12, 5.13) for the dissolution of high-level waste-form glasses.

Precipitation of dissolved species is another process that results in increased removal of species from solution, the replenishment of the solute into solution taking place through an increased rate of mineral dissolution compared to the case for which no precipitation occurs. This commonly observed geochemical phenomenon was reviewed earlier in this program (Ref. 5.14). As discussed in Reference 5.14, various models for simultaneously occurring dissolution/precipitation kinetics have been developed, including models developed at Battelle under this program (Ref. 5.14) for dissolution/precipitation kinetics related to high-level waste-form glasses. As far as UO_2 is concerned, Garisto and Garisto (Ref. 5.15) have pointed out that the dissolution/precipitation process may be important under certain conditions. For example, in saline groundwaters with high concentrations of calcium ions, the mineral calcium uranate can be more stable than UO_2 (Ref. 5.16) for certain conditions related to the groundwater. In addition, in their studies of spent-fuel dissolution, Forsyth et al. (Ref. 5.8) found that the behavior of dissolved plutonium with time was explainable in terms of the crystallization of $PuO_2 \cdot xH_2O$(am.), which is known to have lower solubility. This is also a reasonable explanation for the trends of decreasing plutonium as well as uranium, americium, and curium concentrations observed during the experimental program described above and illustrated in Figures 2.3 and 3.13 through 3.20. Therefore, dissolution/precipitation kinetics must be regarded as potentially important in terms of affecting the long-term dissolution of spent fuel, although this mechanism is not considered further here.

5.1.3 Analyses of Mineral-Dissolution Kinetics

This section presents a brief discussion of how the kinetics of mineral dissolution has been modeled in the past. This information is important, since the analysis of UO_2 dissolution in this study is based largely on some of this past work. Our study focuses on interface-reaction kinetics because of its probable importance to UO_2 dissolution in an aqueous solution.

As major contributors in this area, Dibble and Tiller carried out a detailed study of interface-reaction kinetics in rock-water interactions (Ref. 5.4), including a systematic treatment of the various processes associated with overall transfer of material from the mineral surface to the solution.

Other detailed treatments of the interfacial kinetics associated with mineral-water interactions have also been reported (for example, Lasaga [Ref. 5.2], Aagard and Helgeson [Ref. 5.17], and others). However, rather than concentrating on specific interfacial processes that may relate specifically to UO_2, the present study focuses on some general characteristics of dissolution kinetics summarized by Dibble and Tiller (Ref. 5.4). This approach allowed us to develop a preliminary model of UO_2 dissolution that is not overly complicated by considerations of the actual physical mechanisms that underlie the dissolution process.

As Dibble and Tiller point out, one of the fundamental premises of dissolution kinetics is that the rate at which dissolution takes place is some function of the level of undersaturation. This level, for the ith component, is given by $C_{oi} - C_i$, where C_{oi} is the equilibrium concentration of that species in solution, with respect to the mineral in question, and C_i is its actual, instantaneous concentration in the bulk solution. One quantitative approach to describing the dissolution-induced variation of C_i with time that has been employed is:

$$dC_i/dt = k_d t^{-m} \tag{5-1}$$

where t represents time, k_d is a rate constant for dissolution, and m is a constant that is characteristic of the dissolution reaction (Ref. 5.4). Problems with Eq. 5-1 arise from the fact that only a single mechanism is assumed. Also, the requirement that C_i must, for a closed system, gradually approach C_{oi} is generally not satisfied. An improved and commonly used rate equation is:

$$dC_i/dt = k_d (C_{oi} - C_i)^n \tag{5-2}$$

where $n \geq 0$. For this equation, the undersaturation level does approach zero asymptotically at large times. (The notation used in Eqs. 5-1 and 5-2 is somewhat different from that originally used in Reference 5.4. In addition, the rate constants in these two equations have different units unless both n and m are zero.) As pointed out by Lerman (Ref. 5.18), the dissolution-rate equation given by Eq. 5-2 applies to closed systems for which there are no other sources or sinks for the dissolved species.

5.1.4 Application of Dissolution-Rate Equation

A primary disadvantage of using a semi-empirical dissolution-rate equation (such as Eq. 5-2) is that problems can arise if details of the physical mechanisms are not known. For example, with no prior knowledge of k_d or n, these parameters must be determined experimentally. Moreover, if the rate-controlling process changes as dissolution proceeds, the value of these quantities may likewise change. Another factor of potential importance is that the saturation concentration of the aqueous solution with respect to

the mineral, C_{oi}, may change as the water chemistry changes. In modeling studies of waste-form glasses (Refs. 5.12, 5.13), this effect was found to be an important factor in glass-dissolution kinetics. It should likewise be important for the dissolution of crystalline minerals. However, dissolution of UO_2 should have little effect on the ambient water chemistry due to its generally low solubility, although the water chemistry itself will affect the solubility level of the UO_2.

The magnitude of the constant n, which is the order of the reaction in Eq. 5-2, is also of interest. For example, Christoffersen and Christoffersen (Ref. 5.19) used a rate equation similar to our Eq. 5-2 to describe the dissolution of calcium hydroxyapatite microcrystals in aqueous suspension. They found that, under certain conditions, n exhibited values in the range of 3 to 6. In another study, Keir (Ref. 5.20) measured values for n of 4.2 for aragonitic powder and 4.5 for synthetic calcite in his studies of the dissolution kinetics of calcium carbonate. Also, Morse (Ref. 5.21) has discussed measurements of calcium carbonate dissolution and reported values of n = 3.0, 4.5, and 5.2 for dissolution in the Pacific, Atlantic, and Indian Oceans, respectively.

Variability in the rate constant has also been found. For example, in the two studies just cited (Refs. 5.20, 5.21), substantial variation was exhibited in measured values of the rate constant.

In summary, Eq. 5-2 does provide a reasonably good description of mineral-dissolution kinetics, at least within limited ranges of conditions. However, it must be used with caution, particularly in extrapolating to conditions beyond the limits of experimental data.

5.2 UO_2-Dissolution Model Development

5.2.1 Review of Existing UO_2-Dissolution Models

A number of theoretical models have been developed over the years specifically for describing UO_2 dissolution in assorted aqueous media. Much of this work focused on the processing of uranium-bearing ores, although some recent studies have been directed toward dissolution of spent fuel in a high-level waste repository. Several of these studies are summarized as follows.

As mentioned, some dissolution models were unrelated to nuclear waste. In early work, Schortmann and DeSesa (Ref. 5.22) modeled the dissolution of UO_2 in carbonate/bicarbonate solutions. Effects of the ratio of UO_2 surface area to solution volume, oxygen partial pressure, temperature, and reagent concentrations were included. The dissolution of UO_2 in carbonate solutions was modeled by Pearson and Wadsworth (Ref. 5.23), who used absolute reaction-rate theory to describe dissolution kinetics in terms of competitive adsorption processes between oxygen and the undissociated H_2CO_3. Mackay and Wadsworth (Ref. 5.24) similarly used reaction-rate theory to describe UO_2 dissolution in sulfuric acid. The dissolution of UO_2 in perchloric acid was treated by Kanevskii and Filippov (Ref. 5.25) using a heterogeneous-reaction-rate model, which involved detailed consideration of water chemistry. Models for UO_2 dissolution in acid and carbonate solutions

have been developed by Habashi and Thurston (Ref. 5.26). These models accounted for UO_2 surface area, oxygen partial pressure, hydrogen-ion concentration (for acid solutions), and carbonate-ion concentration (for carbonate solutions). Uraninite dissolution in water was studied by Grandstaff (Ref. 5.27), who developed a semi-empirical dissolution model that accounted for effects of various chemical species contained within the water as well as for effects of temperature and specimen surface area. A largely electrochemical model of UO_2 dissolution in ammonium carbonate was developed by Hiskey (Ref. 5.28) in which both electrode kinetics and adsorption were included.

Some dissolution models have also been developed that were specifically directed toward spent fuel. A "source term" for irradiated UO_2 in a repository was developed by Goodwin et al. (Ref. 5.29) using a largely nonphysical model. This work was based on container-lifetime estimates as well as the assumption that the UO_2 undergoes congruent dissolution to the limit defined by the thermodynamic solubility of uranium for the repository environment. Johnson et al. (Ref. 5.30) described a radionuclide-release model for spent fuel that applies one-dimensional transport equations and accounts for diffusion, convection, and sorption as well as radioactive decay and buildup. Their model is used in the probabilistic safety assessment code, SYVAC (Systems Variability Analysis Code). A model for the gamma-radiation-enhanced dissolution of UO_2, developed by Christensen (Ref. 5.31), describes dissolution that is initiated by reactions of H_2O_2, OH, and HO_2 radicals with the surface of the UO_2.

In summary, considerable effort has been devoted to studying UO_2 dissolution in aqueous solutions, primarily from the standpoint of processing uranium-bearing ores; however, an increasing amount of work has been directed toward gaining an understanding of the long-term behavior of spent fuel in a high-level waste repository.

5.2.2 Battelle UO_2-Dissolution Model

Modeling studies of UO_2 dissolution kinetics have been conducted at Battelle as an extension of previously reported work (Refs. 5.12, 5.13) on the dissolution of glass waste forms. As with those earlier studies, effects of water chemistry have been included in detail. In fact, the same water-chemistry model was used although it was extended to include uranium-bearing species. This model is described in Appendix D. A major difference in water-chemistry effects between glass and spent fuel is that the dissolving glass may significantly alter the ambient water chemistry, whereas by comparison, the dissolving UO_2, because of its relatively low solubility, does not.

The model used in the Battelle studies of UO_2 dissolution is given by Eq. 5-2, which can be expressed in the following form:

$$r = KC_o \left(1 - \frac{C}{C_o}\right)^n \qquad (5\text{-}3)$$

In this equation, r is the dissolution rate of the UO_2 per unit area of surface exposed to the solution, K is a rate constant, C is the instantaneous concentration of uranium in solution (assumed to be spatially invariant within the solution), and C_o is the saturation concentration of uranium for the specific solution composition with respect to the solidified UO_2. Effects of concomitant impurity dissolution (which are important for spent fuel) have not been considered. The advantage of expressing the dissolution rate as shown in Eq. 5-3 is that the units of the rate constant are independent of n. Eqs. 5-2 and 5-3 are equivalent only if C_o is constant. In general, the solubility of UO_2 is so low that the dissolution of UO_2 does not significantly affect the water chemistry, so variation of C_o may be neglected.

Values for K and n are not generally known. However, the rate constant, K, can be eliminated from consideration by "absorbing" it into the measure of time through the creation of a dimensionless time parameter, as was done for the analysis of glass waste forms (Refs. 5.12, 5.13). In addition, the value of n can simply be treated as a variable parameter. Of course, values of K and n can be determined, under given conditions, through direct comparison with experimental data.

Although Eq. 5-3 describes UO_2 dissolution kinetics, its use does not imply any given mechanism for dissolution. However, the dominant kinetics, known independently of this expression, is likely to be an interface-reaction process (because of the low UO_2 solubility). Experimental measurement of n may give some indication of just what that process may be.

Assuming that dissolution takes place into a closed volume, V, of solution, the rate of change of C with time can be expressed as

$$dC/dt = Sr/V \qquad (5\text{-}4)$$

where S is the UO_2 surface area exposed to the solution. As discussed earlier in reference to Eq. 5-2, it is assumed in Eq. 5-4 that the solution contains no "sources" or "sinks" for uranium (such as loss due to precipitation as part of a more stable mineral).

5.3 Application of UO_2 Dissolution Model

The dissolution model described above has been applied to dissolution of UO_2 in both pure water and Grande Ronde basalt groundwater. The results of these calculations are shown in Figures 5.1 through 5.4.

In all these figures, times are expressed as dimensionless normalized times defined as KSt/V. In these terms, the unit of normalized time is the characteristic time for saturation of the solution if n = 1 in Eq. 5-3. The concentration of uranium in solution is specified in units of molality, and dissolution rate is shown as the derivative of concentration with resepct to normalized time.

In Figures 5.1 and 5.2, the dissolution rate and uranium concentration in solution are shown as functions of time for dissolution in pure water at pe = 2. These results were calculated from Eq. 5-3 with various values of n. In Figures 5.3 and 5.4, we show the results of similar calculations for synthetic Grande Ronde basalt groundwater (Ref. 5.32) at pe = 0. Equilibrium solubilities of uranium were calculated to be 2.05×10^{-8} molal for pure water and 3.42×10^{-7} molal for synthetic Grande Ronde basalt groundwater.

While Figures 5.1 and 5.2 differ from Figures 5.3 and 5.4 in terms of their scales, the similarities of the plots are perhaps more striking than the differences. In both cases, the solubility of uranium is sufficiently low such that the water chemistry is not significantly disturbed by the addition of uranium. As a result, C_o is essentially constant. If the uranium concentrations and dissolution rates had been divided by C_o, Figures 5.1 and 5.2 would be nearly identitical to Figures 5.3 and 5.4. This result is notably different from results obtained previously for dissolution of waste glasses, but it is simply the result of the lower solubility of uranium (Ref. 5.12).

5.4 References for Chapter 5

(5.1) K. Stephen, L. Boesch, B. Crane, R. Johnson, R. Moler, S. Smith, and L. Zaremba, "Methodologies for Assessing Long-Term Performance of High-Level Radioactive Waste Packages," NUREG/CR-4477, ATR-85(5810-01)IND (The Aerospace Corp., Washington, DC, 1986), pp. 5-35.

(5.2) A. C. Lasaga, "Chemical Kinetics of Water-Rock Interactions", J. Geophys. Res. 89, 4009 (1984).

(5.3) R. A. Berner, 'Kinetics of Weathering and Diagenesis", in: Rev. in Mineralogy, Vol. 8, Kinetics of Geochemical Processes, A. C. Lasaga and R. J. Kirkpatrick (eds.) (Mineralogical Soc. of Am., Washington, DC, 1981), p. 111.

(5.4) W. E. Dibble, Jr. and W. A. Tiller, "Non-Equilibrium Water/Rock Interactions-I. Model for Interface-Controlled Reactions, Geochim. Cosmochim. Acta 45, 79 (1981).

(5.5) J. S. Newman, Electrochemical Systems (Prentice-Hall, Inc., Englewood Cliffs, NJ, 1973), pp. 217 ff.

(5.6) A. E. Nielsen, Kinetics of Precipitation (Pergamon Press Ltd., Oxford, UK, 1964), p. 121.

(5.7) R. A. Berner, "Rate Control of Mineral Dissolution Under Earth Surface Conditions", Am. J. Sci. 278, 1235 (1978).

(5.8) R. S. Forsyth, L. O. Werme, and J. Bruno, "The Corrosion of Spent UO_2 Fuel in Synthetic Groundwater", J. Nucl. Mater. 138, 1 (1986).

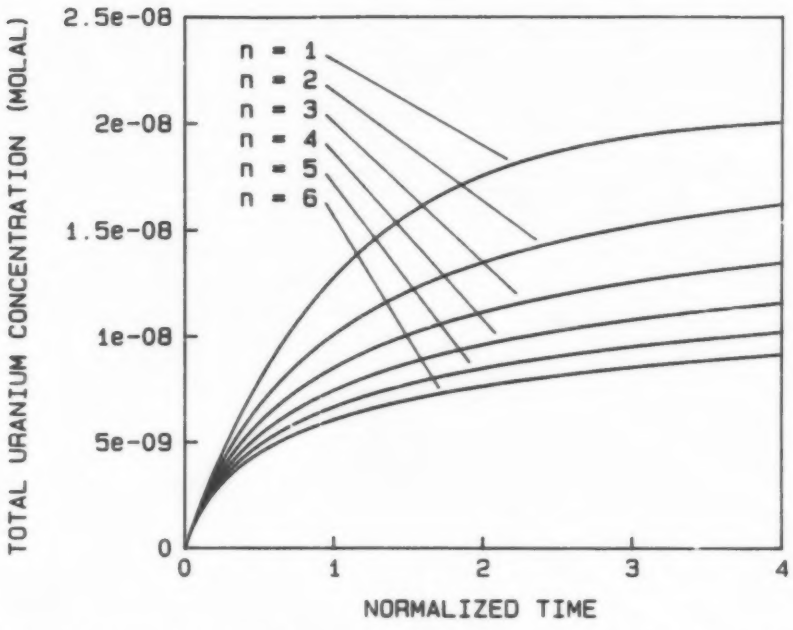

Figure 5.1. Calculated total uranium concentration as a function of time for various values of the kinetic exponent n. Solvent is pure water at pe = 2.

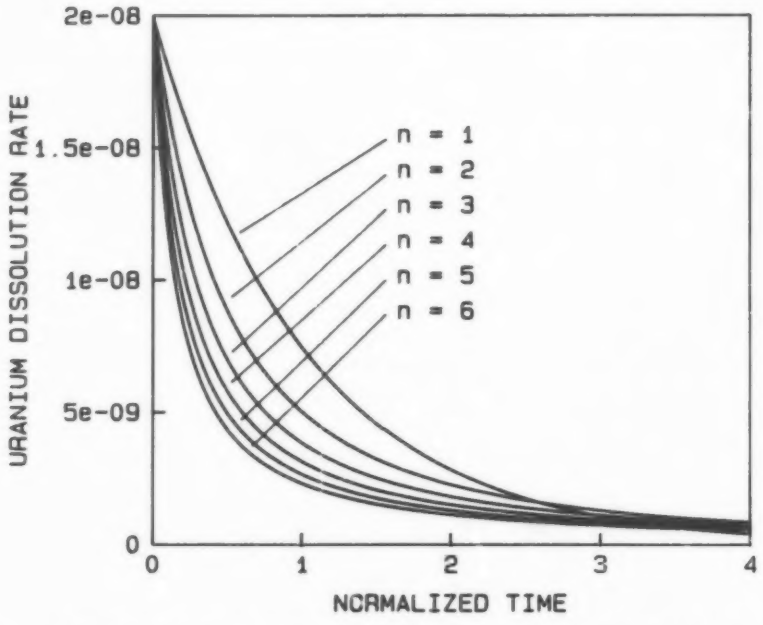

Figure 5.2. Calculated uranium dissolution rate as a function of time for various values of the kinetic exponent n. Solvent is pure water at pe = 2.

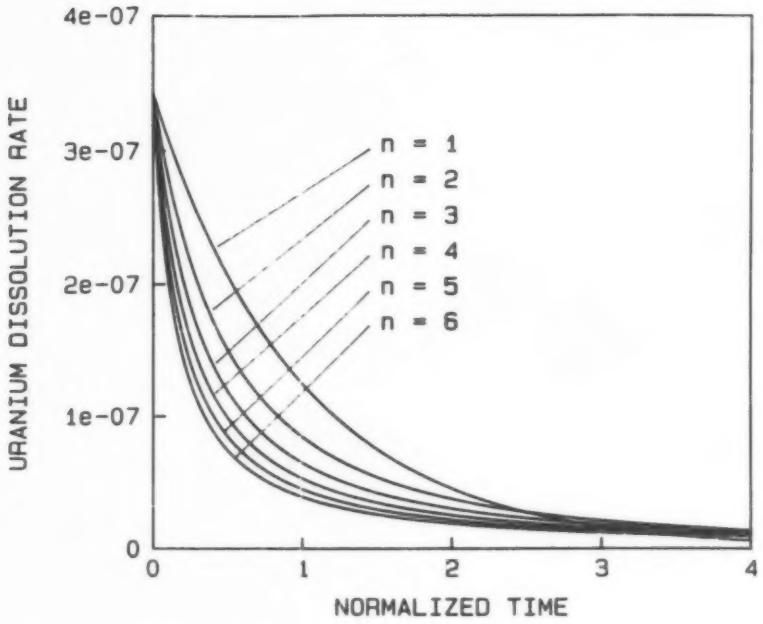

Figure 5.3. Calculated total uranium concentration as a function of time for various values of the kinetic exponent n. Solvent is synthetic Grande Ronde basalt groundwater at pe = 0.

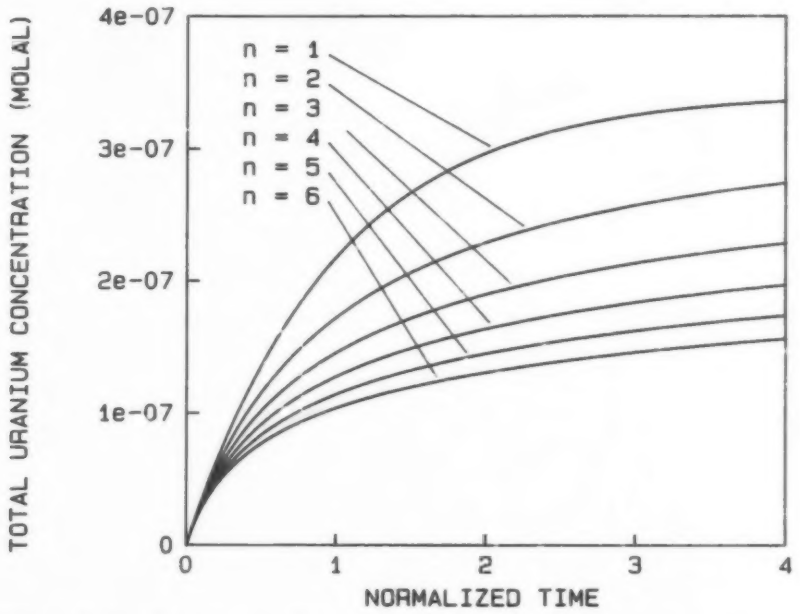

Figure 5.4. Calculated uranium dissolution rate as a function of time for various values of the kinetic exponent n. Solvent is synthetic Grande Ronde basalt groundwater at pe = 0.

(5.9) J. A. van Lier, P. L. de Bruyn, and J. Th. G. Overbeek, "The Solubility of Quartz", J. Phys. Chem. 64, 1675 (1960).

(5.10) H. Kamiya and K. Shimokata, in: Proc. Int. Symp. Water-Rock Interaction, J. Cadek and T. Paces (eds.) (Geol. Sur., Prague, 1976).

(5.11) E. Busenberg and C. V. Clemency, "The Dissolution Kinetics of Feldspars at 25 C and 1 atm CO_2 Partial Pressure", Geochim. Cosmochim. Acta 40, 41 (1976).

(5.12) J. K. McCoy and A. J. Markworth, "Water Chemistry and Dissolution Kinetics of Waste-Form Glasses", J. Non-Crystal. Solids 89, 47 (1987).

(5.13) "Long-Term Performance of High-Level Glass-Waste Forms," D. Stahl (Compiler), NUREG/CR-4795, BMI-2143, in press, pp. 5-1 ff.

(5.14) Ibid., pp. 6-1 ff.

(5.15) F. Garisto and N. C. Garisto, "A UO_2 Solubility Function for the Assessment of Used Nuclear Fuel Disposal", Nucl. Sci. Eng. 90, 103 (1985).

(5.16) M. R. Schweingruber, "Evaluation of Solubility and Speciation of Actinides in Natural Groundwaters", Scientific Basis for Nuclear Waste Management V, W. Lutze (ed.) (Elsevier Science Publ. Co., Inc., New York, 1982), Mater. Res. Soc. Symp. Proc. Vol. 11, 679.

(5.17) P. Aagard and H. C. Helgeson, "Thermodynamic and Kinetic Constraints on Reaction Rates Among Minerals and Aqueous Solutions, I. Theoretical Considerations", Am. J. Sci. 282, 237 (1982).

(5.18) A. Lerman, Geochemical Processes--Water and Sediment Environments (John Wiley & Sons, Inc., New York, 1979), pp. 229 ff.

(5.19) J. Christoffersen and M. R. Christoffersen, "Kinetics of Dissolution of Calcium Hydroxyapatite", Faraday Discuss. Chem. Soc. 77, 235 (1984).

(5.20) R. S. Keir, "The Dissolution Kinetics of Biogenic Calcium Carbonates in Seawater", Geochim. Cosmochim. Acta 44, 241 (1980).

(5.21) J. W. Morse, "Dissolution Kinetics of Calcium Carbonate in Sea Water: VI. The Near-Equilibrium Dissolution Kinetics of Calcium Carbonate-Rich Deep Sea Sediments", Am. J. Sci. 278, 344 (1978).

(5.22) W. E. Schortmann and M. A. DeSesa, "Kinetics of the Dissolution of Uranium Dioxide in Carbonate-Bicarbonate Solutions", in: Proc. Second U.N. Conf. on the Peaceful Uses of Atomic Energy, Vol. 3, Processing of Raw Materials, (United Nations, Geneva, 1958), p. 333.

(5.23) R. L. Pearson and M. E. Wadsworth, "A Kinetic Study of the Dissolution of UO_2 In Carbonate Solution", Trans. Metall. Soc. of AIME 212, 294 (1958).

(5.24) T. L. Mackay and M. E. Wadsworth, "A Kinetic Study of the Dissolution of UO_2 in Sulfuric Acid", Trans. Metall. Soc. of AIME 212, 597 (1958).

(5.25) E. A. Kanevskii and A. P. Filippov, "Kinetics of the Interactions of UO_2 and Fe (III) in Perchloric Acid Solutions", Soviet Radiochem. 7, 205 (1965).

(5.26) F. Habashi and G. Thurston, "Kinetics and Mechanisms of the Dissolution of Uranium Dioxide", Energia Nucleare 14, 238 (1967).

(5.27) D. E. Grandstaff, "A Kinetic Study of the Dissolution of Uraninite", Econ. Geol. 71, 1493 (1976).

(5.28) J. B. Hiskey, "Kinetics of Uranium Dioxide Dissolution in Ammonium Carbonate", Trans. Instn. Min. Metall. (Sect. C: Mineral Process. Extr. Metall.) 88, C145 (1979).

(5.29) B. W. Goodwin, L. H. Johnson, and D. M. Wuschke, "Radionuclide Source Terms for Irradiated UO_2 Fuel", in: Proc. Workshop on Near-Field Phenomena in Geologic Repositories for Radioactive Waste (Nuclear Energy Agency, Organization for Economic Cooperation and Development, Paris, 1981), p. 33.

(5.30) L. H. Johnson, N. C. Garisto, and S. Stroes-Gascoyne, "Used-Fuel Dissolution Studies in Canada", in: Waste Management 85, Vol. 1--Waste Policies and Programs, High-Level Waste, R. G. Post (ed.), Proc. Symp. on Waste Manag. (Tucson, AZ, 1985), p. 479.

(5.31) H. Christensen and E. Bjergbakke, "Radiation Induced Dissolution of UO_2", in: Scientific Basis for Nuclear Waste Management X, J. K. Bates and W. B. Seefeldt (eds.) Mater. Res. Soc. Symp. Proc., Vol. 84, (Mater. Res. Soc., Pittsburgh, 1987), p 115.

(5.32) "Reference Material Chemistry--Synthetic Groundwater Composition", T. E. Jones, RHO-BW-ST-37 P (April 1982).

6. CONCLUSIONS

These experiments were conducted in order to generate some basic data on spent-fuel leach and dissolution characteristics and to identify areas of interest for future research. Simulated tuff, basalt, and brine groundwaters were tested to determine whether there were any major distinctions between the spent-fuel dissolution characteristics attributable to the expected chemical compositions of fluids from the proposed repository sites. There were some differences, but they were minor.

Past research has been conducted where experimental design did not appear to evenly remotely resemble scenarios applicable to the deep geologic repository environment. For example, Soxhlet-type (refluxing hydrothermal) experiments appear to overestimate groundwater flow rates. The intentional inclusion of oxygen seems unrealistic unless loss of containment occurs early after emplacement, except perhaps for the tuff repository, which will be located in the vadose zone. Other experimental programs have simply neglected to define the leaching environment, so it is impossible to understand which aspects of the deep geologic disposal scenario, if any, relate to the results. The group of experiments in the present study were designed specifically to relate to ambient, long-term conditions in a deep repository where groundwater flow rates are expected to be slow and where redox conditions will be influenced and perhaps buffered by the large amount of iron present in the repository environment from canisters, overpacks, and their corrosion products. Surface-area-to-volume ratio was included as a variable because the magnitude of this parameter in the repository environment depends upon numerous other parameters and cannot be specified with confidence.

The leach and dissolution characteristics of uranium are critical because many of the fission by-products and presumably all of the actinides are dissolved or dispersed in some way in the UO_2 matrix. Hence, these will be released congruently (at least initially, until other precipitation reactions take control) with uranium. Uranium release from both unirradiated and irradiated UO_2 appeared to be solubility controlled, and any relative leachate compositional effects on the uranium concentrations were not very pronounced. When leached in the presence of an external radiation field, unirradiated UO_2 gave rise to some highly elevated uranium concentrations in only the brine leachates. The effect was most pronounced in the high S/V experiments, although it was also evident at the lower S/V, and was first observed at a cumulative gamma dose rate of approximately 10^7 rads. The mechanism giving rise to these elevated uranium concentrations is unclear; however, two possibilities are suggested by the data. The preferred explanation is that gamma radiolysis produced species that oxidized some uranium, which then dissolved. A second possibility is that uranium was released as grains as opposed to truly dissolved species. Intergranular attack (IGA) is a well-known mechanism for the degradation of certain metallic alloys in certain chemical environments. Because of the granular structure of UO_2 fuel pellets, IGA may also apply to spent fuel. Both radiolysis and spent-fuel IGA are recommended as subjects for further research.

There appears to be a highly soluble component of cesium and iodine in spent fuel, and other studies have suggested that the percentage of a fuel's total inventory of volatile fission by-product occurring as part of this highly leachable fraction depends primarily upon fuel burn-up history. While the percentage of this mobile cesium and iodine appears fixed for a given fuel burn-up history, the total mass of either nuclide (and hence, the ultimate nuclide concentration in solution) depends greatly upon S/V ratio and is unconstrained by the solubility of a cesium or iodine solid phase. The major principles governing the dissolution of these radionuclides appear to be well recognized.

The results for strontium-90 were enigmatic. A strong leachate compositional effect was observed wherein the leaching of strontium in brine > tuff > deionized water > basalt groundwater. Overall, the data suggest non-equilibrium behavior. Because of its short half-life (30 years), strontium-90 is not a major issue in licensing, but it may be a good analogue for the much longer lived isotopes of radium.

The leaching of plutonium, americium, and curium was congruent with that of uranium at the outset, but then the transuranics appeared to equilibrate with phases having lower solubilities, hence reducing their concentrations in solution relative to uranium. The principal exception was the high S/V brine experiments, where fairly uniform transuranic concentrations were observed throughout the course of the experiment. These were low relative to the other leachates early in the experiment but relatively high by the conclusion. In all cases, the very low transuranic element concentrations in spent fuel leachates at the conclusion of the experiments suggest that transuranic release will probably conform to regulatory limits, at least in scenarios similar to this one. However, these experiments were conducted in anaerobic environments. This was shown by the platinum electrode measurements, but could also be deduced by the fact that leachates were equilibrated with metallic iron. It will be necessary in a license application to provide a convincing argument that anaerobic geochemical environments will prevail at the point of loss of containment, if release rates are based on low actinide concentrations such as those reported here.

To develop a predictive model for radionuclide release from spent fuel, a relatively simple, semi-empirical model was used to describe the dissolution kinetics. The model is based on analogous studies that have been conducted in the area of mineral-water interactions. Research focused on evaluating the effects of groundwater chemistry on dissolution kinetics using a Battelle-developed water chemistry model in conjunction with a crystal-dissolution model.

The model that was developed predicts that the effect of water chemistry on spent fuel dissolution is largely limited to affecting the saturation concentration of uranium in the aqueous solution. These results contrast sharply with those obtained previously for glass dissolution. The apparent cause of this different behavior is that glass dissolves in sufficient quantities and significantly changes the composition of the groundwater, while spent fuel dissolves only in small quantities, leaving the groundwater composition barely disturbed.

57

APPENDIX A

SPENT FUEL CHARACTERISTICS

SPENT FUEL CHARACTERISTICS

1. INTRODUCTION

The spent fuel used in the leaching experiments described in this report was obtained from one rod (F10) from an H.B. Robinson pressurized water reactor (PWR) fuel assembly. A sample from an adjacent rod (P8) in the same fuel assembly had been previously analyzed and the burnup was determined to be 30,920 MWD/MTU (Ref. A.1). This value, together with an initial U-235 fuel enrichment of 2.55 percent, was used to estimate the fission product inventories in the spent-fuel samples.

2. FISSION PRODUCT INVENTORY

The ORIGEN2 code was used to calculate the activity and mass of fission products in the fuel samples. A burnup of 30,920 MWD/MTU and an initial enrichment of 2.55 percent U-235 was used. This fuel was part of the initial core which first went critical in September 1970. Until January 1971, the reactor underwent low-power testing and generated an average of 2 percent maximum power output. From January 1971 until September 1971, the reactor still had low monthly power generation. Because this implies that there will be a low burnup rate in the fuel, the ORIGEN2 calculation only included the reactor operating history from September 1971 until shutdown for refueling in May 1974. The operating history depicted in Figure A.1 shows that the only significant outages occurred in 1973. Linear heat generation rates of 212 to 327 W/cm were used, but the duration of each period was adjusted to achieve the desired burnup. Impurities in the fuel were assumed to be the same as given in the "standard" PWR case. After the fuel was irradiated in the core, it was allowed to decay. The inventory of actinides plus daughters, activation products, and fission products present at 12.1 and 12.4 years after shutdown (corresponding to June and October 1986, respectively) was then determined.

The results of the calculation are given in Attachment A.1. The activities for the individual isotopes or elements are given in curies and the weights are given in grams. The elemental concentrations of the activation products, actinides plus daughters, and fission products are listed in grams per metric tonne of uranium (g/MTU).

To compare these estimated fission product inventories with the values measured for total cesium, iodine, strontium and the actinides uranium, plutonium, curium, and americium in our leaching experiments, the calculated values were converted for the total spent-fuel inventory used in the present study. These results are given in Table A.1.

H. B. Robinson Power History

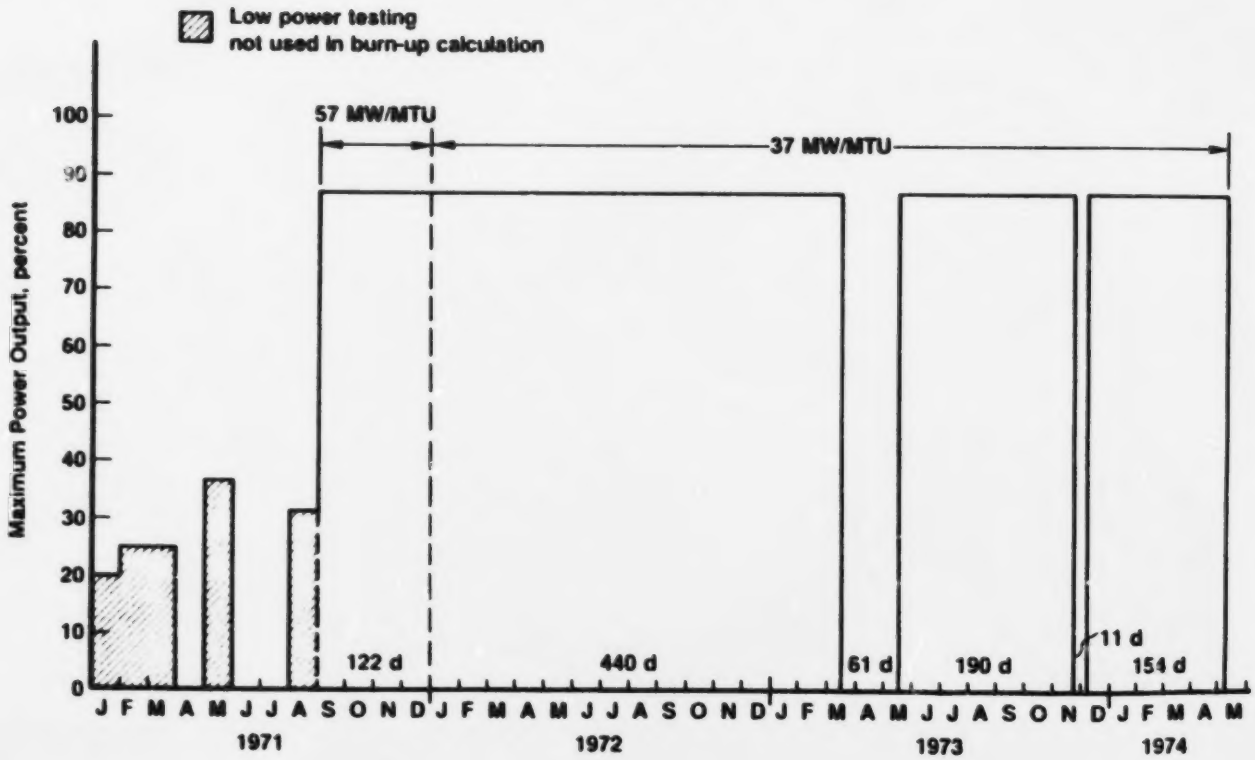

Figure A.1. H.B. Robinson PWR power history.

BEST COPY AVAILABLE

Table A.1. Spent-fuel inventory.*

Radionuclide	Calculated Inventory (g) 12.1 Year	12.4 Year
U-234	0.206	0.207
U-235	9.433	9.433
U-236	5.197	5.197
U-238	1534.617	1534.617
Pu-238	0.213	0.213
Pu-239	8.180	8.180
Pu-240	3.792	3.793
Pu-241	1.171	1.152
Pu-242	0.845	0.845
Am-241	0.972	0.989
Am-243	0.170	0.170
Cm-243	5.337×10^{-4}	5.294×10^{-4}
Cm-244	3.229×10^{-2}	3.189×10^{-2}
Sr-88	0.496	0.496
Sr-90	0.566	0.562
I-127	0.090	0.090
I-129	0.282	0.282
Cs-133	1.693	1.693
Cs-134	0.003	0.003
Cs-135	0.446	0.446
Cs-137	1.364	1.353

* Total quantity of spent fuel used = 1616.918 g.

3. REFERENCES FOR APPENDIX A

(A.1) L. M. Lowry, A. J. Markworth, J. S. Perrin, and M. P. Manahan, "Evaluating Strength and Ductility of Irradiated Zircaloy", NUREG/CR-1729, BMI-2066 (1981).

(A.2) A. G. Cross, "ORIGEN2 - A Revised and Updated Version of the Oak Ridge Isotope Generation and Depletion Code," ORNL-5621 (July 1980).

(A.3) A. G. Croff, "A User's Manual for the ORIGEN2 Computer Code," ORNL/TM-7175 (July 1980).

(A.4) A. G. Croff, M. A. Bjerke, G. W. Morrison, and L. M. Petrie, "Revised Uranium-Plutonium Cycle PWR and BWR Models for the ORIGEN Computer Code," ONRL/TM-6051 (September 1978).

(A.5) A. G. Croff and M. A. Bjerke, "Alternative Fuel Cycle PWR Models for the ORIGEN Computer Code," ORNL/TM-7005 (February 1980).

(A.6) A. G. Croff, R. L. Haese, and N. B. Gove, "Updated Decay and Photon Libraries for the ORIGEN Code," ORNL/TM-6055 (February 1979).

* IRRADIATION OF ONE METRIC TON OF PWRU FUEL ACTIVATION PRODUCTS
POWER= 1.00000E+00 MW, BURNUP= 1.00000E+00 MWD, FLUX= 1.00E+00 N/CM**2-SEC

5 SUMMARY TABLE: CONCENTRATIONS, GRAMS
ONE METRIC TON OF PWRU FUEL

		12.1YR	12.4YR
H	1	1.110E-02	1.110E-02
H	3	1.433E-02	1.407E-02
HE	3	1.416E-02	1.442E-02
HE	4	2.516E+00	2.516E+00
LI	6	7.419E-03	7.419E-03
LI	7	1.064E+00	1.064E+00
BE	9	6.730E-04	6.730E-04
BE	10	8.062E-05	8.062E-05
B	11	8.282E-01	8.282E-01
C	12	8.832E+01	8.832E+01
C	13	8.839E+00	8.839E+00
C	14	1.427E-01	1.427E-01
N	14	2.476E+01	2.476E+01
N	15	1.059E-01	1.059E-01
O	16	1.341E+05	1.341E+05
O	17	5.430E+01	5.430E+01
O	18	3.085E+02	3.085E+02
F	19	1.070E+01	1.070E+01
NE	20	4.127E-04	4.127E-04
NE	21	1.659E-05	1.659E-05
NE	22	2.467E-05	2.467E-05
NA	23	1.496E+01	1.496E+01
MG	24	1.596E+00	1.596E+00
MG	25	2.057E-01	2.057E-01
MG	26	2.355E-01	2.355E-01
AL	27	1.669E+01	1.669E+01
SI	28	1.112E+01	1.112E+01
SI	29	5.873E-01	5.873E-01
SI	30	4.006E-01	4.006E-01
P	31	3.498E+01	3.498E+01
S	32	1.578E-02	1.578E-02
CL	35	3.577E+00	3.577E+00
CL	36	3.899E-01	3.899E-01
CL	37	1.343E+00	1.343E+00
AR	38	1.519E-03	1.519E-03
K	40	6.980E-04	6.980E-04
K	41	2.638E-05	2.638E-05
CA	40	1.930E+00	1.930E+00
CA	41	1.905E-03	1.905E-03
CA	42	1.351E-02	1.351E-02
CA	43	2.763E-03	2.763E-03
CA	44	4.578E-02	4.578E-02
CA	46	8.051E-05	8.051E-05
CA	48	4.535E-03	4.535E-03
SC	45	1.138E-04	1.138E-04
TI	46	7.908E-02	7.908E-02
TI	47	7.285E-02	7.285E-02
TI	48	7.248E-01	7.248E-01
TI	49	6.898E-02	6.898E-02
TI	50	5.460E-02	5.460E-02
V	50	6.104E-03	6.104E-03
V	51	2.965E+00	2.965E+00

BEST COPY AVAILABLE

• IRRADIATION OF ONE METRIC TON OF PWRU FUEL ACTIVATION PRODUCTS
POWER= 1.00000E+00 MW, BURNUP= 1.00000E+00 MWD, FLUX= 1.00E+00 N/CM**2-SEC

5 SUMMARY TABLE: CONCENTRATIONS, GRAMS
ONE METRIC TON OF PWRU FUEL

	12 1YR	12 4YR
CR 50	1.608E-01	1.608E-01
CR 52	3.355E+00	3.355E+00
CR 53	3.995E-01	3.995E-01
CR 54	1.161E-01	1.161E-01
MN 55	1.640E+00	1.640E+00
FE 54	1.004E+00	1.004E+00
FE 55	1.756E-04	1.608E-04
FE 56	1.650E+01	1.650E+01
FE 57	5.098E-01	5.098E-01
FE 58	6.173E-02	6.173E-02
CO 59	8.831E-01	8.831E-01
CO 60	2.059E-02	1.971E-02
NI 58	1.596E+01	1.596E+01
NI 59	1.786E-01	1.786E-01
NI 60	6.480E+00	6.481E+00
NI 61	3.248E-01	3.248E-01
NI 62	8.804E-01	8.804E-01
NI 63	2.754E-02	2.748E-02
NI 64	2.433E-01	2.433E-01
CU 63	5.796E-01	6.796E-01
CU 65	3.632E-01	3.632E-01
ZN 64	1.910E+01	1.910E+01
ZN 66	1.131E+01	1.131E+01
ZN 67	1.671E+00	1.671E+00
ZN 68	7.873E+00	7.873E+00
ZN 70	2.671E-01	2.671E-01
GA 69	3.481E-02	3.481E-02
GA 71	5.959E-05	5.959E-05
GE 70	2.398E-04	2.398E-04
ZR 92	1.132E-04	1.132E-04
MO 92	1.417E+00	1.417E+00
MO 93	6.348E-04	6.347E-04
MO 94	9.094E-01	9.094E-01
MO 95	1.410E+00	1.410E+00
MO 96	1.804E+00	1.804E+00
MO 97	9.836E-01	9.836E-01
MO 98	2.462E+00	2.462E+00
MO100	9.959E-01	9.959E-01
TC 99	1.708E-03	1.708E-03
RU100	2.118E-04	2.118E-04
RU101	3.763E-03	3.763E-03
RU102	1.482E-04	1.482E-04
PD108	2.021E-04	2.029E-04
PD110	9.201E-05	9.201E-05
AG107	4.381E-02	4.381E-02
AG108M	4.994E-04	4.985E-04
AG109	1.749E-02	1.749E-02
CD108	3.055E-01	3.055E-01
CD108	2.197E-01	2.197E-01
CD110	2.912E+00	2.912E+00
CD111	3.047E+00	3.047E+00
CD112	6.140E+00	6.140E+00

Attachment A.1. Continued

BEST COPY AVAILABLE

ACTIVATION PRODUCTS

* IRRADIATION OF ONE METRIC TON OF PWRU FUEL
POWER= 1.00000E+00 MW, BURNUP= 1.00000E+00 MWD, FLUX= 1.00E+00 N/CM**2-SEC

5 SUMMARY TABLE: CONCENTRATIONS, GRAMS
ONE METRIC TON OF PWRU FUEL

	12 1YR	12 4YR
CD113	9.703E-04	9.703E-04
CD114	1.028E+01	1.028E+01
CD116	1.928E+00	1.928E+00
IN113	6.212E-02	6.212E-02
IN115	2.556E-02	2.556E-02
SN112	3.698E-02	3.698E-02
SN114	4.788E-02	4.788E-02
SN115	1.310E-02	1.310E-02
SN116	2.464E+00	2.464E+00
SN117	3.382E-01	3.382E-01
SN118	9.619E-01	9.619E-01
SN119	3.521E-01	3.521E-01
SN120	1.310E+00	1.310E+00
SN122	1.888E-01	1.888E-01
SN124	2.314E-01	2.314E-01
SB121	1.892E-03	1.892E-03
SB123	2.047E-04	2.047E-04
SB125	8.494E-05	7.821E-05
TE122	1.331E-04	1.331E-04
TE125	2.324E-03	2.331E-03
TE126	2.485E-05	2.485E-05
EU153	2.280E-03	2.280E-03
EU154	3.392E-04	3.303E-04
EU155	5.474E-05	5.228E-05
GD152	6.836E-05	6.836E-05
GD154	3.677E-02	3.678E-02
GD155	4.216E-04	4.241E-04
GD156	8.114E-01	8.114E-01
GD157	2.627E-04	2.627E-04
GD158	1.052E+00	1.052E+00
GD160	5.489E-01	5.489E-01
TB159	4.057E-02	4.057E-02
DY160	5.413E-03	5.413E-03
DY161	4.256E-03	4.256E-03
DY162	2.394E-03	2.394E-03
DY163	1.318E-03	1.318E-03
DY164	1.465E-04	1.465E-04
HO165	3.002E-04	3.002E-04
ER166	4.177E-05	4.177E-05
TA181	2.735E-04	2.735E-04
W180	2.221E-03	2.221E-03
W182	3.405E-01	3.405E-01
W183	3.825E-01	3.825E-01
W184	6.891E-01	6.891E-01
W186	3.873E-01	3.873E-01
RE185	5.276E-03	5.276E-03
RE187	1.601E-01	1.601E-01
OS186	2.934E-03	2.934E-03
OS188	3.150E-02	3.150E-02
OS189	9.552E-04	9.552E-04
OS190	1.360E-04	1.360E-04
PB204	1.375E-02	1.375E-02

Attachment A.1. Continued

BEST COPY AVAILABLE

BLANK PAGE

ACTIVATION PRODUCTS

* IRRADIATION OF ONE METRIC TON OF PWRU FUEL
POWER= 1 00000E+00 MW, BURNUP= 1 00000E+00 MWD, FLUX= 1 00E+00 N/CM**2-SEC

5 SUMMARY TABLE: CONCENTRATIONS, GRAMS
ONE METRIC TON OF PWRU FUEL

	12 1YR	12 4YR
PB205	3 447E-05	3 447E-05
PB206	2 246E-01	2 246E-01
PB207	2 354E-01	2 354E-01
PB208	5 263E-01	5 263E-01
BI209	3 999E-01	3 999E-01
BI210M	3 274E-05	3 274E-05
SUMTOT	1 348E+05	1 348E+05
TOTAL	1 348E+05	1 348E+05

Attachment A.1. Continued

BEST COPY AVAILABLE

* IRRADIATION OF ONE METRIC TON OF PWRU FUEL ACTIVATION PRODUCTS
POWER= 1 00000E+00 MW. BURNUP= 1 00000E+00 MWD. FLUX= 1 00E+00 N/CM**2-SEC

5 SUMMARY TABLE: CONCENTRATIONS, GRAMS
ONE METRIC TON OF PWRU FUEL

	12.1YR	12.4YR
H	2.545E-02	2.518E-02
HE	2.530E+00	2.531E+00
LI	1.072E+00	1.072E+00
BE	7.537E-04	7.537E-04
B	8.282E-01	8.282E-01
C	9.731E+01	9.731E+01
N	2.487E+01	2.487E+01
O	1.344E+05	1.344E+05
F	1.070E+01	1.070E+01
NE	4.539E-04	4.539E-04
NA	1.496E+01	1.496E+01
MG	2.037E+00	2.037E+00
AL	1.669E+01	1.669E+01
SI	1.211E+01	1.211E+01
P	3.498E+01	3.498E+01
S	1.580E-02	1.590E-02
CL	5.310E+00	5.310E+00
AR	1.539E-03	1.539E-03
K	7.244E-04	7.244E-04
CA	1.999E+00	1.999E+00
SC	1.138E-04	1.138E-04
TI	1.000E+00	1.000E+00
V	2.971E+00	2.971E+00
CR	4.032E+00	4.032E+00
MN	1.840E+00	1.840E+00
FE	1.807E+01	1.807E+01
CO	9.036E-01	9.028E-01
NI	2.410E+01	2.410E+01
CU	1.043E+00	1.043E+00
ZN	4.022E+01	4.022E+01
GA	3.487E-02	3.487E-02
GE	2.407E-04	2.407E-04
ZR	1.318E-04	1.318E-04
MO	9.983E+00	9.983E+00
TC	1.708E-03	1.708E-03
RU	4.123E-03	4.123E-03
PD	2.947E-04	2.956E-04
AG	6.180E-02	6.180E-02
CD	2.483E+01	2.483E+01
IN	8.768E-02	8.768E-02
SN	5.944E+00	5.944E+00
SB	2.181E-03	2.175E-03
TE	2.494E-03	2.500E-03
EU	2.674E-03	2.663E-03
GD	2.450E+00	2.450E+00
TB	4.057E-02	4.057E-02
DY	1.353E-02	1.353E-02
HO	3.021E-04	3.021E-04
ER	4.344E-05	4.344E-05
TA	2.735E-04	2.735E-04
W	1.802E+00	1.802E+00
RE	1.654E-01	1.654E-01
OS	3.553E-02	3.553E-02
PB	1.000E+00	1.000E+00
BI	4.000E-01	4.000E-01
SUMTOT	1.348E+05	1.348E+05

Attachment A.1. Continued

BEST COPY AVAILABLE

90

ACTIVATION PRODUCTS

* IRRADIATION OF ONE METRIC TON OF PWRU FUEL
POWER= 1.00000E+00 MW, BURNUP= 1.00000E+00 MWD, FLUX= 1.00E+00 N/CM**2-SEC

7 SUMMARY TABLE: RADIOACTIVITY CURIES
ONE METRIC TON OF PWRU FUEL

	12 1YR	12 4YR
H 3	1.384E+02	1.358E+02
BE 10	1.802E-06	1.802E-06
C 14	6.363E-01	6.363E-01
SI 32	3.163E-08	3.162E-08
P 32	3.163E-08	3.162E-08
CL 36	1.287E-02	1.287E-02
AR 39	7.482E-05	7.475E-05
CA 41	2.052E-04	2.052E-04
MN 54	9.259E-05	7.087E-05
FE 55	4.391E-01	4.021E-01
CO 60	2.329E+01	2.230E+01
NI 59	1.353E-02	1.353E-02
NI 63	1.700E+00	1.695E+00
ZN 65	4.882E-04	3.466E-04
NB 94	1.073E-06	1.073E-06
MO 93	6.978E-04	6.978E-04
TC 99	2.897E-05	2.897E-05
AG108	1.159E-03	1.157E-03
AG108M	1.302E-02	1.300E-02
AG109M	1.692E-03	1.413E-03
AG110	1.186E-07	8.491E-08
AG110M	8.918E-06	6.384E-06
CD109	1.692E-03	1.413E-03
SN119M	2.515E-05	1.788E-05
SN121M	5.813E-04	5.787E-04
SB125	8.774E-02	8.079E-02
TE125M	2.111E-02	1.971E-02
EU152	1.529E-06	1.503E-06
EU154	9.160E-02	8.919E-02
EU155	2.547E-02	2.432E-02
GD153	7.083E-06	5.015E-06
HO166M	3.484E-06	3.483E-06
TL206	1.851E-08	1.851E-08
BI208	2.824E-08	2.824E-08
BI210M	1.859E-08	1.859E-08
SUMTOT	1.647E+02	1.611E+02
TOTAL	1.647E+02	1.611E+02

TOTAL	1.348E+05	1.348E+05

CUMULATIVE TABLE TOTALS

AP+FP	1.348E+05	1.348E+05
ACT+FP	0.0	0.0
AP+ACT+FP	1.348E+05	1.348E+05

Attachment A.1. Continued

BEST COPY AVAILABLE

* IRRADIATION OF ONE METRIC TON OF PWRU FUEL
POWER= 1.00000E+00 MW, BURNUP= 1.00000E+00 MWD, FLUX= 1.00E+00 N/CM**2-SEC

ACTIVATION PRODUCTS

7 SUMMARY TABLE: RADIOACTIVITY, CURIES
ONE METRIC TON OF PWRU FUEL

	12.1YR	12.4YR
H	1.384E+02	1.358E+02
BE	1.802E-06	1.802E-06
C	6.363E-01	6.363E-01
SI	3.163E-08	3.162E-08
P	3.163E-08	3.162E-08
CL	1.287E-02	1.287E-02
AR	7.482E-05	7.475E-05
CA	2.052E-04	2.052E-04
MN	9.259E-05	7.087E-05
FE	4.391E-01	4.021E-01
CO	2.329E+01	2.230E+01
NI	1.713E+00	1.709E+00
ZN	4.882E-04	3.466E-04
NB	1.078E-06	1.078E-06
MO	6.978E-04	6.978E-04
TC	2.897E-05	2.897E-05
AG	1.588E-02	1.557E-02
CD	1.692E-03	1.413E-03
SN	6.065E-04	5.966E-04
SB	8.774E-02	8.079E-02
TE	2.141E-02	1.971E-02
EU	1.171E-01	1.135E-01
GD	7.083E-06	5.015E-06
HO	3.484E-06	3.483E-06
TL	1.851E-08	1.851E-08
BI	4.682E-08	4.682E-08
SUMTOT	1.647E+02	1.611E+02
TOTAL	1.647E+02	1.611E+02

CUMULATIVE TABLE TOTALS

AP+FP	1.647E+02	1.611E+02
ACT+FP	0.0	0.0
AP+ACT+FP	1.647E+02	1.611E+02

BEST COPY AVAILABLE

* IRRADIATION OF ONE METRIC TON OF PWRU FUEL
POWER= 1.00000E+00 MW, BURNUP= 1.00000E+00 MWD, FLUX= 1.00E+00 N/CM**2-SEC

ACTINIDES·DAUGHTERS

5 SUMMARY TABLE: CONCENTRATIONS, GRAMS
ONE METRIC TON OF PWRU FUEL

	12.1YR	12.4YR
HE 4	1.226E+00	1.244E+00
TH230	4.889E-03	5.006E-03
TH232	1.293E-03	1.324E-03
PA231	2.511E-04	2.530E-04
U232	1.256E-03	1.256E-03
U233	2.522E-03	2.564E-03
U234	1.276E+02	1.280E+02
U235	5.834E+03	5.834E+03
U236	3.214E+03	3.214E+03
U238	9.491E+05	9.491E+05
NP236	3.775E-04	3.775E-04
NP237	4.021E+02	4.025E+02
PU238	1.320E+02	1.317E+02
PU239	5.059E+03	5.059E+03
PU240	2.345E+03	2.346E+03
PU241	7.240E+02	7.128E+02
PU242	5.226E+02	5.226E+02
PU244	2.952E+02	2.952E-02
AM241	6.010E+02	6.121E+02
AM242M	8.031E-01	8.019E-01
AM243	1.052E+02	1.052E+02
CM242	1.943E-03	1.941E-03
CM243	3.301E-01	3.274E-01
CM244	1.997E+01	1.972E+01
CM245	1.174E+00	1.174E+00
CM246	1.505E-01	1.505E-01
CM247	1.432E-03	1.432E-03
SUMTOT	9.682E+05	9.682E+05
TOTAL	9.682E+05	9.682E+05

Attachment A.1. Continued

BEST COPY AVAILABLE

* IRRADIATION OF ONE METRIC TON OF PWRU FUEL
POWER= 1.00000E+00 MW, BURNUP= 1.00000E+00 MWD, FLUX= 1.00E+00 N/CM**2-SEC ACTINIDES+DAUGHTERS

5 SUMMARY TABLE: CONCENTRATIONS, GRAMS
ONE METRIC TON OF PWRU FUEL

	12.1YR	12.4YR
HE	1.226E+00	1.244E+00
TH	6.227E-03	6.376E-03
PA	2.648E-04	2.667E-04
U	9.583E+05	9.583E+05
NP	4.021E+02	4.025E+02
PU	8.783E+03	8.772E+03
AM	7.071E+02	7.182E+02
CM	2.163E+01	2.138E+01
SUMTOT	9.682E+05	9.682E+05
TOTAL	9.682E+05	9.682E+05

CUMULATIVE TABLE TOTALS

AP+FP	1.348E+05	1.348E+05
ACT+FP	9.682E+05	9.682E+05
AP+ACT+FP	1.103E+06	1.103E+06

Attachment A.1. Continued

BEST COPY AVAILABLE

* IRRADIATION OF ONE METRIC TON OF PWRU FUEL ACTINIDES+DAUGHTERS
POWER= 1 00000E+00 MW, BURNUP= 1 00000E+00 MWD, FLUX= 1 00E+00 N/CM**2-SEC

7 SUMMARY TABLE: RADIOACTIVITY, CURIES
ONE METRIC TON OF PWRU FUEL

	12 1YR	12 4YR
TL208	9 189E-03	9 283E-03
PB212	2 557E-02	2 584E-02
BI212	2 557E-02	2 584E-02
PO212	1 639E-02	1 655E-02
PO216	2 557E-02	2 584E-02
RN220	2 557E-02	2 584E-02
RA224	2 557E-02	2 584E-02
TH228	2 557E-02	2 572E-02
TH230	9 872E-05	1 011E-04
TH231	1 262E-02	1 262E-02
TH234	3 192E-01	3 192E-01
PA231	1 187E-05	1 195E-05
PA233	2 836E-01	2 837E-01
PA234M	3 192E-01	3 192E-01
PA234	4 150E-04	4 150E-04
U232	2 688E-02	2 689E-02
U233	2 442E-05	2 483E-05
U234	7 979E-01	8 000E-01
U235	1 262E-02	1 262E-02
U236	2 080E-01	2 080E-01
U237	1 830E+00	1 802E+00
U238	3 192E-01	3 192E-01
NP237	2 836E-01	2 838E-01
NP238	3 904E-02	3 898E-02
NP239	2 099E+01	2 099E+01
PU236	3 117E-02	2 876E-02
PU238	2 261E+03	2 255E+03
PU239	3 146E+02	3 146E+02
PU240	5 346E+02	5 347E+02
PU241	7 461E+04	7 344E+04
PU242	1 996E+00	1 996E+00
AM241	2 064E+03	2 102E+03
AM242M	7 808E+00	7 796E+00
AM242	7 769E+00	7 758E+00
AM243	2 099E+01	2 099E+01
CM242	6 426E+00	6 419E+00
CM243	1 705E+01	1 691E+01
CM244	1 617E+03	1 596E+03
CM245	2 016E-01	2 016E-01
CM246	4 624E-02	4 624E-02
CF250	8 899E-06	8 745E-06
SUMTOT	8 149E+04	8 033E+04
TOTAL	8 149E+04	8 033E+04

Attachment A.1. Continued

BEST COPY AVAILABLE

* IRRADIATION OF ONE METRIC TON OF PWRU FUEL ACTINIDES+DAUGHTERS
POWER= 1.00000E+00 MW, BURNUP= 1.00000E+00 MWD, FLUX= 1.00E+00 N/CM**2-SEC

7 SUMMARY TABLE: RADIOACTIVITY, CURIES
ONE METRIC TON OF PWRU FUEL

	12 1YR	12 4YR
TL	9.192E-03	9.287E-03
PB	2.558E-02	2.584E-02
BI	2.558E-02	2.584E-02
PO	4.196E-02	4.239E-02
RN	2.558E-02	2.584E-02
RA	2.558E-02	2.584E-02
TH	3.575E-01	3.577E-01
PA	6.032E-01	6.034E-01
U	3.195E+00	3.168E+00
NP	2.131E+01	2.131E+01
PU	7.773E+04	7.655E+04
AM	2.100E+03	2.138E+03
CM	1.640E+03	1.620E+03
CF	1.301E-05	1.279E-05
SUMTOT	8.149E+04	8.033E+04
TOTAL	8.149E+04	8.033E+04

CUMULATIVE TABLE TOTALS

AP+FP	1.647E+02	1.611E+02
ACT+FP	8.149E+04	8.033E+04
AP+ACT+FP	8.166E+04	8.049E+04

BEST COPY AVAILABLE

• IRRADIATION OF ONE METRIC TON OF PWRU FUEL FISSION PRODUCTS
POWER= 1.00000E+00 MW, BURNUP= 1.00000E+00 MWD, FLUX= 1.00E+00 N/CM**2-SEC

5 SUMMARY TABLE: CONCENTRATIONS, GRAMS
ONE METRIC TON OF PWRU FUEL

	12.1YR	12.4YR
H 3	2.784E-02	2.733E-02
LI 6	1.584E-04	1.584E-04
LI 7	9.434E-06	9.434E-06
BE 9	1.815E-05	1.815E-05
BE 10	1.212E-04	1.212E-04
C 14	2.447E-05	2.447E-05
GE 72	2.205E-02	2.205E-02
GE 73	4.404E-02	4.404E-02
GE 74	9.354E-02	9.354E-02
AS 75	1.907E-01	1.907E-01
GE 76	4.609E-01	4.609E-01
SE 76	5.376E-03	5.376E-03
SE 77	9.367E-01	9.367E-01
SE 78	2.256E+00	2.256E+00
SE 79	5.428E+00	5.428E+00
BR 79	7.916E-04	8.107E-04
SE 80	1.225E+01	1.225E+01
KR 80	2.325E-04	2.325E-04
BR 81	1.975E+01	1.975E+01
KR 81	2.410E-05	2.410E-05
SE 82	3.038E+01	3.038E+01
KR 82	9.404E-01	9.404E-01
KR 83	3.640E+01	3.640E+01
KR 84	1.016E+02	1.016E+02
KR 85	9.632E+00	9.429E+00
RB 85	9.788E+01	9.808E+01
KR 86	1.672E+02	1.672E+02
SR 86	3.815E-01	3.815E-01
RB 87	2.142E+02	2.142E+02
SR 87	3.239E-03	3.239E-03
SR 88	3.069E+02	3.069E+02
Y 89	3.994E+02	3.994E+02
SR 90	3.501E+02	3.473E+02
Y 90	8.779E-02	8.710E-02
ZR 90	1.355E+02	1.383E+02
ZR 91	5.212E+02	5.212E+02
ZR 92	5.701E+02	5.701E+02
ZR 93	6.468E+02	6.468E+02
NB 93	1.274E-03	1.325E-03
NB 93M	2.735E-03	2.781E-03
ZR 94	6.718E+02	6.718E+02
NB 94	7.934E-04	7.933E-04
MO 95	6.901E+02	6.901E+02
ZR 96	7.331E+02	7.331E+02
MO 96	3.231E+01	3.231E+01
MO 97	7.324E+02	7.324E+02
MO 98	7.680E+02	7.680E+02
TC 98	6.102E-03	6.102E-03
TC 99	7.181E+02	7.181E+02
RU 99	3.151E-02	3.227E-02
MO100	8.700E+02	8.700E+02
RU100	9.217E+01	9.217E+01

Attachment A.1. Continued

BEST COPY AVAILABLE

* IRRADIATION OF ONE METRIC TON OF PWRU FUEL FISSION PRODUCTS
POWER= 1.00000E+00 MW, BURNUP= 1.00000E+00 MWD, FLUX= 1.00E+00 N/CM**2-SEC

5 SUMMARY TABLE: CONCENTRATIONS, GRAMS
ONE METRIC TON OF PWRU FUEL

	12 1YR	12.4YR
RU101	7.274E+02	7.274E+02
RU102	7.381E+02	7.381E+02
RH102	5.662E-05	5.233E-05
RH103	4.500E+02	4.500E+02
RU104	5.466E+02	5.466E+02
PD104	2.228E+02	2.228E+02
PD105	3.876E+02	3.876E+02
RU106	4.114E-02	3.279E-02
PD106	3.835E+02	3.835E+02
PD107	2.349E+02	2.349E+02
AG107	3.304E-04	3.387E-04
PD108	1.627E+02	1.627E+02
CD108	4.505E-04	4.505E-04
AG109	8.180E+01	8.180E+01
PD110	5.327E+01	5.327E+01
AG110M	4.654E-06	3.331E-06
CD110	3.821E+01	3.821E+01
CD111	2.944E+01	2.944E+01
CD112	1.747E+01	1.747E+01
CD113	1.530E-01	1.530E-01
CD113M	1.543E-01	1.519E-01
IN113	1.337E-01	1.361E-01
CD114	2.316E+01	2.316E+01
SN114	1.420E-03	1.420E-03
IN115	2.371E+00	2.371E+00
SN115	3.264E-01	3.264E-01
CD116	8.341E+00	8.341E+00
SN116	7.560E+00	7.560E+00
SN117	8.430E+00	8.430E+00
SN118	8.490E+00	8.490E+00
SN119	8.468E+00	8.468E+00
SN120	8.624E+00	8.624E+00
SN121M	3.001E-03	2.987E-03
SB121	8.371E+00	8.371E+00
SN122	9.471E+00	9.471E+00
TE122	5.816E-01	5.816E-01
SB123	1.030E+01	1.030E+01
TE123	8.280E-03	8.280E-03
SN124	1.272E+01	1.272E+01
TE124	4.397E-01	4.397E-01
SB125	6.859E-01	6.215E-01
TE125	1.855E+01	1.861E+01
TE125M	9.593E-03	8.833E-03
SN126	2.761E+01	2.761E+01
TE126	7.770E-01	7.770E-01
I127	5.580E+01	5.580E+01
TE128	1.081E+02	1.081E+02
XE128	3.103E+00	3.103E+00
I129	1.742E+02	1.742E+02
XE129	1.777E-02	1.777E-02
TE130	3.407E+02	3.407E+02
XE130	1.231E+01	1.231E+01

BEST COPY AVAILABLE

FISSION PRODUCTS

* IRRADIATION OF ONE METRIC TON OF PWRU FUEL
POWER= 1.00000E+00 MW, BURNUP= 1.00000E+00 MWD, FLUX= 1.00E+00 N/CM**2-SEC

5 SUMMARY TABLE: CONCENTRATIONS, GRAMS
ONE METRIC TON OF PWRU FUEL

	12.1YR	12.4YR
XE131	4.028E+02	4.028E+02
XE132	1.025E+03	1.025E+03
BA132	1.813E-03	1.813E-03
CS133	1.047E+03	1.047E+03
XE134	1.367E+03	1.367E+03
CS134	1.912E+00	1.711E+00
BA134	1.482E+02	1.484E+02
CS135	2.758E+02	2.758E+02
BA135	2.677E-01	2.677E-01
XE136	2.202E+03	2.202E+03
BA136	1.698E+01	1.698E+01
CS137	8.434E+02	8.370E+02
BA137	3.090E+02	3.154E+02
BA137M	1.290E-04	1.281E-04
BA138	1.176E+03	1.176E+03
LA138	4.729E-03	4.729E-03
LA139	1.123E+03	1.123E+03
CE140	1.145E+03	1.145E+03
PR141	1.030E+03	1.030E+03
CE142	1.036E+03	1.036E+03
ND142	2.474E+01	2.474E+01
ND143	7.052E+02	7.052E+02
CE144	6.651E-03	4.957E-03
ND144	1.219E+03	1.219E+03
ND145	8.146E+02	8.146E+02
ND146	6.357E+02	6.357E+02
PM146	1.475E-03	1.415E-03
SM146	6.906E-03	6.928E-03
PM147	5.337E+00	4.891E+00
SM147	1.811E+02	1.815E+02
ND148	3.459E+02	3.459E+02
SM148	1.591E+02	1.591E+02
SM149	2.460E+00	2.460E+00
ND150	1.705E+02	1.705E+02
SM150	2.346E+02	2.346E+02
SM151	1.073E+01	1.070E+01
EU151	1.053E+00	1.081E+00
SM152	1.221E+02	1.221E+02
EU152	1.727E-02	1.699E-02
GD152	1.508E-02	1.516E-02
EU153	1.043E+02	1.043E+02
SM154	3.797E+01	3.797E+01
EU154	1.448E+01	1.410E+01
GD154	2.666E+01	2.704E+01
EU155	2.584E+00	2.449E+00
GD155	1.137E+01	1.149E+01
GD156	7.118E+01	7.118E+01
GD157	1.063E-01	1.063E-01
GD158	1.983E+01	1.983E+01
TB159	2.791E+00	2.791E+00
GD160	1.360E+00	1.360E+00
DY160	3.094E-01	3.094E-01

Attachment A.1. Continued

BEST COPY AVAILABLE

* IRRADIATION OF ONE METRIC TON OF PWRU FUEL
POWER= 1.00000E+00 MW, BURNUP= 1 00000E+00 MWD, FLUX= 1 00E+00 N/CM**2-SEC

FISSION PRODUCTS

5 SUMMARY TABLE: CONCENTRATIONS, GRAMS
ONE METRIC TON OF PWRU FUEL

	12 1YR	12.4YR
DY161	4.440E-01	4.440E-01
DY162	3.972E-01	3.972E-01
DY163	3.195E-01	3.195E-01
DY164	4.674E-02	4.674E-02
HO165	1.606E-01	1.606E-01
HO166M	1.686E-03	1.686E-03
ER166	5.203E-02	5.203E-02
ER167	3.284E-03	3.284E-03
ER168	9.153E-03	9.153E-03
TM169	6.546E-05	6.546E-05
YB170	2.124E-05	2.124E-05
SUMTOT	3.175E+04	3.175E+04
TOTAL	3.175E+04	3.175E+04

BEST COPY AVAILABLE

* IRRADIATION OF ONE METRIC TON OF PWRU FUEL
POWER= 1.00000E+00 MW, BURNUP= 1.00000E+00 MWD, FLUX= 1.00E+00 N/CM**2-SEC

FISSION PRODUCTS

5 SUMMARY TABLE: CONCENTRATIONS, GRAMS
ONE METRIC TON OF PWRU FUEL

	12.1YR	12.4YR
H	2.784E-02	2.733E-02
LI	1.679E-04	1.679E-04
BE	1.394E-04	1.394E-04
C	2.447E-05	2.447E-05
GE	6.205E-01	6.205E-01
AS	1.907E-01	1.907E-01
SE	5.125E+01	5.125E+01
BR	1.975E+01	1.975E+01
KR	3.158E+02	3.156E+02
RB	3.120E+02	3.122E+02
SR	6.574E+02	6.547E+02
Y	3.995E+02	3.995E+02
ZR	3.279E+03	3.281E+03
NB	4.803E-03	4.899E-03
MO	3.093E+03	3.093E+03
TC	7.181E+02	7.161E+02
RU	2.104E+03	2.104E+03
RH	4.500E+02	4.500E+02
PD	1.445E+03	1.445E+03
AG	8.180E+01	8.180E+01
CD	1.169E+02	1.169E+02
IN	2.505E+00	2.507E+00
SN	9.170E+01	9.170E+01
SB	1.935E+01	1.930E+01
TE	4.692E+02	4.692E+02
I	2.300E+02	2.300E+02
XE	5.012E+03	5.012E+03
CS	2.168E+03	2.161E+03
BA	1.650E+03	1.657E+03
LA	1.123E+03	1.123E+03
CE	2.181E+03	2.181E+03
PR	1.030E+03	1.030E+03
ND	3.715E+03	3.715E+03
PM	5.338E+00	4.893E+00
SM	7.480E+02	7.484E+02
EU	1.224E+02	1.219E+02
GD	1.305E+02	1.310E+02
TB	2.791E+00	2.791E+00
DY	1.517E+00	1.517E+00
HO	1.623E-01	1.623E-01
ER	6.447E-02	6.447E-02
TM	6.547E-05	6.547E-05
YB	2.283E-05	2.284E-05
SUMTOT	3.175E+04	3.175E+04
TOTAL	3.175E+04	3.175E+04

CUMULATIVE TABLE TOTALS

AP+FP	1.666E+05	1.666E+05
ACT+FP	1.000E+06	1.000E+06
AP+ACT+FP	1.135E+06	1.135E+06

Attachment A.1. Continued

BEST COPY AVAILABLE

* IRRADIATION OF ONE METRIC TON OF PWRU FUEL FISSION PRODUCTS
POWER= 1.00000E+00 MW, BURNUP= 1.00000E+00 MWD, FLUX= 1.00E+00 N/CM**2-SEC

7 SUMMARY TABLE: RADIOACTIVITY, CURIES
ONE METRIC TON OF PWRU FUEL

	12.1YR	12.4YR
H 3	2.687E+02	2.638E+02
C 14	1.091E-04	1.091E-04
SE 79	3.783E-01	3.783E-01
KR 85	3.781E+03	3.701E+03
SR 90	4.777E+04	4.740E+04
Y 90	4.778E+04	4.741E+04
ZR 93	1.626E+00	1.626E+00
NB 93M	7.734E-01	7.863E-01
NB 94	1.487E-04	1.487E-04
TC 99	1.215E+01	1.215E+01
RH102	6.846E-02	6.327E-02
RU106	1.377E+02	1.098E+02
RH106	1.377E+02	1.098E+02
PD107	1.208E-01	1.208E-01
AG108M	2.996E-05	2.990E-05
AG110	2.941E-04	2.105E-04
AG110M	2.212E-02	1.583E-02
CD113M	3.347E+01	3.295E+01
SN119M	8.636E-04	6.141E-04
SN121M	1.775E-01	1.767E-01
SB125	7.085E+02	6.523E+02
TE125M	1.729E+02	1.592E+02
SN126	7.835E-01	7.835E-01
SB126	1.097E-01	1.097E-01
SB126M	7.835E-01	7.835E-01
I 129	3.077E-02	3.077E-02
CS134	2.475E+03	2.215E+03
CS135	3.177E-01	3.177E-01
CS137	7.340E+04	7.284E+04
BA137M	6.943E+04	6.891E+04
CE144	2.123E+01	1.582E+01
PR144	2.124E+01	1.582E+01
PR144M	2.549E-01	1.898E-01
PM146	6.571E-01	8.304E-01
PM147	4.949E+03	4.536E+03
SM151	2.824E+02	2.817E+02
EU152	2.988E+00	2.938E+00
GD153	1.505E-04	1.066E-04
EU154	3.911E+03	3.808E+03
EU155	1.193E+03	1.139E+03
HO166M	3.027E-03	3.027E-03
SUMTOT	2.565E+05	2.536E+05
TOTAL	2.565E+05	2.536E+05

Attachment A.1. Continued

BEST COPY AVAILABLE

* IRRADIATION OF ONE METRIC TON OF PWRU FUEL
POWER= 1.00000E+00 MW, BURNUP= 1.00000E+00 MWD, FLUX= 1.00E+00 N/CM**2-SEC

FISSION PRODUCTS

7 SUMMARY TABLE: RADIOACTIVITY, CURIES
ONE METRIC TON OF PWRU FUEL

	12.1YR	12.4YR
H	2.687E+02	2.638E+02
C	1.091E-04	1.091E-04
SE	3.783E-01	3.783E-01
KR	3.781E+03	3.701E+03
SR	4.777E+04	4.740E+04
Y	4.778E+04	4.741E+04
ZR	1.626E+00	1.626E+00
NB	7.736E-01	7.864E-01
TC	1.215E+01	1.215E+01
RU	1.377E+02	1.098E+02
RH	1.378E+02	1.098E+02
PD	1.208E-01	1.208E-01
AG	2.244E-02	1.608E-02
CD	3.347E+01	3.295E+01
SN	9.619E-01	9.608E-01
SB	7.094E+02	6.532E+02
TE	1.729E+02	1.592E+02
I	3.077E-02	3.077E-02
CS	7.587E+04	7.505E+04
BA	6.943E+04	6.891E+04
CE	2.123E+01	1.582E+01
PR	2.149E+01	1.601E+01
PM	4.950E+03	4.537E+03
SM	2.824E+02	2.817E+02
EU	5.107E+03	4.951E+03
GD	1.505E-04	1.066E-04
HO	3.027E-03	3.027E-03
SUMTOT	2.565E+05	2.536E+05
TOTAL	2.565E+05	2.536E+05

CUMULATIVE TABLE TOTALS

AP+FP	2.567E+05	2.538E+05
ACT+FP	3.380E+05	3.339E+05
AP+ACT+FP	3.382E+05	3.341E+05

Attachment A.1. Continued

BEST COPY AVAILABLE

IRRADIATION OF ONE METRIC TON OF PWRU FUEL
SPONTANEOUS FISSION NEUTRON SOURCE, NEUTRONS/SEC
BASIS= ONE METRIC TON OF PWRU FUEL

	12 1YR	12 4YR
PU238	3.508E+05	3.499E+05
PU240	2.136E+08	2.136E+08
PU242	8.809E+05	8.809E+05
CM244	2.221E+08	2.193E+08
CM246	1.339E+06	1.339E+06
TOTALS		
TABLE	2.269E+08	2.241E+08
ACTUAL	2.269E+08	2.241E+08
OVERALL TOTALS		
TABLE	2.336E+08	2.308E+08
ACTUAL	2.336E+08	2.308E+08

Attachment A.1. Continued

BEST COPY AVAILABLE

APPENDIX B

DISTRIBUTION OF RADIONUCLIDES IN SPENT FUEL

DISTRIBUTION OF RADIONUCLIDES IN SPENT FUEL

1. INTRODUCTION

The spent-fuel radionuclide release studies described in this report require quantitative information on the types, amounts, and chemical forms of radionuclides present in spent fuel and on their partitioning behavior between the UO_2 grains and the grain boundaries. This appendix presents an assessment of the data in the literature that help explain the present results.

2. RADIONUCLIDES CONSIDERED

Although some 40 fission products are generated during irradiation of UO_2 (Ref. B.1), the long-lived radionuclides are of most concern with respect to their release to the environment from a high-level waste repository. Based on the EPA standard (Ref. B.2), the specific radionuclides for which release limits are defined are listed as follows. The present assessment is focused on the distribution of these radionuclides.

Am-241, Am-243, Np-237, Pu-238, Pu-239, Pu-240
Pu-242, Sr-90, Ra-226, Th-230, Th-232, U-233
U-234, U-235, U-236, U-238
C-14, Cs-135, Cs-137, I-129, Tc-99, Sn-126.

3. EXPERIMENTAL TECHNIQUES FOR ANALYSIS OF SPENT FUEL

Various experimental techniques (Ref. B.3) are available for analyzing irradiated UO_2 fuel to obtain information on radionuclide distribution. Table B.1 lists these methods along with their lateral resolution. Since light water reactor (LWR) fuel irradiated to a burnup of about 40,000 MWD/MTU has a grain size in the range of 13-20 μm, only the electron beam analytical techniques (SEM, EMPA, SIMS, and AES) in Table B.1 have the lateral resolution to provide quantitative (EMPA) or semiquantitative (SEM, SIMS, AES) information on the partitioning of radionuclides between the grains and grain boundaries. Direct analysis of the grain boundaries is feasible only with AES.

4. CHEMICAL STATE OF RADIONUCLIDES

The main parameters that determine the chemical state of the radionuclides are the oxygen potential and the temperature of the fuel.

4.1 Oxygen Potential

For each uranium atom two oxygen atoms are generated during fission of UO_2 fuel. Due to its large excess, oxygen will dominate the chemical environment and oxidize UO_2 according to the following reaction:

$$UO_2 + (x/2)\ O_2 = UO_{2+x} \qquad \text{(B-1)}$$

Table B.1. Experimental methods for analyzing irradiated fuel.

Analysis Method	Lateral Resolution (μm)
1. Micro-Gamma Scanning	∿ 250 to 500
2. Core Drilling	∿ 300
3. Laser Microanalysis	∿ 25
4. Nuclear Microanalysis	∿ 10
5. X-Ray Microanalysis	∿ 2
a. SEM-EDX	
b. EMPA-WDX	
c. SIMS	
6. Auger Electron Spectroscopy (AES)	∿ 0.1

Note:

SEM = Scanning Electron Microscopy
EMPA = Electron Microprobe Analysis
SIMS = Secondary Ion Mass Spectrometry
EDX = Energy Dispersive X-Ray Analysis
WDX = Wavelength Dispersive X-Ray Analysis.

for which the partial molar free energy is given by

$$\Delta\bar{G}(O_2) = - RT \ln (P_{O_2}) \qquad \text{(B-2)}$$

Here R is the gas constant, T is the temperature in degrees Kelvin, and p_{O_2} is the partial pressure of O_2 in equilibrium with UO_2/UO_{2+x}.

From Eq. B-1, it is obvious that for each value of UO_{2+x} there is a unique value of $\Delta\bar{G}(O_2)$ associated with it. Thus, Eq. B-2 expresses the oxygen potential of the system. Direct in-pile measurements (Refs. B.4, B.5) of this quantity in irradiated fuel are in very good agreement with values calculated from electron microprobe analysis of irradiated fuel cross-sections (Refs. B.6, B.7). In general, the oxygen potential in irradiated UO_2 fuel rods ranges uniformly between -400 and -500 kJ/mol from the centerline of the fuel pellet to the periphery of the fuel.

4.2 Fuel Temperature

Irradiation induces large temperature gradients within the fuel. Since radionuclide distribution is affected by the prevailing temperatures, it is important to know the radial dependence of the fuel temperature. This can be determined by finding appropriate solutions to the basic heat conduction equation for a solid cylindrical rod in which heat is conducted only in the radial direction. Computer codes such as SATURN-3 (Ref. B.6) and COMETHE (Ref. B.8) have been used to perform thermal analyses of LWR fuel rods, and these codes give average fuel temperatures ranging from about 1300 K at the centerline to about 800 K at the periphery.

5. CHEMISTRY OF THE RADIONUCLIDES

As noted earlier, oxygen will dominate the fuel/fission-products system in irradiated UO_2. Hence, the reactions of the radionuclides with oxygen need to be considered first. This can be accomplished on the basis of a $\Delta\bar{G}(O_2)$-T diagram for UO_2/UO_{2+x} (Ref. B.9) and the radionuclides under consideration (Refs. B.1, B.10), as shown in Figure B.1. The cross-hatched region on the diagram defines the $\Delta\bar{G}(O_2)$-T conditions in irradiated UO_2 fuel.

This diagram shows that the oxides of the actinide nuclides and strontium have free energies that are much more negative than those of the fuel. Hence, they will be present either dissolved in the fuel (actinides) or as a separate phase ($SnO \cdot ZrO_2$).

Of the other nuclides, Tc-99 should be present as the oxide in the system. However, the free energies of formation of compounds in the U-Pu-Tc system are more negative (Ref. B.3), and technetium is usually present in the five-component Mo-Tc-Ru-Rh-Pd alloy inclusions observed in irradiated fuel (Ref. B.3). Similarly, tin will also be present in its elemental state in the fuel.

The chemistry of cesium and iodine is more complicated than that shown in Figure B.1. At low temperatures, Cs_2O is thermodynamically stable; but at temperatures above about 1000 K, cesium should be present as the element. However, cesium is very reactive and forms several very stable ternary compounds in the Cs-U-O (Refs. B.11, B.12), Cs-Mo-O (Ref. B.13), and Cs-Zr-O (Ref. B.14) systems. In addition, cesium will also tie up all of the iodine as CsI because the fission yield of cesium is nearly ten times greater than iodine (Ref. B.1) and CsI is one of the most stable compounds known (Ref. B.1). Cesium iodide can be dissociated according to the reaction

$$2\,CsI + UO_2 + O_2 = Cs_2UO_4 + 2I \qquad \text{(B-3)}$$

However, it requires an oxygen potential of about -160 kJ/mol at 900 K (Ref. B.15).

The behavior of C-14 is relatively straightforward. It will tend to oxidize to form CO and CO_2 by the reaction

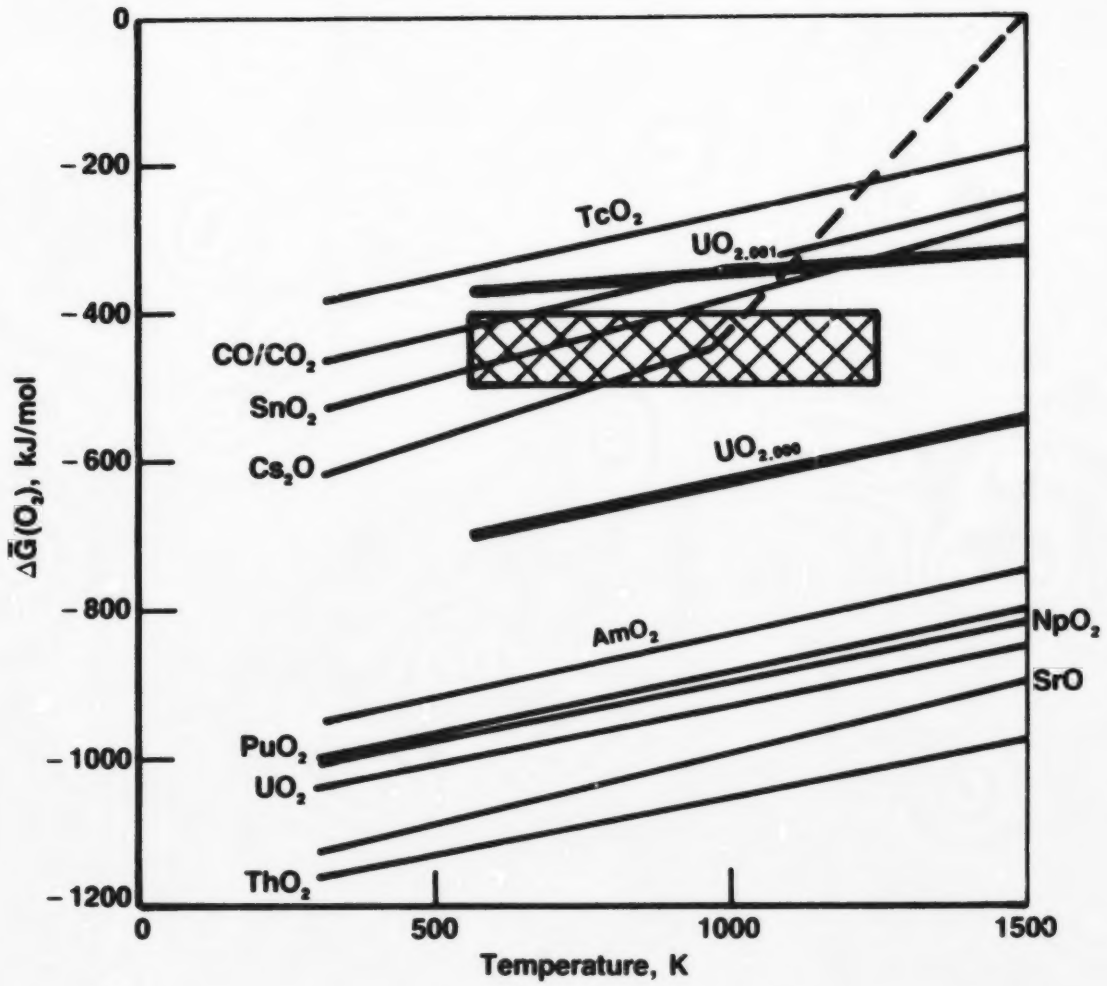

Figure B.1. Partial molar free energies of radionuclide oxides and UO_{2+x} as a function of temperature.

Information on the free energy of the radium oxides is presently unavailable.

BEST COPY AVAILABLE

$$2\ CO + O_2 = 2\ CO_2 \qquad \text{(B-4)}$$

for which the free energy can be written as

$$\Delta G = -2\ RT\ \ln \frac{P_{CO_2}}{P_{CO}} + \Delta\bar{G}(O_2) \qquad \text{(B-5)}$$

From Reaction B-5, it can be seen that the oxygen potential of the system controls the CO/CO_2 equilibrium in Reaction B-4.

6. PHYSICAL DISTRIBUTION OF THE RADIONUCLIDES

To consider the distribution of the radionuclides and their partitioning behavior between the grains and grain boundaries in irradiated UO_2 fuel, one needs to consider their transport behavior in conjunction with the chemical state described earlier, as well as their solubility in the fuel matrix.

6.1 Vapor Pressure

The oxides of the actinide nuclides have very low vapor pressures and are relatively immobile since they form solid solutions with UO_2 (Ref. B.3).

CsI is highly volatile (Ref. B.16) and will tend to migrate from the hotter center to the cooler fuel periphery. In the ternary systems, there are no known volatile compounds in the Cs-U-O system (Ref. B.17). Cs_2MoO_4, which is the stable Cs-Mo-O phase in LWR fuel (Ref. B.18), is a stable gaseous molecule (Ref. B.19). There is no information on any compounds in the Cs-Zr-O system, although Cs_2ZrO_3 is predicted to be thermodynamically very stable (Ref. B.14). Of the remaining nuclides, both carbon oxides are stable gaseous compounds, while the alloy inclusions containing technetium will tend to have very low mobility.

Table B.2 lists the vapor pressures of the present radionuclides in their most probable chemical states in the fuel.

6.2 Phase Diagrams and Solubility

Phase diagram and solubility information on plutonium, neptunium, thorium, and carbon in UO_2 has been critically evaluated and summarized (Refs. B.20, B.21). The maximum solubility of SrO in UO_2 is 12 atom percent at 1773 K (Ref. B.22), but no information is currently available for the solubility of americium, radium, technetium, or tin in UO_2.

The phase relations in the Cs-U-O system have been well established (Ref. B.17), but cesium also has limited solubility in UO_2 (about 0.5 weight percent at 1273 K (Ref. B.3).

Table B.2. Vapor pressures of the radionuclide compounds.

Compound/Element	Vapor Pressure (MPa) at Temperature 600K	1000K	2000K
AmO_2, NpO_2, PuO_2, ThO_2, UO_2	$<10^{-60}$	$<10^{-32}$	$<10^{-8}$
SrO	$<10^{-37}$	10^{-19}	10^{-8}
CsI	10^{-9}	10^{-3}	>1
Tc	$<10^{-41}$	$<10^{-22}$	$<10^{-7}$
Sn	10^{-21}	10^{-10}	10^{-3}
CO, CO_2	*	*	*

*Gases.

7. THEORETICAL MODELING OF RADIONUCLIDE DISTRIBUTION

Various models have been proposed to predict the distribution of fission products in LWR fuel rods. The FASTGRASS model (Refs. B.23-B.25) was developed at Argonne National Laboratory to describe the distribution and migration behavior of fission gases (xenon, krypton) and other volatile fission products (cesium, iodine, CsI, ruthenium, barium, tellurium, ternary cesium compounds) in LWR fuel rods under normal and accident conditions. The model assumes that the volatile fission products exist in the fission gas bubbles and that further transport occurs by bubble diffusion. By solving the classical diffusion equation for spherical geometry and including key variables (gas atom trapping and resolution, grain size, grain boundary migration, etc.), the percentage of retained fission gas in the grains and the grain boundaries can be determined. The results of one such calculation at 1200 K for fuel irradiated to 3-atom-percent burnup suggest that the retained fission gas is present in approximately equal quantities in the grains and the grain boundaries (Refs. B.23-B.25).

A similar methodology has been adopted in fuel performance codes such as ELESIM (Ref. B.26) to predict fission gas release. By assuming that the volatile fission products (cesium and iodine) behave similarly to the fission gases, the typical calculated distribution shows that the grain inventory is approximately ten times the grain boundary inventory.

There is no apparent explanation for the wide disparity in the predicted results from these models. As a result, these models may have only limited applicability to the present work.

8. REFERENCES FOR APPENDIX B

(B.1) R. Kohli, "Thermodynamics of the System Uranium Dioxide-Fission Products-Zircaloy", Report SGAE-3014, Austrian Research Center, Vienna, December, 1978.

(B.2) "Environmental Standards for the Management and Disposal of Spent Nuclear Fuel, High-Level and Transuranic Wastes; Final Rule," 40 CFR Part 191, Environmental Protection Agency, (September 19, 1985).

(B.3) H. Kleykamp, J. Nucl Mater. 131, 221 (1985).

(B.4) E. A. Aitken, S. K. Evans, M. G. Adamson, and J. H. Davies, in Proc. IAEA Symp. on Thermodynamics of Nuclear Materials--1974, International Atomic Energy Agency, Vienna, 1975, p. 59.

(B.5) M. G. Adamson, E. S. Darlin, and J. H. Davies, in IWGFPT/3 Specialists' Meeting on Internal Fuel Rod Chemistry, International Atomic Energy Agency, Vienna, 1979, p. 83.

(B.6) H. Kleykamp, J. Nucl. Mater. 84, 109 (1979).

(B.7) R. Kohli, "Electron Microprobe Analysis of High Burnup Fuel Rods", Battelle Internal Report BCL-382-85-2, September, 1985.

(B.8) P. Verbeck and N. Hoppe, Report BN7609-01, Belgonucleaire S.A., Belgium, September, 1976.

(B.9) Gmelin Handbook of Inorganic Chemistry, 8th Ed., Uranium, Supplement Vol. C5, Uranium Dioxide, UO_2 Physical Properties and Electrochemical Behavior (Springer Verlag, Berlin, 1986).

(B.10) J. Fuger and F. L. Oetting, "The Chemical Thermodynamics of Actinide Elements and Compounds. Part 2. The Actinide Aqueous Ions", International Atomic Energy Agency, Vienna, 1976.

(B.11) A. B. van Egmond, J. Inorg. Nucl. Chem. 38, 1645 (1976).

(B.12) A. B. van Egmond, op cit. 38, 2105 (1976).

(B.13) H. R. Hoekstra, Inorg. Nucl. Chem. Letters 9, 1291 (1973).

(B.14) R. Kohli, Thermochim. Acta 65, 285 (1983).

(B.15) R. Kohli, "Chemical Thermodynamic Analysis of Halogen Stress Corrosion Cracking of Zircaloy Cladding", Paper IAEA-TC-544/13, Proc. Tech. Comm. on Fuel Rod Internal Chemistry and Fission Products Behavior, International Atomic Energy Agency, Vienna, 1986.

(B.16) O. Kubaschewski and C. B. Alcock, Metallurg. Thermochem., 5th Ed., Pergamon Press, New York, 1979.

(B.17) D. C. Fee and C. E. Johnson, J. Nucl. Mater. 99, 107 (1981).

(B.18) R. Kohli, "Chemical Metallurgy--A Tribute to Carl Wagner", N. A. Gokcen, ed., Met. Soc. AIME, Warrendale, PA., June, 1981, p. 309.

(B.19) I. Johnson, J. Phys. Chem. 79, 722 (1975).

(B.20) "The Chemical Thermodynamics of Actinide Elements and Compounds. Parts 1-14", International Atomic Energy Agency, Vienna, 1976-to date.

(B.21) "Thorium Dioxide: Properties and Nuclear Applications", J. Belle and R. M. Berman, eds., Office of Naval Reactors, U.S. Department of Energy, 1984.

(B.22) E. J. McIver, Report AERE-M-1612, Atomic Energy Research Establishment, Harwell, 1966.

(B.23) J. Rest, Nucl. Technol. 56, 553 (1982).

(B.24) J. Rest, op cit. 61, 33 (1983).

(B.25) J. Rest, J. Nucl. Mater. 120, 195 (1984).

(B.26) M.J.F. Notely, Nucl. Technol. 44, 445 (1979).

APPENDIX C

TABULATED LEACHATE DATA

Table C.1. Total uranium concentrations (mg/L) in UO_2 leachates--no external radiation field (Experiment No. 1).

Reaction Vessel No.	Leachate	S/V (meter^{-1})	Day 20	Day 50	Day 97	Day 127	Day 162	Day 188	Day 218	Day 246	Day 274	Day 305	Day 328
1	Brine	5	0.027	0.029	0.026	0.026	0.026	0.026	0.023	0.027	0.033	0.034	0.028
2	Brine	5	0.023	0.027	0.029	0.030	0.028	0.025	0.024	0.027	0.047	0.034	0.039
3	Brine	5	0.023	NA[a]	0.022	0.028	0.025	0.026	0.024	0.026	0.042	0.031	0.027
4	Brine	50	0.024	NA	0.023	0.029	0.045	0.026	0.036	0.027	0.044	0.029	0.034
5	Brine	50	0.024	NA	0.071	0.15	0.039	0.028	0.029	0.028	0.052	0.030	0.030
6	Tuff	5	0.062	NA	0.035	0.025	0.040	0.033	0.028	NA	NA	0.056	0.030
7	Tuff	5	0.036	NA	0.038	0.025	0.040	0.046	0.010	0.026	0.027	0.053	0.023
8	Tuff	5	0.049	NA	0.028	0.022	0.033	0.038	0.003	0.035	0.019	0.047	0.023
9	Tuff	50	0.064	NA	0.036	0.018	0.042	0.050	0.030	0.031	NA	0.040	0.016
10	Tuff	50	0.030	NA	0.036	0.028	0.033	0.043	0.007	NA	0.024	0.042	0.021
11	Basalt	5	0.031	NA	0.028	0.021	0.031	0.031	0.028	0.028	0.025	0.039	0.021
12	Basalt	5	0.033	NA	0.031	0.003	0.036	0.036	0.014	0.027	NA	0.051	0.026
13	Basalt	5	0.051	NA	0.037	0.026	0.054	0.029	0.007	NA	NA	0.054	0.029
14	Basalt	50	0.064	NA	0.047	0.025	0.030	0.029	0.009	0.028	0.028	0.058	0.035
15	Basalt	50	0.031	NA	0.039	0.028	0.025	0.029	0.030	0.025	NA	0.056	0.031
16	H_2O[b]	5	0.032	NA	0.043	0.026	0.032	0.028	0.014	NA	0.026	0.058	0.028

(a)Not analyzed.
(b)Deionized.

Table C.2. Total uranium concentrations (mg/L) in UO_2 leachates--external radiation field (Experiment No. 2).

Reaction Vessel No.	Leachate	S/V (meter^{-1})	Day 10	Day 42	Day 71	Day 101	Day 126	Day 156	Day 182	Day 213	Day 238
1	Brine	5	0.054	0.021	0.020	0.007	0.014	0.021	0.026	0.011	0.031
2	Brine	5	0.012	0.025	0.020	0.011	0.025	0.200	0.022	0.015	0.016
3	Brine	5	0.006	0.020	0.018	0.018	0.086	0.240	0.210	0.014	0.019
4	Brine	50	0.018	0.036	0.025	0.049	0.130	2.680	0.840	0.029	0.290
5	Brine	50	0.021	0.053	0.026	0.033	0.540	0.450	1.330	0.024	1.480
6	Tuff	5	0.060	0.025	0.031	0.049	0.029	0.043	0.030	0.029	0.118
7	Tuff	5	0.074	0.048	0.038	0.038	0.030	0.034	0.030	0.030	0.075
8	Tuff	5	0.080	0.040	0.032	0.038	0.029	0.011	0.029	0.040	0.083
9	Tuff	50	0.045	0.048	0.028	0.032	0.028	0.027	0.072	0.057	0.036
10	Tuff	50	0.065	0.030	0.038	0.032	0.038	0.053	0.036	0.041	0.030
11	Basalt	5	0.023	0.020	0.033	0.048	0.030	0.007	0.043	0.044	0.063
12	Basalt	5	0.026	0.005	0.033	0.029	0.028	0.048	0.029	0.040	0.055
13	Basalt	5	0.034	0.010	0.032	0.031	0.039	0.097	0.033	0.045	0.053
14	Basalt	50	0.043	0.017	0.029	0.048	0.042	0.042	0.033	0.057	0.054
15	Basalt	50	0.045	0.017	0.029	0.033	0.044	0.036	0.027	0.048	0.044
16	H_2O*	5	0.023	0.183	0.041	0.028	0.071	0.214	0.058	0.053	0.045

*Deionized

Table C.3. Total uranium concentrations (mg/L) in spent fuel leachates.

Reaction Vessel No.	Synthetic Leachate Composition	S/V (meter^{-1})	Day 27	Day 54	Day 84	Day 111	Day 146
1	Brine	5	0.035	0.032	0.032	0.026	0.026
2	Brine	5	0.030	0.029	0.045	0.028	0.033
3	Brine	50	0.069	0.084	0.097	0.105	0.055
4	Brine	50	0.056	0.102	0.108	0.063	0.052
5	Tuff	5	0.080	0.035	0.034	0.040	0.032
6	Tuff	5	0.088	0.057	0.030	0.028	0.030
7	Tuff	50	0.263	0.152	0.121	0.105	0.034
8	Tuff	50	0.582	0.471	0.143	0.355	0.045
9	Basalt	5	0.068	0.102	0.059	0.049	0.046
10	Basalt	5	0.070	0.052	0.033	0.038	0.039
11	Basalt	50	0.082	0.077	0.089	0.030	0.027
12	Basalt	50	0.855	0.468	0.249	0.116	0.024
13	Deionized H_2O	5	1.080	0.082	0.057	0.046	0.058

Table C.4. Total Cs-137 concentrations (mg/L) in spent fuel leachates.

Reaction Vessel No.	Synthetic Leachate Composition	S/V (meter^{-1})	Day 27	Day 54	Day 84	Day 111	Day 146
1	Brine	5	0.29	0.35	0.43	0.35	0.33
2	Brine	5	0.41	0.39	0.35	0.30	0.26
3	Brine	50	3.98	4.10	3.26	2.43	1.86
4	Brine	50	4.24	3.40	2.82	2.32	1.93
5	Tuff	5	0.41	0.37	0.34	0.29	0.26
6	Tuff	5	0.40	0.37	0.31	0.30	0.25
7	Tuff	50	3.89	3.58	2.99	2.41	1.96
8	Tuff	50	2.97	2.61	2.27	2.04	1.67
9	Basalt	5	0.24	0.19	0.19	0.18	0.24
10	Basalt	5	0.29	0.26	0.24	0.19	0.19
11	Basalt	50	3.12	3.03	2.51	2.02	1.95
12	Basalt	50	4.42	4.12	3.26	3.06	2.65
13	Deionized H_2O	5	0.48	0.43	0.36	0.34	0.26

Table C.5. Total Cs-134 concentrations (μg/L) in spent fuel leachates.

Reaction Vessel No.	Synthetic Leachate Composition	S/V (meter^{-1})	Day 27	Day 54	Day 84	Day 111	Day 146
1	Brine	5	0.53	0.65	0.81	0.69	0.64
2	Brine	5	0.70	0.76	0.68	0.56	0.44
3	Brine	50	7.39	8.01	6.27	4.63	3.36
4	Brine	50	8.07	6.58	5.38	4.42	3.63
5	Tuff	5	0.77	0.70	0.66	0.55	0.48
6	Tuff	5	0.78	0.72	0.59	0.61	0.46
7	Tuff	50	7.56	6.94	5.91	4.64	3.56
8	Tuff	50	5.53	4.84	4.19	3.57	2.96
9	Basalt	5	0.43	0.35	0.36	0.30	0.39
10	Basalt	5	0.51	0.48	0.44	0.33	0.33
11	Basalt	50	5.84	5.71	4.65	3.72	3.42
12	Basalt	50	8.49	7.90	6.37	5.81	5.01
13	Deionized H_2O	5	0.85	0.81	0.68	0.60	0.44

Table C.6. Total I-129 concentrations (mg/L) in spent fuel leachates.

Reaction Vessel No.	Synthetic Leachate Composition	S/V (meter^{-1})	Day 27	Day 54	Day 84	Day 111	Day 146
1	Brine	5	0.14	0.12	0.13	0.13	0.11
2	Brine	5	0.14	0.19	0.15	0.08	0.08
3	Brine	50	1.38	1.15	1.09	0.92	0.57
4	Brine	50	1.55	1.03	0.43	0.92	0.74
5	Tuff	5	0.05	0.13	0.07	0.03	0.07
6	Tuff	5	0.10	0.10	0.07	0.04	0.06
7	Tuff	50	0.97	1.20	0.80	0.57	0.45
8	Tuff	50	0.92	0.63	0.60	0.34	0.36
9	Basalt	5	0.05	<0.05	0.06	<0.01	0.05
10	Basalt	5	0.06	0.17	0.05	0.04	<0.01
11	Basalt	50	0.52	0.74	0.46	0.43	0.29
12	Basalt	50	0.69	0.69	0.80	0.77	0.34
13	Deionized H_2O	5	0.09	0.11	0.08	0.05	0.05

Table C.7. Total Sr-90 concentrations (μg/L) in spent fuel leachates.

Reaction Vessel No.	Synthetic Leachate Composition	S/V (meter^{-1})	Day 27	Day 54	Day 84	Day 111	Day 146
1	Brine	5	3.35	3.89	5.61	5.35	5.42
2	Brine	5	3.95	5.31	5.21	5.10	4.12
3	Brine	50	27.8	44.9	42.0	36.5	29.0
4	Brine	50	30.5	43.3	41.4	35.4	32.6
5	Tuff	5	0.62	0.62	0.71	0.88	1.00
6	Tuff	5	0.44	0.44	0.54	0.61	0.70
7	Tuff	50	3.88	4.29	5.41	7.14	6.95
8	Tuff	50	4.37	3.57	3.54	3.08	3.47
9	Basalt	5	0.036	0.058	0.029	0.018	0.018
10	Basalt	5	0.024	0.022	0.014	0.025	0.014
11	Basalt	50	0.16	0.19	0.22	0.23	0.33
12	Basalt	50	0.59	0.56	0.44	0.46	0.53
13	Deionized H_2O	5	0.46	0.24	0.22	0.26	0.36

Table C.8. Total Am-241 (μg/L) concentrations* in spent fuel leachates.

Reaction Vessel No.	Synthetic Leachate Composition	S/V (meter^{-1})	Day 27	Day 54	Day 84	Day 111	Day 146
1	Brine	5	<0.006	<0.011	0.012	0.010	<0.006
2	Brine	5	<0.007	<0.011	0.007	0.004	<0.007
3	Brine	50	0.096	0.029	0.058	0.088	0.026
4	Brine	50	0.029	0.110	0.130	0.051	<0.022
5	Tuff	5	0.170	0.013	0.022	<0.008	<0.008
6	Tuff	6	0.130	0.032	<0.010	<0.008	<0.010
7	Tuff	50	0.230	0.210	0.160	0.170	<0.012
8	Tuff	50	0.580	0.430	0.170	0.160	<0.008
9	Basalt	5	0.047	0.049	0.028	<0.008	<0.008
10	Basalt	5	0.023	0.007	0.010	0.015	<0.009
11	Basalt	50	0.058	0.050	0.110	0.011	<0.008
12	Basalt	50	0.800	0.280	0.380	0.050	<0.008
13	Deionized H_2O	5	1.170	0.051	0.044	<0.012	0.025

*Typical uncertainty measurement is ±25 percent.

Table C.9. Total Cm-244* (ng/L) concentrations in spent fuel leachates.

Reaction Vessel Number	Synthetic Leachate Composition	S/V (meter^{-1})	Day 27	Day 54	Day 74	Day 111	Day 146
1	Brine	5	0.063	1.1	0.37	0.42	0.063
2	Brine	5	0.022	0.055	0.33	0.10	0.059
3	Brine	50	3.8	0.98	2.9	4.6	2.6
4	Brine	50	1.3	5.2	5.0	2.2	1.7
5	Tuff	5	4.8	0.62	0.85	2.8	0.08
6	Tuff	5	5.4	1.8	0.41	0.21	0.06
7	Tuff	50	14	8.7	5.7	6.3	0.28
8	Tuff	50	15	11	4.5	7.7	0.41
9	Basalt	5	2.2	1.8	1.2	0.25	0.11
10	Basalt	5	1.1	0.37	0.28	0.15	0.02
11	Basalt	50	2.1	2.2	3.6	0.29	0.20
12	Basalt	50	26	10	14	2.2	0.09
13	Deionized H_2O	5	24	1.5	1.8	0.39	0.74

*Cm-243/Cm-244 <1 percent.

Table C.10. Total Pu-238 (ng/L) concentrations in spent fuel leachates.

Reaction Vessel Number	Synthetic Leachate Composition	S/V ($meter^{-1}$)	Day 27*	Day 54*	Day 84*	Day 111**	Day 146**
1	Brine	5	0.20**	1.7**	0.52	0.93	0.29
2	Brine	5	0.03**	0.17**	0.99	0.35	0.23
3	Brine	50	7.6	6.1	7.0	15	8.2
4	Brine	50	4.2	12	11	7.6	5.8
5	Tuff	5	9.9	0.82	1.9	5.8**	0.13
6	Tuff	5	9.6	2.3	2.5**	5.3**	0.18
7	Tuff	50	26	11	13	23	1.3
8	Tuff	50	38	24	11	48**	2.0
9	Basalt	5	3.4	1.7	2.4	4.1	0.70
10	Basalt	5	2.7	0.26	1.2	1.5	0.08
11	Basalt	50	5.1	3.3	7	1.3	0.88
12	Basalt	50	61	20	33	7.0	0.44
13	Deionized H_2O	5	62	5.3	6.5	2.8	1.7

*Typical uncertainty is ±30 percent.
**Typical uncertainty is ±50 percent.

Table C.11. Total Pu-239 (μg/L) concentrations in spent fuel leachates.

Reaction Vessel Number	Synthetic Leachate Composition	S/V (meter^{-1})	Day 27*	Day 54*	Day 84*	Day 111**	Day 146**
1	Brine	5	0.008	0.039	0.039	0.066	0.007
2	Brine	5	0.010	0.019	0.035	0.017	0.004
3	Brine	50	0.320	0.150	0.310	0.680	0.210
4	Brine	50	0.120	0.430	0.490	0.320	0.140
5	Tuff	5	0.420	0.035	0.065	0.180	0.010
6	Tuff	5	0.410	0.099	0.060	0.110	0.009
7	Tuff	50	1.070	0.500	0.600	1.010	0.017
8	Tuff	50	2.200	1.430	0.570	1.520	0.047
9	Basalt	5	0.140	0.100	0.042	0.089	0.015
10	Basalt	5	0.120	0.021	0.059	0.029	0.030
11	Basalt	50	0.230	0.150	0.300	0.039	0.021
12	Basalt	50	2.440	0.830	1.280	0.270	0.005
13	Deionized H_2O	5	3.930	0.260	0.120	0.071	0.047

*Typical uncertainty is ±30 percent.
**Typical uncertainty is ±50 percent.

Table C.12. Total Pu-240 (μg/L) concentrations in spent fuel leachates.

Reaction Vessel Number	Synthetic Leachate Composition	S/V (meter^{-1})	Day 27*	Day 54*	Day 84*	Day 111**	Day 146**
1	Brine	5	0.004	0.018	0.018	0.030	0.003
2	Brine	5	0.004	0.009	0.016	0.008	0.002
3	Brine	50	0.150	0.072	0.140	0.320	0.100
4	Brine	50	0.058	0.200	0.230	0.150	0.064
5	Tuff	5	0.200	0.016	0.030	0.083	0.005
6	Tuff	5	0.190	0.046	0.028	0.050	0.005
7	Tuff	50	0.500	0.230	0.280	0.470	0.008
8	Tuff	50	1.020	0.660	0.270	0.710	0.022
9	Basalt	5	0.064	0.047	0.019	0.042	0.007
10	Basalt	5	0.058	0.010	0.027	0.013	0.014
11	Basalt	50	0.110	0.069	0.140	0.018	0.010
12	Basalt	50	1.140	0.390	0.600	0.120	0.002
13	Deionized H_2O	5	1.830	0.120	0.058	0.033	0.022

*Typical uncertainty is ±30 percent.
**Typical uncertainty is ±50 percent.

APPENDIX D

WATER CHEMISTRY

WATER CHEMISTRY

1. INTRODUCTION

A water chemistry model was developed and was found to be useful in a previous study of glass waste form performance (Ref. D.1). For our study of UO_2 dissolution, we have developed a similar model with three versions that predict: (1) the speciation of a groundwater without considering any interaction with a waste form; (2) the equilibrium composition and speciation of a groundwater when saturated with respect to a waste form; and (3) the dissolution rate of a waste form in a groundwater unsaturated with respect to the waste form. These three versions of the model treat water chemistry similarly; the differences among them lie in the addition of new subroutines for altering the groundwater chemistry to account for interaction with the waste form. This appendix presents a description of the model and results of calculations performed with the first two versions. The results of applying the third version to UO_2 dissolution are described in Chapter 5.

2. SCOPE OF MODEL

The water chemistry code that was developed for glass waste form studies accounts for 13 chemical elements. This code includes the most important of those elements comprising waste glasses and many natural groundwaters. A complete listing of the species is given elsewhere (Ref. D.2). Since most of these elements are found in groundwater even in the absence of waste glass, we have included all of them in the new model for spent-fuel waste forms. To more fully account for spent fuel, however, it is necessary to add actinide elements, perhaps the most important of which is uranium.

Aqueous uranium species of interest (Refs. D.3,D.4) include: $U(OH)^{3+}$, $U(OH)_2^{2+}$, $U(OH)_3^{+}$, $U(OH)^4(aq)$, $U(OH)_5^{-}$, UO_2^{+}, UO_2^{2+}, UO_2OH^{+}, and $UO_2(OH)_2(aq)$. This list was developed from thermodynamic data (Ref. D.5) for uranium solution chemistry. For any plausible combination of pH and Eh, one of these uranium species is expected to be dominant. In compiling this list, it was assumed that the species do not form complexes with other ions. In actual groundwaters, however, there may be some complexation with carbonate, chloride, and sulfate, particularly under oxidizing conditions.

Since the set of aqueous species under consideration includes uranium in three oxidation states (U(IV), U(V), and U(VI)), the tendency of the water to oxidize or reduce is important. Therefore, the model requires, as part of its input, a value of pe, where $pe = -\log_{10}[e^-]$ and $[e^-]$ is the activity of (hypothetical) aqueous electrons (Ref. D.6).

As mentioned above, the model versions differ in their treatment of the interaction of groundwater with solid spent fuel. In the first version, water chemistry is treated exclusively, without consideration of interactions of the groundwater with spent fuel. In the second version, the dissolution of spent fuel is treated by adding UO_2 to the solution until saturation is reached. Saturation is reached when equilibrium is achieved with respect to the chemical reaction for dissolution of UO_2. In the third

version, a kinetic equation specifies the rate of change in the concentration of uranium as a function of the current concentration. The program takes a series of small time steps and calculates the concentration of uranium as a function of time.

3. SAMPLE CALCULATIONS

As a test of the first version of the model, we determined the speciation of uranium as a function of pH for pe = 6.0 (Eh = 0.355 V) at 25 C. For this calculation, we assumed that uranium was dissolved in water at a concentration of 10^{-9} molal. The pH was controlled by assuming a fixed concentration of 10^{-3} molal HCl, while the concentration of NaOH was varied from zero to 2×10^{-3} molal. No other solutes were included in the calculation.

In Figure D.1, the concentrations of the various uranium species are plotted as a function of pH. For convenience, the concentrations have been normalized so that the total concentration of all uranium species is unity. Since these calculations were performed for relatively oxidizing conditions (pe = 6.0), the fraction of uranium in the U(IV) and U(V) oxidation states never exceeds about 0.0005. These concentrations are so small that they would not be visible in Figure D.1; therefore, we have plotted only the concentrations of the species containing U(VI). As pH increases, the activity of OH^- also increases, and it is observed that UO_2^{++} complexes with OH^- to form UO_2OH^+ and $UO_2(OH)_2(aq)$.

As a test of the second version of the model, we determined the solubility of UO_2 as a function of pe for a nearly fixed pH. The pH was controlled by assuming a fixed concentration of 10^{-4} molal HCl. Solubility was calculated from the thermodynamics of formation of aqueous species from crystalline UO_2. Chloride and uranium species were the only solutes included in the calculation. For most of the range of pe values considered, the concentration of chloride greatly exceeded that of the uranium species. As a result, the pH was fixed at nearly 4. At high pe values, pH also increased slightly, reaching 4.1 at pe = 4.4 and 4.7 at pe = 4.8. Complexation of uranium species with chloride was not taken into account.

Solid uranium oxides exist in several different crystal structures, and uranium solubility depends on the crystal structure of the oxide being dissolved. Depending on pH and pe, the thermodynamically stable solid oxide phase may or may not be UO_2. However, because solid-state phase changes are extremely slow at ordinary temperatures, the solid phase was assumed to be UO_2 throughout this calculation, even though the equilibrium phase at higher pe values may be U_3O_8 or U_4O_9. If phase changes of this type occur, this assumption will have the effect of overestimating uranium solubility.

In Figure D.2, the calculated uranium solubility in 10^{-4} molal HCl is given as a function of pe. The figure begins at the lowest pe value at which water is stable. The solubility of uranium at this point is just above 10^{-13} molal, which is near the minimum solubility resulting from the reaction

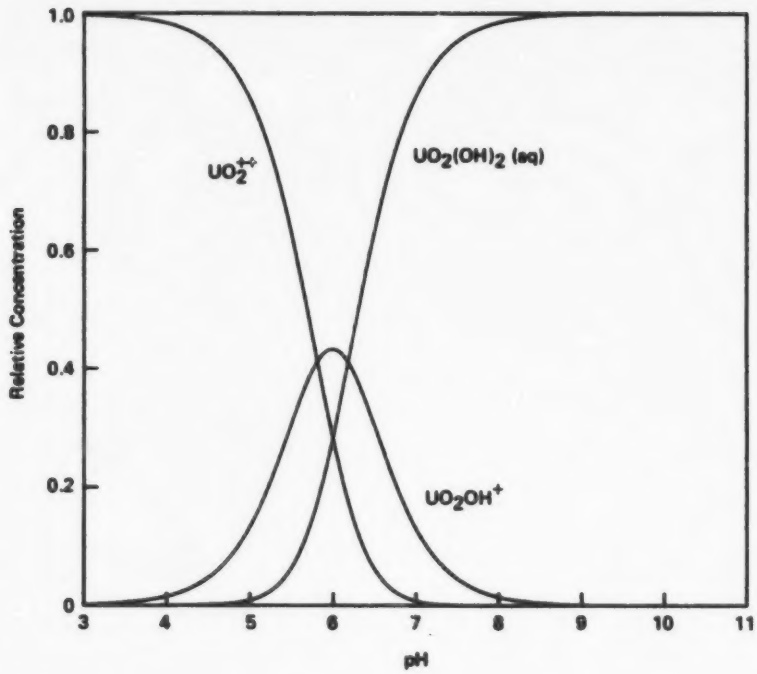

Figure D.1. Relative concentrations of uranium species as a function of pH at pe = 6.0.

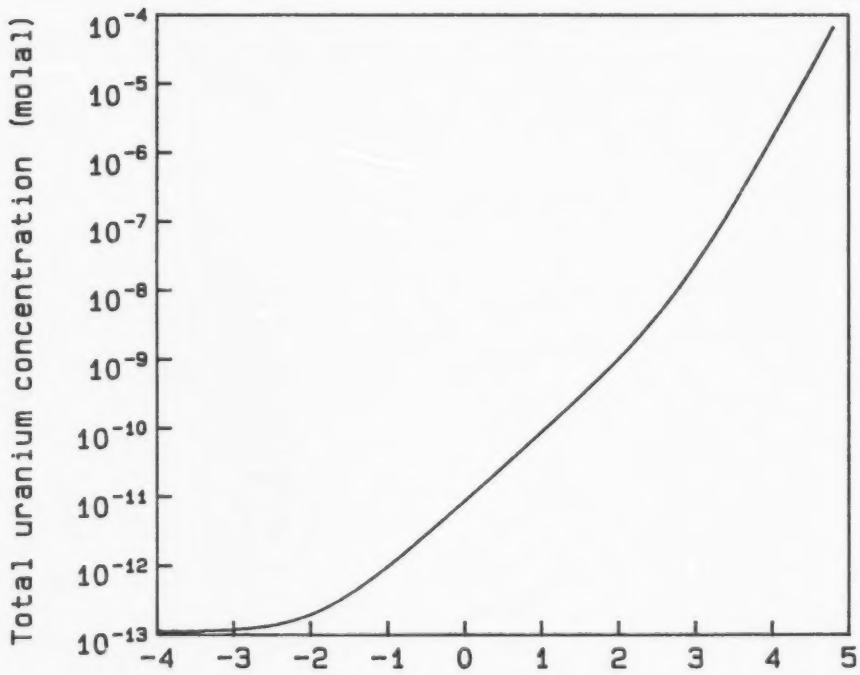

Figure D.2. Calculated total uranium solubility in 10^{-4} molal HCl as a function of pe.

$$UO_2 + 2H_2O = U(OH)_4(aq). \qquad (D\text{-}1)$$

The activity of UO_2 is fixed at unity because it is a solid phase, and the activity of H_2O is essentially constant for dilute solutions. Therefore, the activity of $U(OH)_4(aq)$ at equilibrium (saturation) is independent of pH, pe, or the presence of other solutes. Near the solubility minimum, $U(OH)_4(aq)$ is the dominant aqueous species, although $U(OH)_3^+$ and $U(OH)_5^-$ are also significant.

As pe increases, U(V) becomes more stable than U(IV). This is reflected in an increased solubility due primarily to the reaction

$$U(OH)_4(aq) = UO_2^+ + 2H_2O + e^-. \qquad (D\text{-}2)$$

Note that $U(OH)_4(aq)$ contains U(IV) while UO_2^+ contains U(V). As pe increases, the activity of e^- decreases, while the activities of H_2O and $U(OH)_4(aq)$ are constant, as discussed above. The decreasing electron activity causes production of additional UO_2^+, increasing the total amount of uranium in solution. Eq. D-2 results in the roughly linear portion of Figure D.2 for pe values between -2 and 3. As pe increases beyond 3, U(VI) becomes more stable than U(V). U(VI) is produced through the reaction

$$U(OH)_4(aq) = UO_2^{++} + 2H_2O + 2e^- \qquad (D\text{-}3)$$

since UO_2^{++} contains U(VI). Like Eq. D-2, Eq. D-3 results in increased uranium solubility through the production of additional aqueous uranium species. However, Eq. D-3 has a stronger dependence of the solubility on pe because more electrons are involved than in Eq. D-2. Eq. D-3 is responsible for the linear region of Figure D.2 for pe > 3.

The calculations reported in Figure D.2 may be extended to allow both pH and pe to vary. In Figure D.3, we show total uranium solubility as a function of pH and pe as calculated with the model. In these calculations, the solvent was water with a fixed concentration of HCl of 10^{-3} molal and a concentration of NaOH which varied between 0 and 2×10^{-3} molal. This range of compositions gives a pH between about 3 and 11.

The solubility of uranium reflects the various chemical reactions among solid and aqueous species. Near pe = -3 and pH = 4, the solubility goes through a minimum. The minimum solubility is that resulting from Eq. D-1, and $U(OH)_4(aq)$ is the dominant species. At lower pH, solubility increases due to the reaction

$$U(OH)_4(aq) + H^+ = U(OH)_3^+ + H_2O \qquad (D\text{-}4)$$

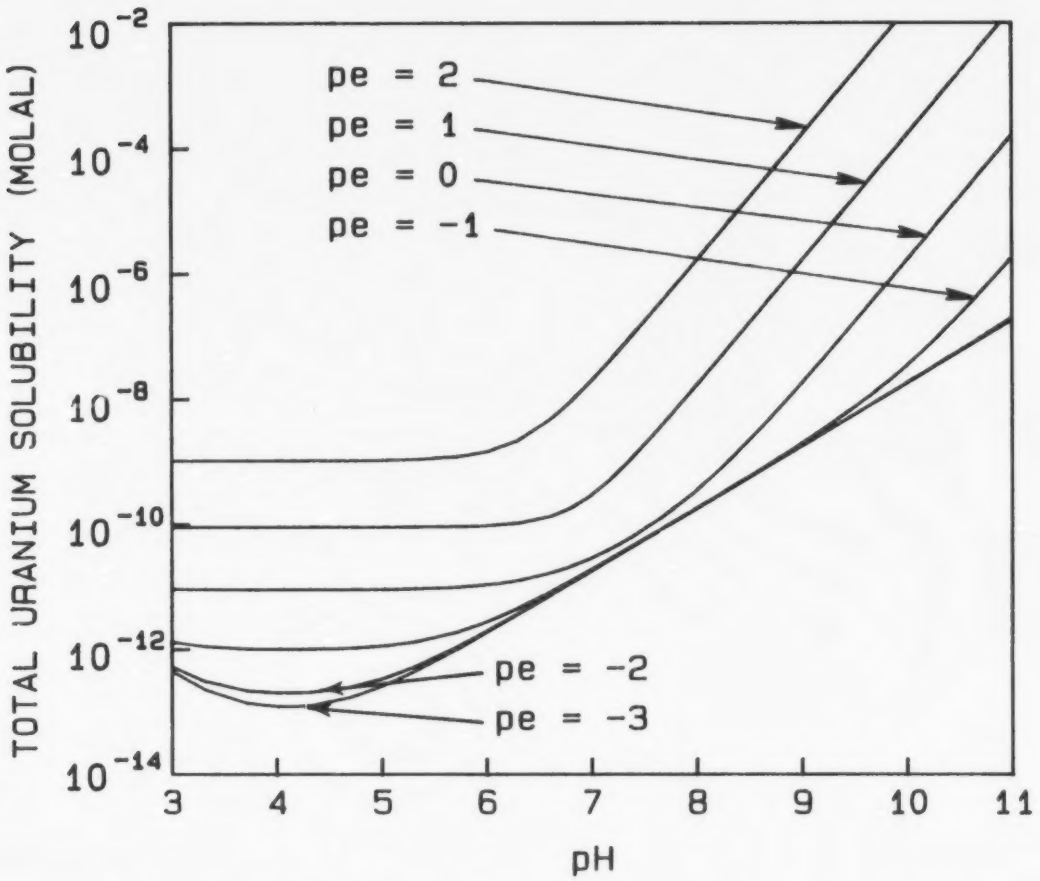

Figure D.3. Total solubility of uranium in dilute aqueous solutions as a function of pH and pe. (See text for description of solutions.)

while at higher pH, solubility increases due to the reaction

$$U(OH)_4(aq) + OH^- = U(OH)_5^-. \qquad (D\text{-}5)$$

Since Eq. D-1 does not depend on the composition of the solvent, the concentration of $U(OH)_4(aq)$ at saturation is constant. Eqs. D-4 and D-5 provide additional solubility since uranium goes into other species.

At pH = 4, solubility increases as pe increases. Over the range of pe = -1 to pe = 2, the solubility increases roughly inversely with the activity of aqueous electrons. This is due to the reaction

$$U(OH)_4(aq) = UO_2^+ + 2H_2O + e^-. \qquad (D\text{-}6)$$

At pe = 2, the dominant species changes from UO_2^+ to $UO_2(OH)_2(aq)$ as pH increases. Again referring everything to the base species $U(OH)_4(aq)$, the following reaction can be written:

$$U(OH)_4(aq) + 2OH^- = UO_2(OH)_2(aq) + 2H_2O + 2e^-. \qquad (D\text{-}7)$$

From this reaction, we expect solubility to vary as the square of the OH^- activity and as the inverse square of the activity of aqueous electrons; this is exactly the variation seen for the large pe and pH.

4. REFERENCES FOR APPENDIX D

(D.1) "Long-Term Performance of High-Level Glass Waste Forms," D. Stahl (Compiler), NUREG/CR-4795, BMI-2143, pp 5-1 ff (1987).

(D.2) "System Performance of High-Level Waste Package Components," D. Stahl (Compiler), NUREG/CR-4956, BMI-2156, Appendix B (1987).

(D.3) L. H. Johnson et al., "Mechanisms of Leaching and Dissolution of UO_2 Fuel," Nucl. Technol. 56, 238 (1982).

(D.4) R. J. Lemire and P. R. Tremaine, "Uranium and Plutonium Equilibria in Aqueous Solutions to 200 C," J. Chem. Eng. Data 25, 361 (1980).

(D.5) J. Paquette and R. J. Lemire, "A Description of the Chemistry of Aqueous Solutions of Uranium and Plutonium to 200 C Using Potential-pH Diagrams," Nucl. Sci. Eng. 79, 26 (1981).

(D.6) W. Stumm and J. J. Morgan, Aquatic Chemistry: An Introduction Emphasizing Chemical Equilibria in Natural Waters, 2nd Ed. (John Wiley and Sons, Inc., New York, 1981), 422.

APPENDIX E

QUALITY ASSURANCE PROCEDURES

QUALITY ASSURANCE PROCEDURES

Quality assurance (QA) procedures were established for all experimental activities. Procedures were revised and new ones prepared as necessary to meet program requirements. Seven approved procedures are applicable to this task.

These QA procedures are summarized in Table E.1 which lists each procedure number, the current revision number, the title, and the procedure status.

Table E.1. NRC waste package program QA procedures.

Procedure	Title	Status
WF-PP-17 Revision 1	Laboratory Procedures for the Fluorometric Analysis of Uranium in Ground Water and Brine	Approved
WF-PP-18 Revision 0	Experimental Procedure for Flow-Through Leaching of Unirradiated UO_2 and Spent Fuel	Approved
WF-PP-19 Revision 1	Iodine-129 Analysis of Aqueous Samples with Separation of Interfering Activity	Approved
WF-PP-21 Revision 0	The Analysis of Strontium-90 in Simulated Basalt, Brine, and Tuff Groundwaters	Approved
WF-PP-32 Revision 1	Laboratory Procedures for Preparation of Simulated WIPP Brine A	Approved
WF-PP-33 Revision 0	Procedure for Preparation of Simulated Basalt Groundater Solution	Approved
WF-PP-34 Revision 0	Laboratory Procedure for Preparation of Simulated Tuff Groundwater Solutions	Approved

DISTRIBUTION LIST

Office of Nuclear Regulatory Research
Division of Engineering
Mail Stop NL-007
U.S. Nuclear Regulatory Commission, Washington, D.C. 20555

Attn: Division Director/Deputy Director
F. A. Costanzi, Chief, Waste Management Branch
J. R. Randall
M. B. McNeil
G. F. Birchard, Project Manager (15)

Division of High Level Waste Management, NMSS
Mail Stop 623 SS
U.S. Nuclear Regulatory Commission, Washington, D.C. 20555

Attn: Division Director/Deputy Director
Chief, System Engineering and Evaluation Branch
E. A. Wick
M. Tokar
K. C. Chang
Document Control Center

Division of Waste Management, NMSS
U.S. Nuclear Regulatory Commission
1955 Jadwin Ave - Suite 310A
Richland, WA 99352

Attn: R. Cook, BWIP Site Rep.

Advisory Committee on Reactor Safeguards
Mail Stop H-1016
U.S. Nuclear Regulatory Commission, Washington, D.C. 20555

Attn: Waste Management Subcommittee
R. C. Tang

Battelle Columbus Division
505 King Avenue
Columbus, Ohio 43201-2693

Attn: B. Saffell, Program Manager (50)

DISTRIBUTION LIST (Continued)

Martin A. Molecke
Sandia National Lab.
Albuquerque, NM 87185

Neville Pugh
National Bureau of Standards
Washington, D.C. 20234

Nicholas Grant
Department of Metallurgy
Massachusetts Institute
of Technology
Cambridge, MA 02139

Jerome Kruger
Corrosion Section
National Bureau of Standards
Washington, D.C. 20234

Don J. Bradley
Waste Package Programs
Battelle Pacific Northwest Labs
Richland, WA 99352

Allen G. Croff
Oak Ridge National Laboratory
P.O. Box X
Oak Ridge, TN 37830

Lynn Hobbs
Department of Materials Science
Massachusetts Institute of
Technology
77 Massachusetts Avenue
Cambridge, MA 02139

Richard E. Westerman
Pacific Northwest Lab.
P.O. Box 999
Richland, WA 99352

Edward J. Hennelly
Savannah River Lab.
Aiken, SC 29808

Arthur A. Bauer
Office of Crystalline Rock
Development
Battelle Memorial Institute
505 King Avenue
Columbus, OH 43201-2693

Robert Williams
Electric Power Research Institute
P.O. Box 10412
Palo Alto, CA 94301

William P. Reed
U.S. Department of Commerce
National Bureau of Standards
Washington, D.C. 20234

Ray Walton
U.S. Department of Energy
Washington, D.C. 20545

John E. Mendel
Materials Characterization Center
Pacific Northwest Lab.
P.O. Box 999
Richland, WA 99352

Larry Hench
University of Florida
Gainesville, FL 32611

David E. Clark
University of Florida
Gainesville, FL 32611

Joseph Muscara
Mail Stop NL 007
U.S. NRC
Washington, D.C. 20555

Ken W. Stephens
The Aerospace Corp., Suite 400
955 L'Enfant Plaza, S.W.
Washington, D.C. 20024

Robert S. Dyer
Office of Radiation Programs
(ANR-461)
U.S. Environmental Protection Agency
401 M Street, S.W.
Washington, D.C. 20460

Lorenzo Ricks
U.S. DOE/BES
Washington, D.C. 20545

DISTRIBUTION LIST (Continued)

James Burnell
Basalt Waste Isolation Projects
Rockwell Hanford Operation
Richland, WA 99352

Kenneth Russell
Department of Materials Science
and Engineering
Massachusetts Institute of
Technology
Cambridge, MA 02139

Robert H. Doremus
Materials Engineering Department
Rensselaer Polytechnic Institute
Troy, NY 12181

David C. Kocher
Oak Ridge National Lab.
P.O. Box X
Oak Ridge, TN 37830

Neville Moody
Sandia Livermore Lab.
Livermore, CA 94550

Donald E. Clark
ONWI
Battelle Memorial Institute
505 King Avenue
Columbus, OH 43201

Martin J. Steindler
Argonne National Lab.
Argonne, IL 60439

Donald G. Schweitzer
Brookhaven National Lab.
Upton, NY 11973

Peter Soo
Brookhaven National Lab.
Upton, NY 11973

Nestor Ortiz
Sandia National Lab.
Albuquerque, NM 87185

Pedro B. Macedo
Catholic University of America
Washington, D.C. 20064

Larry Evans
Armco Research Center
703 Curtis St.
Middletown, OH 45043

Robert R. Gaugh
Armco Research Center
703 Curtis St.
Middletown, OH 45043

M. John Plodinec
Savannah River Laboratory
Aiken, SC 29808

Robert H. Frost
Colorado School of Mines
Center for Welding Research
Golden, CO 80401

D. Stahl
Science Applications Intl. Corp.
101 Convention Center Dr., Suite 407
Las Vegas, NV 89109

T.C. Johnson
Mail Stop 623 SS
U.S. NRC
Washington, D.C. 20555

John Voglewede
Mail Stop 623 SS
U.S. NRC
Washington, D.C. 20555

Document Control Center, NMSS
Mail Stop 623 SS
U.S. NRC
Washington, D.C. 20555

R.E. Browning/M.J. Bell
Mail Stop 623 SS
U.S. NRC
Washington, D.C. 20555

P.T. Prestholt
U.S. NRC
1050 Flamingo Rd. Suite 319
Las Vegas, NV 89119

DISTRIBUTION LIST (Continued)

W. Ott
Mail Stop NL 007
U.S. NRC
Washington, D.C. 20555

J.T. Greeves
Mail Stop 623 SS
U.S. NRC
Washington, D.C. 20555

T.L. Jungling
Mail Stop 623 SS
U.S. NRC
Washington, D.C. 20555

Tilak Verma
U.S. NRC - SRPO/ONWI
505 King Ave.
Columbus, OH 43201

Metal Component Subcommittee
Mail Stop H-1016, ACRS
U.S. NRC
Washington, D.C. 20555

Jack L. McElroy
Pacific Northwest Lab
P.O. Box 999
Richland, WA 99352

Harold Wallenberg
Lawrence Berkeley Lab
Berkeley, CA 94720

Don Alexander
U.S. DOE
Washington, D.C. 20545

E. Gause
Weston Consultants
2301 Research Boulevard, 3rd Floor
Rockville, MD 20850

Kyo S. Kim
United Engineers & Constructors, Inc.
P.O. Box 179
Philadelphia, PA 19105

NRC FORM 335 (2-84) NRCM 1102, 3201, 3202

U.S. NUCLEAR REGULATORY COMMISSION

BIBLIOGRAPHIC DATA SHEET

SEE INSTRUCTIONS ON THE REVERSE

1 REPORT NUMBER (Assigned by TIDC add Vol No., if any)

NUREG/CR-4954
BMI 2154

2 TITLE AND SUBTITLE

Long-Term Performance of Spent Fuel Waste Forms

3 LEAVE BLANK

4 DATE REPORT COMPLETED

MONTH: June | YEAR: 1987

5 AUTHOR(S)

J.L. Means, A.J. Markworth, J.K. McCoy, M.P. Failey, M.J. Stenhouse, R. Kohli, and G.C. Taylor

6 DATE REPORT ISSUED

MONTH: September | YEAR: 1987

7 PERFORMING ORGANIZATION NAME AND MAILING ADDRESS (Include Zip Code)

Battelle Columbus Division
505 King Avenue
Columbus, Ohio 43201-2693

8 PROJECT/TASK/WORK UNIT NUMBER

9 FIN OR GRANT NUMBER

B6764
NRC-04-82-015

10 SPONSORING ORGANIZATION NAME AND MAILING ADDRESS (Include Zip Code)

Division of Engineering
Office of Nuclear Regulatory Research
U.S. Nuclear Regulatory Commission
Washington, DC 20555

11a TYPE OF REPORT

Technical

b PERIOD COVERED (Inclusive dates)

April 1982--August 1987

12 SUPPLEMENTARY NOTES

13 ABSTRACT (200 words or less)

This report describes the results of a 2-year experimental program to investigate the leaching/dissolution characteristics of spent fuel in simulated groundwaters. Experiments were conducted to evaluate the leaching of unirradiated UO_2 in simulated groundwaters both in the presence and absence of an external radiation field. Other experiments characterized the dissolution behavior of spent fuel under the same conditions as for UO_2. Leach data were interpreted in terms of rates and mechanisms of radionuclide release, thus providing insight on leach behavior under realistic repository conditions.

Uranium release from both unirradiated and irradiated UO_2 appeared to be solubility controlled, with only minor leachate compositional effects on the uranium concentrations. When leached in the presence of a radiation field, unirradiated UO_2 produced elevated uranium concentrations only in the brine leachates. The leaching of both cesium and iodine from spent fuel was rapid and linear with the surface-area-to-volume (S/V) ratio. Similar to cesium and iodine, strontium release was nearly proportional to S/V. However, unlike cesium and iodine, strontium release was strongly affected by leachate composition, with greater release associated with lower pH.

A model describing spent fuel/UO_2 dissolution was developed, complementing the experimental studies.

14 DOCUMENT ANALYSIS - a KEYWORDS/DESCRIPTORS

High-level waste
Waste form
Spent fuel
Leaching mechanism
Spent fuel dissolution modeling

b IDENTIFIERS/OPEN ENDED TERMS

15 AVAILABILITY STATEMENT

Unlimited

16 SECURITY CLASSIFICATION

(This page) Unclassified
(This report) Unclassified

17 NUMBER OF PAGES

18 PRICE

* U. S. GOVERNMENT PRINTING OFFICE: 1987-181-582:50224

UNITED STATES
NUCLEAR REGULATORY COMMISSION
WASHINGTON, D.C. 20555

OFFICIAL BUSINESS
PENALTY FOR PRIVATE USE, $300

SPECIAL FOURTH CLASS RATE
POSTAGE & FEES PAID
USNRC
PERMIT No. G-67